Forschungszentrum Karlsruhe
Technik und Umwelt

Wissenschaftliche Berichte
FZKA 6170

T-stresses for Components with One-dimensional Cracks

T. Fett
Institut für Materialforschung

Dezember 1998

FORSCHUNGSZENTRUM KARLSRUHE

Technik und Umwelt

Wissenschaftliche Berichte

FZKA 6170

T-stresses for components with one-dimensional cracks

T. Fett

Institut für Materialforschung

Forschungszentrum Karlsruhe GmbH, Karlsruhe

1998

Als Manuskript gedruckt

Forschungszentrum Karlsruhe GmbH
Postfach 3640, 76021 Karlsruhe

Mitglied der Hermann von Helmholtz-Gemeinschaft
Deutscher Forschungszentren (HGF)

ISSN 0947-8620

T-stresses for components with one-dimensional cracks

Abstract:

The failure of cracked components is governed by the stresses in the vicinity of the crack tip. The singular stress contribution is characterised by the stress intensity factor K, the first regular stress term is represented by the so-called T-stress. Sufficient information about the stress state is available, if the stress intensity factor and the constant stress term, the T-stress, are known.

While stress intensity factor solutions are reported in handbooks for many crack geometries and loading cases, T-stress solutions are available only for a small number of test specimens and simple loading cases as for instance pure tension and bending.

T-stress solutions for components containing two-dimensional internal cracks and edge cracks were computed by application of the Boundary Collocation Method (BCM). The results are compiled in form of tables, diagrams or approximative relations.

In addition a Green's function for T-stresses is proposed for internal and external cracks which enables to compute T-stress terms for any given stress distribution in the uncracked body.

T-Spannungen für Komponenten mit eindimensionalen Rissen

Kurzfassung:

Das Versagen von Bauteilen mit Rissen wird durch die unmittelbar an der Rißspitze auftretenden Spannungen verursacht. Der singuläre Anteil diese Spannungen wird durch den Spannungsintensitätsfaktor K charakterisiert. Der erste reguläre Term wird durch die sogenannte T-Spannung beschrieben. Eine für die meisten Anwendungsfälle ausreichende Beschreibung des Spannungsfeldes vor Rissen ist möglich bei Kenntnis dieser beiden bruchmechanischen Parameter. Während Lösungen für Spannungsintensitätsfaktoren in Handbüchern verfügbar sind, besteht ein Mangel an T-Spannungs-Lösungen.

Im vorliegenden Bericht werden Ergebnisse für Bauteile mit zweidimensionalen Innenrissen sowie Außenrissen mitgeteilt, die mit der "Boundary Collocation Methode" (BCM) bestimmt wurden. Die Resultate werden in Form von Tabellen, Diagrammen und Näherungsformeln wiedergegeben.

Zusätzlich werden Greensfunktionen für Innen- und Außenrisse angegeben. Diese erlauben die Berechnung des T-Spannungsterms für beliebige Spannungsverteilungen in der ungerissenen Struktur.

Contents

1 Introduction

The fracture behaviour of cracked structures is dominated by the near-tip stress field. In fracture mechanics, interest focusses on stress intensity factors, which describe the singular stress field ahead of a crack tip and govern fracture of a specimen when a critical stress intensity factor is reached. Nevertheless, there is experimental evidence (e.g. [1-4]) that also the constant stress contributions acting over a longer distance from the crack tip may affect fracture mechanics properties.

Two experimental results may illustrate this for nonelastic fracture mechanics. As a first example results for the plastic component of the crack opening displacement (COD) during crack extension are plotted in Fig. 1a as reported by Cotterell et al.[3] for steel 1204-350. It can be seen that the initiation value (obtained by extrapolation to zero crack growth) is by a factor of about 2 higher for a shallow crack ($a/W = 0.1$) compared with a deep crack ($a/W = 0.5$).

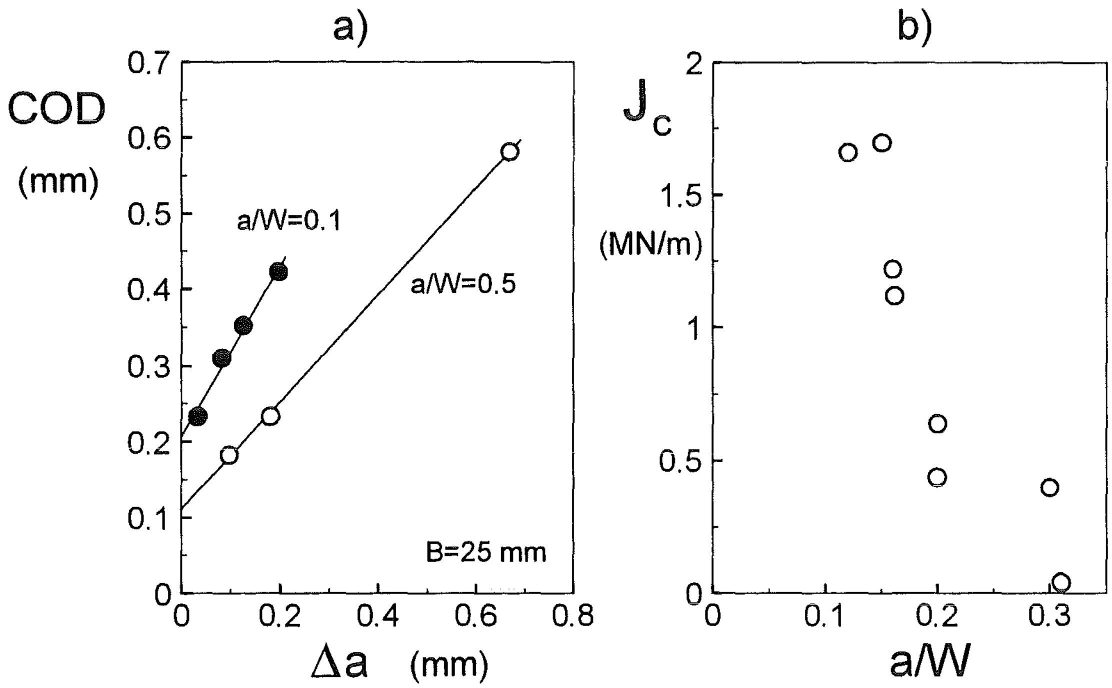

Fig. 1.1 a) Crack opening displacement (COD) of specimens with shallow and deep notches for 25 mm thick bend specimens made of structural steel [3]; b) J_c at cleavage instability for HY80 MMA weld measured with 3-point bending specimens after Sumpter and Hancock [4].

In Fig. 1.1b the influence of the crack length on the critical J-integral value at cleavage instability for HY80 weld metal is shown as measured by Sumpter and Hancock [4]. These results show that the parameters of plastic fracture mechanics (J, COD) cannot characterise the fracture behaviour sufficiently. An interpretation of such crack length effects is possible by including the T stress as an additional parameter for crack tip stress triaxiality.

Sufficient information about the stress state is available, if the stress intensity factor and the constant stress term, the T-stress, are known.

While stress intensity factor solutions are reported in handbooks for many crack geometries and loading cases, T-stress solutions are available only for a small number of test specimens and simple loading cases as for instance pure tension and bending.

Different methods were applied in the past to compute the T-stress term for fracture mechanics standard test specimens. Regarding one-dimensional cracks, Leevers and Radon [5] made a numerical analysis based on a variational method. Kfouri [6] applied the Eshelby technique. Sham [7,8] developed a second-order weight function based on a work-conjugate integral and evaluated it for the SEN specimen using the FE method. In [9,10] a Green's function for T-stresses was determined on the basis of Boundary Collocation results. Wang and Parks [11] extended the T-stress evaluation to two-dimensional surface cracks using the line-spring method. A compendium of results from the literature has been given by Sherry et al. [12].

In earlier reports the T-stress terms for edge-cracked structures [13] and internal one-dimensional cracks were reported [14].

In the present report T-stress solutions derived by the author are compiled. Most of the results were obtained with the Boundary Collocation Procedure and with the Green's function technique. Therefore, these methods are described in detail in Sections 2-4. For the numerical computations the Boundary Collocation Method (BCM) is applied. This procedure provides all coefficients of a Williams expansion of the stress function. Therefore, additional coefficients are reported, especially the coefficient of the singular stress term, i.e. the stress intensity factor and in some cases weight functions are given which enable to compute the stress intensity factor under arbitrary stress distributions in the uncracked component.

2 T-stress term

The complete stress state in a cracked body is known if a related stress function is known. In most cases, the Airy stress function Φ is an appropriate tool which results as the solution of

$$\Delta\Delta\Phi = 0 \tag{2.1}$$

For a cracked body a series representation for Φ was given by Williams [15]. Its symmetric part can be written in polar coordinates with the crack tip as the origin

$$\Phi = \sigma^* W^2 \sum_{n=0}^{\infty} (r/W)^{n+3/2} A_n \left[\cos(n+\tfrac{3}{2})\varphi - \frac{n+\frac{3}{2}}{n-\frac{1}{2}} \cos(n-\tfrac{1}{2})\varphi \right]$$

$$+\sigma^* W^2 \sum_{n=0}^{\infty} (r/W)^{n+2} A^*_n [\cos(n+2)\varphi - \cos n\varphi] \tag{2.2}$$

where σ^* is a characteristic stress and W is a characteristic dimension. The geometric data are explained by Fig. 2.1. The stress components are given by

$$\frac{\sigma_r}{\sigma^*} = \sum_{n=0}^{\infty} A_n (r/W)^{n-1/2} (n+3/2) \left[\frac{n^2-2n-5/4}{n-1/2} \cos(n-1/2)\varphi - (n+1/2)\cos(n+3/2)\varphi \right]$$

$$+\sum_{n=0}^{\infty} A^*_n (r/W)^n [(n^2-n-2)\cos n\varphi - (n+2)(n+1)\cos(n+2)\varphi] \tag{2.3}$$

$$\frac{\sigma_\varphi}{\sigma^*} = \sum_{n=0}^{\infty} A_n (r/W)^{n-1/2} (n+3/2)(n+1/2) \left[\cos(n+3/2)\varphi - \frac{n+3/2}{n-1/2} \cos(n-1/2)\varphi \right]$$

$$+\sum_{n=0}^{\infty} A^*_n (r/W)^n (n+2)(n+1)[\cos(n+2)\varphi - \cos n\varphi] \tag{2.4}$$

$$\frac{\tau_{r\varphi}}{\sigma^*} = \sum_{n=0}^{\infty} A_n (r/W)^{n-1/2} (n+3/2)(n+1/2)[\sin(n+3/2)\varphi - \sin(n-1/2)\varphi]$$

$$+\sum_{n=0}^{\infty} A^*_n (r/W)^n (n+1)[(n+2)\sin(n+2)\varphi - n\sin n\varphi] \tag{2.5}$$

From (2.3) the x-component of stresses results with $\varphi=0$

$$\sigma_x/\sigma^* = -\sum_{n=0}^{\infty} A_n \left(\frac{a-x}{W}\right)^{n-1/2} \frac{(2n+3)(2n+1)}{2n-1} - \sum_{n=0}^{\infty} 4A^*_n \left(\frac{a-x}{W}\right)^n (n+1) \tag{2.6}$$

The term with coefficient A_0 is related to the stress intensity factor K_I by

$$K_I = \sigma * F\sqrt{\pi a} \tag{2.7}$$

with the geometric function F

$$\boxed{F = A_0\sqrt{18/\alpha}} \tag{2.8}$$

with the relative crack depth $\alpha = a/W$.

The term with the coefficient A^*_0 represents the total constant σ_x-stress contribution appearing at the crack tip ($x = a$) of a cracked structure, which is called the T-stress

$$\boxed{T = \sigma_x\big|_{x=a} = -4\sigma * A^*_0}\,. \tag{2.9}$$

This total x-stress includes stress contributions which are already present at the location $x = a$ in the uncracked body, $\sigma^{(0)}_{x,a}$, and an additional stress term which is generated by the crack exclusively. This stress separation gives rise to define two T-stress contributions. The contribution determined by the x-stress in the uncracked structure may be denoted here by $T^{(0)}$

$$T^{(0)} = \sigma^{(0)}_{x,a} \tag{2.10}$$

and the contribution caused by the crack by T_c. Therefore, we can write

$$T = T^{(0)} + T_c\ . \tag{2.11}$$

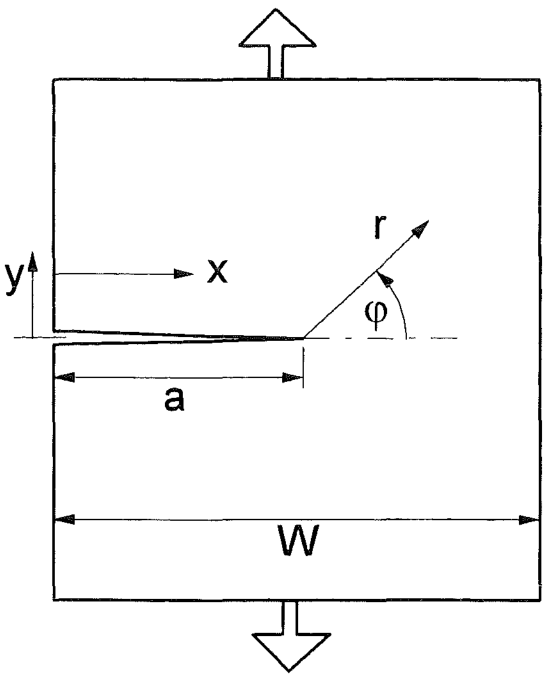

Fig. 2.1 Geometrical data of a crack in a component.

Leevers and Radon [5] proposed a dimensionless representation by the stress biaxiality ratio β which reads

$$\beta = \frac{T\sqrt{\pi a}}{K_I} = \frac{T}{\sigma * F} \tag{2.12}$$

or expressed in terms of stress function coefficients

$$\beta = -\sqrt{\frac{8\alpha}{9}}\frac{A^*_0}{A_0} \tag{2.13}$$

Taking into consideration the singular stress term and the first regular term, the near-tip stress field can be described by

$$\sigma_{ij} = \frac{K_I}{\sqrt{2\pi a}} f_{ij}(\varphi) + \sigma_{ij,0} \tag{2.14}$$

$$\sigma_{ij,0} = \begin{pmatrix} \sigma_{xx,0} & \sigma_{xy,0} \\ \sigma_{yx,0} & \sigma_{yy,0} \end{pmatrix} = \begin{pmatrix} T & 0 \\ 0 & 0 \end{pmatrix} \tag{2.15}$$

where f_{ij} are the well-known angular functions for the singular stress contribution.

The determination of the biaxiality ratio obviously needs the stress intensity factor solution to be known. Fortunately, in the application of the BCM-Method also the coefficient A_0 related to the stress intensity factor via eqs.(2.7) and (2.8) is determined. Therefore, for all crack problems the stress intensity factor solution will be given too.

In special cases it may be of advantage to know also higher coefficients of the Williams expansion, eq.(2.2). This is desirable e.g. for the computation of stresses over a somewhat wider distance from a crack tip. Therefore, additional coefficients are compiled in some cases.

I METHODS

For the determination of T-stress solutions occurring in this report the following methods were applied:

- Westergaard stress function
- Williams (Airy) stress function
- Boundary Collocation method
- Green's function method
- Principle of superposition.

The methods are outlined in Sections 3 and 4.

3 Green's function for T-stress

3.1 Representation of T-stresses by a Green's function

As a consequence of the principle of superposition, stress fields for different loadings can be added in the case of single loadings acting simultaneously. This leads to an integration representation of the loading parameters and was applied very early to the singular stress field and the computation of the related stress intensity factor by Bückner [16]. Similarly, the T-stress contribution T_c caused by the crack exclusively can be expressed by an integral [7-10]. The integral representations read

$$K_I = \int_0^a h(x,a)\,\sigma_y(x)\,dx \tag{3.1.1a}$$

$$T_c = \int_0^a t(x,a)\,\sigma_y(x)\,dx \tag{3.1.1b}$$

where the integration has to be performed with the stress field σ_y in the uncracked body (Fig.3.1.1). The stress contributions are weighted by a weight function (h, t) dependent on the location x where the stress σ_y acts.

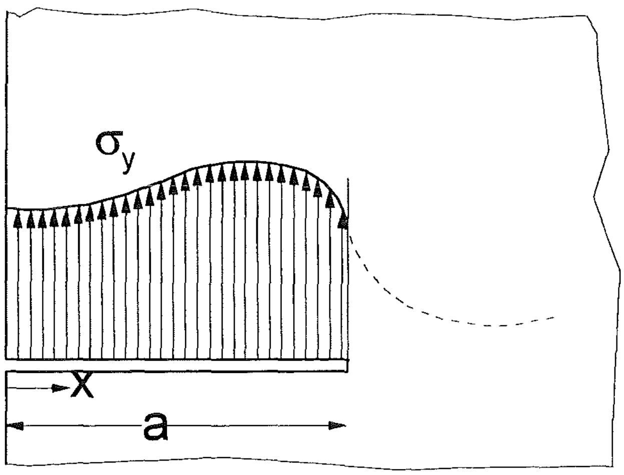

Fig. 3.1.1 Crack loaded by continuously distributed normal tractions (present in the uncracked body).

The weight functions h and t can be interpreted as the stress intensity factor and as the T-term for a pair of single forces P acting at the crack face at the location x_0 (Fig. 3.1.2), i.e. the weight functions (h, t) are Green's functions for K_I and T_c. This can be shown easily. The single forces are represented by a stress distribution

$$\sigma(x) = \frac{P}{B}\delta(x - x_0) \tag{3.1.2}$$

where δ is the Dirac Delta-function and B is the thickness of the plate (often chosen to be B = 1). By introducing these stress distribution into (3.1.2) we obtain

$$K_P = \frac{P}{B}\int_0^a \delta(x - x_0)h(x,a)\,dx = \frac{P}{B}h(x_0,a) \tag{3.1.3}$$

$$T_P = \frac{P}{B}\int_0^a \delta(x - x_0)t(x,a)\,dx = \frac{P}{B}t(x_0,a) \tag{3.1.4}$$

i.e. the weight function terms $h(x_0,a)$ and $t(x_0,a)$ are the Green's functions for the stress intensity factor and T-stress term.

3.2 Set-up of the Green's function

3.2.1 Asymptotic term

In order to describe the Green's function, a separation is made consisting of a term t_0 representing the asymptotic limit case of near-tip behaviour and a correction term t_{corr} which includes information about the special shape of the component and the finite dimensions,

$$t = t_0 + t_{corr} \tag{3.2.1}$$

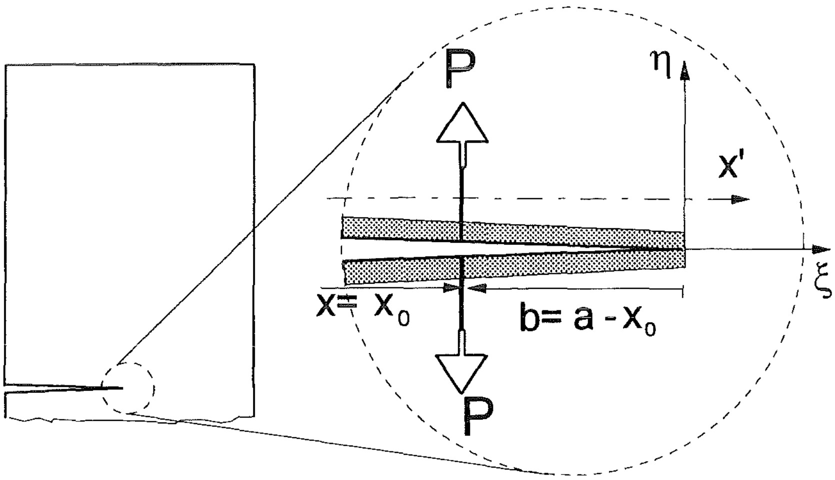

Fig. 3.2.1 Situation at the crack tip for asymptotic stress consideration.

In order to obtain information on the asymptotic behaviour of the weight or Green's function, we consider exlusively the near-tip behaviour. Therefore, we take into consideration a small section of the body (dashed circle) very close to the crack tip (Fig.3.2.1). The near-tip zone is zoomed very strongly. Consequently, the outer borders of the component move to infinity. Now, we have the case of a semi-infinite crack in an infinite body. If we load the crack faces by a couple of forces P at location $x=x_0<<a$, the stress state can be described in terms of the Westergaard stress function [17]:

$$Z = \frac{P}{\pi}\frac{1}{z+b}\sqrt{\frac{b}{z}} \quad , \quad z = \xi + i\eta \tag{3.2.2}$$

The regular contribution to the stress function is (z, $b \neq 0$)

$$Z_{reg} = -\frac{P}{\pi}\frac{1}{z+b}\sqrt{\frac{z}{b}} \tag{3.2.3}$$

from which the regular part of the x-stress component results as

$$\sigma_x = \operatorname{Re} Z - y \operatorname{Im}(dZ/dz) \;\Rightarrow\; \sigma_x\big|_{y=0} = \operatorname{Re}\{Z\}\big|_{y=0} \tag{3.2.4}$$

$$\sigma_{x,reg}\big|_{y=0} = \operatorname{Re}\{Z_{reg}\}\big|_{y=0} = -\frac{P}{\pi}\frac{\sqrt{x'-a}}{(x'-x)\sqrt{a-x}} \quad , \quad x' > a \tag{3.2.5}$$

The constant x-stress term, i.e. the regular x-stress at $x' = 0$ is then given by

$$\sigma_{x,reg}\big|_{x\to 0} = -\frac{P}{\pi}\lim_{x'\to a}\frac{\sqrt{x'-a}}{(x'-x)\sqrt{a-x}} \tag{3.2.6}$$

and the Green's function reads

$$\Rightarrow \qquad t_0 = -\frac{1}{\pi}\lim_{x'\to a}\frac{\sqrt{x'-a}}{(x'-x)\sqrt{a-x}} \; . \tag{3.2.7}$$

From (3.2.7), the T-stress can be derived for a couple of forces for a semi-infinite crack in an infinite body, namely

$$T = \begin{cases} 0 & \text{for } x < a \\ \infty & \text{for } x = a \end{cases} \; . \tag{3.2.8}$$

Let us consider the crack loading p to be represented by a Taylor series with respect to the crack tip as

$$p(x) = p\big|_{x=a} - \frac{dp}{dx}\bigg|_{x=a}(a-x) + \frac{1}{2}\frac{d^2 p}{dx^2}\bigg|_{x=a}(a-x)^2 \text{ -+..} \tag{3.2.9}$$

The corresponding T-stress contribution, resulting from the asymptotic part of the Green's function, is given by

$$T_{c,0} = \int_0^a t_0(x', a, x)\sigma(x)\,dx = -\frac{1}{\pi}\sigma_y\big|_{x=a}\lim_{x'\to a}\sqrt{x'-a}\int_0^a \frac{dx}{(x'-x)\sqrt{a-x}} + R \tag{3.2.10}$$

with the remainder R containing integrals of the type

$$I_n = \int_0^a \frac{(a-x)^{n-1/2}}{x'-x}\,dx \quad , \quad n \geq 1 \tag{3.2.11}$$

which yield (see e.g. integral 212.14a in [18])

$$I_n = 2\sum_{\nu=0}^{n-1} \frac{(a-x')^{\nu}}{2n-1-2\nu} a^{n-\nu-1/2} + a^{n-1/2} \ln \frac{\sqrt{a}-\sqrt{x'-a}}{\sqrt{a}+\sqrt{x'-a}} \tag{3.2.12}$$

Consequently, the limit value is

$$\lim_{x'\to a} \sqrt{x'-a}\; I_n = 0 \quad \Rightarrow R = 0 \tag{3.2.13}$$

and the term T_0 is exclusively represented by the first integral term in (3.2.10). Integration of this term results in

$$-\frac{1}{\pi} p\big|_{x=a} \lim_{x'\to a} \sqrt{x'-a} \int_0^a \frac{dx}{(x'-x)\sqrt{a-x}} = -\frac{1}{\pi} p\big|_{x=a} \lim_{x'\to a} \sqrt{x'-a} \left[\frac{2}{\sqrt{x'-a}} \arctan \sqrt{\frac{x'-a}{a-x}} \right]_0^a =$$

$$= -\frac{1}{\pi} p\big|_{x=a} \lim_{x'\to a} \left[\pi - \arctan \sqrt{\frac{x'-a}{a}} \right] = -p\big|_{x=a} \tag{3.2.14}$$

$$\Rightarrow \quad T_{c,0} = -p\big|_{x=a} = -\sigma_y\big|_{x=a} \tag{3.2.15}$$

3.2.2 Correction terms for the Green's function

3.2.2.1 Edge cracks

By the considerations made before, only the asymptotic part of the x-stress is derived. Since a small region around the crack tip was chosen, the component boundaries were shifted to infinity. Now, a set-up has to be chosen for the weight function contribution $t_{\rm corr}$ which includes the finite size of the component.

Let us assume the difference between the complete Green's function $t(b)$ and its asymptotic part $t_0(b)$ to be expressible in a Taylor series for $b=a-x\to 0$

$$t_{corr}(b) = t(b) - t_0(b) = f(b) = 0 + \frac{\partial t}{\partial b}\bigg|_{b=0} b + \tfrac{1}{2} \frac{\partial t^2}{\partial b^2}\bigg|_{b=0} b^2 + \ldots \tag{3.2.16}$$

Then the complete Green's function can be written as

$$t = t_0 + \sum_{\nu=1}^{\infty} C_{\nu} (1 - x/a)^{\nu} \tag{3.2.17}$$

If we restrict the expansion to the leading term, we obtain as an approximation

$$t \cong t_0 + C\left(1 - \frac{x}{a}\right) \tag{3.2.18}$$

A simple procedure to determine approximative Green's functions is possible by determination of the unknown coefficients in the series representation (3.2.17) to known T-solutions for reference loading cases [10]. The general treatment may be shown for the determination of the coefficient C for an approximative weight function representation according to (3.2.18).

Let us assume the T-term T_t of an edge-cracked plate under pure tension σ_0 to be known. Introducing (3.2.18) into (3.1.1) yields (with $T^{(0)}=0$)

$$T_t = \sigma_0 \int_0^a t(x,a)\,dx = \sigma_0 \int_0^a t_0\,dx + \sigma_0 C \int_0^a (1 - x/a)\,dx = \sigma_0\left(-1 + C\frac{a}{2}\right) \tag{3.2.19}$$

and the coefficient C results as

$$C = \frac{2}{a}\left(1 + \frac{T_t}{\sigma_0}\right) \tag{3.2.20}$$

Knowledge of additional reference solutions for T allows to determine further coefficients.

3.2.2.2 Internal crack

The derivation of an approximate Green's function for internal cracks is similar to those of edge cracks. Due to the symmetry at $x=0$, the general set-up must be modified. An improved description that fulfills eq.(3.2.16) and is symmetric with respect to x=0 is

$$t = t_0 + \sum_{\nu=1}^{\infty} C_\nu (1 - x^2/a^2)^\nu \tag{3.2.21}$$

with the first approximation

$$t \cong t_0 + C(1 - x^2/a^2) \tag{3.2.22}$$

In this case, the coefficient C results from the pure tension case as

$$C = \frac{3}{2a}\left(1 + \frac{T_t}{\sigma_0}\right) \tag{3.2.23}$$

4 Boundary Collocation Procedure

4.1 Boundary conditions

A simple possibility to determine the coefficients A_0 and A^*_0 is the application of the Boundary Collocation Method (BCM) [19-21]. For practical application of eq.(2.2), which is used to determine A_0 and A^*_0, the infinite series for the Airy stress function must be truncated after the Nth term for which an adequate value must be chosen. The still unknown coefficients are determined by fitting the stresses and displacements to the specified boundary conditions. The stresses result from the relations

$$\sigma_r = \frac{1}{r}\frac{\partial \Phi}{\partial r} + \frac{1}{r^2}\frac{\partial^2 \Phi}{\partial \varphi^2} \tag{4.1.1}$$

$$\sigma_\varphi = \frac{\partial^2 \Phi}{\partial r^2} \tag{4.1.2}$$

$$\tau_{r\varphi} = \frac{1}{r^2}\frac{\partial \Phi}{\partial \varphi} - \frac{1}{r}\frac{\partial^2 \Phi}{\partial r \partial \varphi} \tag{4.1.3}$$

The stresses resulting from these relations by use of the Williams stress function are given in eqs.(2.3-2.5). The displacements read

$$\frac{u}{\sigma^* W} = \frac{1+\nu}{E}\sum_{n=0}^{\infty} A_n \left(\frac{r}{W}\right)^{n+1/2} \frac{2n+3}{2n-1}[(n+4\nu-\tfrac{5}{2})\cos(n-\tfrac{1}{2})\varphi - (n-\tfrac{1}{2})\cos(n+\tfrac{3}{2})\varphi] +$$
$$+\frac{1+\nu}{E}\sum_{n=0}^{\infty} A^*_n \left(\frac{r}{W}\right)^{n+1} [(n+4\nu-2)\cos n\varphi - (n+2)\cos(n+2)\varphi] \tag{4.1.4}$$

$$\frac{v}{\sigma^* W} = \frac{1+\nu}{E}\sum_{n=0}^{\infty} A_n \left(\frac{r}{W}\right)^{n+1/2} \frac{2n+3}{2n-1}[(n-\tfrac{1}{2})\sin(n+\tfrac{3}{2})\varphi - (n-4\nu+\tfrac{7}{2})\sin(n-\tfrac{1}{2})\varphi] +$$
$$+\frac{1+\nu}{E}\sum_{n=0}^{\infty} A^*_n \left(\frac{r}{W}\right)^{n+1} [(n+2)\sin(n+2)\varphi - (n-4\nu+4)\sin n\varphi] \tag{4.1.5}$$

(ν=Poisson's ratio), from which the needed Cartesian component results as

$$u_x = u\cos\varphi - v\sin\varphi \tag{4.1.6}$$

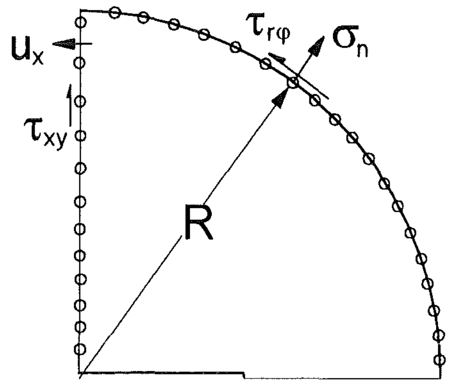

Fig. 4.1.1 Node selection and boundary conditions for an internally cracked disk.

In the special case of an internally cracked circular disk of radius R, the stresses at the boundaries are:

$$\sigma_n = \tau_{r\varphi} = 0 \tag{4.1.7}$$

along the quarter circle. Along the perpendicular symmetry line, the boundary conditions are:

$$u_x = \text{const.} \rightarrow \frac{\partial u_x}{\partial y} = 0 \tag{4.1.8}$$

$$\tau_{xy} = 0 \tag{4.1.9}$$

About 100 coefficients for eq.(2.2) were determined from 600-800 stress and displacement equations at 400 nodes along the outer contour (symbolized by the circles in Fig. 4.1.1). For a selected number of (N+1) collocation points, the related stress components (or displacements) are computed, and a system of 2(N+1) equations allows to determine up to 2(N+1) coefficients. The expenditure of computation can be reduced by the selection of a rather large number of edge points and by solving subsequently the then overdetermined system of equations using a least squares routine.

In the case of the edge-cracked rectangular plate of width W and hight $2H$ (Fig. 4.1.2) the stresses at the border are

$$\sigma_x = 0,\ \tau_{xy} = 0 \qquad \text{for } x = 0 \tag{4.1.10}$$

$$\sigma_y = \sigma^*,\ \tau_{xy} = 0 \qquad \text{for } y = H \tag{4.1.11}$$

$$\sigma_x = 0,\ \tau_{xy} = 0 \qquad \text{for } x = W \tag{4.1.12}$$

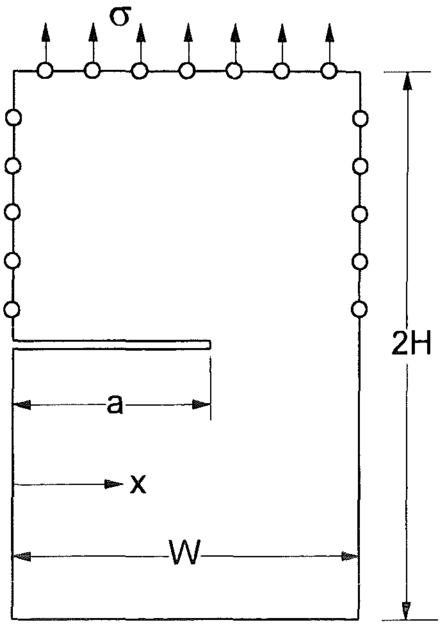

Fig. 4.1.2 Collocation points for the edge-cracked rectangular plate

and in the case of the Double-edge-cracked plate (Fig. 4.1.3) it holds

$$\sigma_x = 0, \ \tau_{xy} = 0 \qquad \text{for } x = 0 \tag{4.1.13}$$

$$\sigma_y = \sigma^*, \ \tau_{xy} = 0 \qquad \text{for } y = H \tag{4.1.14}$$

$$\frac{\partial u_x}{\partial y} = 0, \ \tau_{xy} = 0 \qquad \text{for } x = W \tag{4.1.15}$$

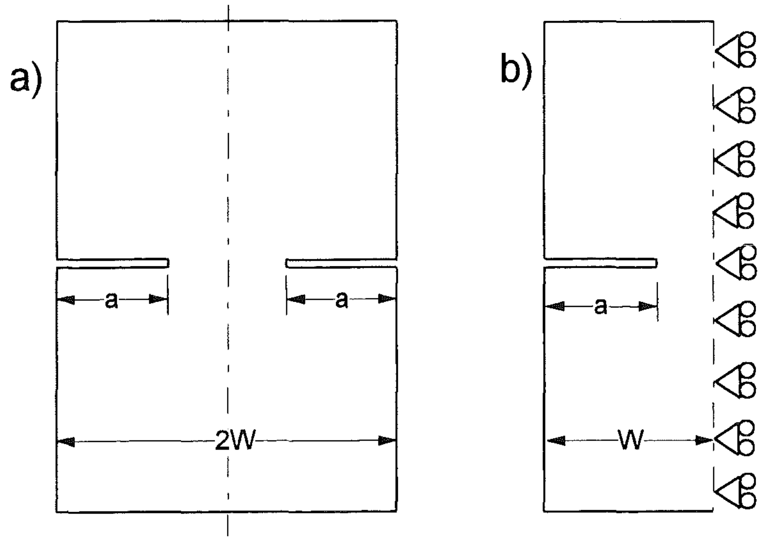

Fig. 4.1.3 Double-edge-cracked plate a) geometric data, b) half-specimen with symmetry boundary conditions.

4.2 Boundary Collocation procedure for point forces

The treatment of point forces at the crack face in case of a finite body is illustrated in the following sections for a circular disk with an internal crack loaded by a couple of forces at $x = y = 0$. In order to describe the crack-face loading by concentrated forces, we superimpose two loading cases. First, the singular crack-face loading is modelled by the centrally loaded crack in an infinite body described by the Westergaard stress function

$$Z = \frac{Pa}{\pi} \frac{1}{z\sqrt{z^2 - a^2}} \tag{4.2.1}$$

The stresses resulting from this stress function disappear only at infinite distances from the crack. In the finite body, consequently, the stress-free boundary condition is not fulfilled. To nullify the tractions at the outer boundaries, stresses resulting from the Airy stress function, eq.(2.2), are added which do not superimpose additional stresses at the crack faces. The basic principle used for such calculations, the principle of superposition, is illustrated in more detail in Section 5.

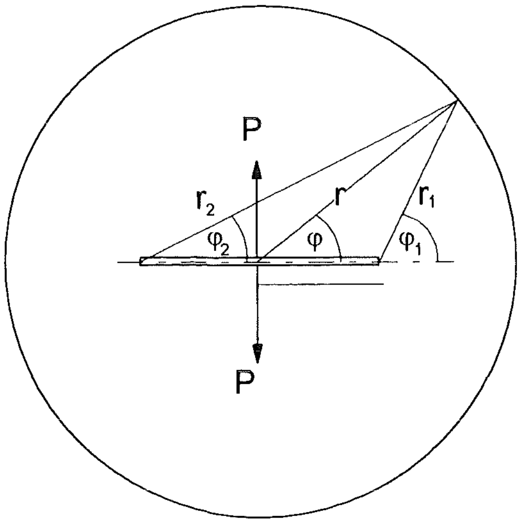

Fig.4.2.1 Coordinate system for the application of the Westergaard stress function to a finite component.

The stresses caused by Z are

$$\sigma_x = \operatorname{Re} Z - y \operatorname{Im} Z' \tag{4.2.2}$$

$$\sigma_y = \operatorname{Re} Z + y \operatorname{Im} Z' \tag{4.2.3}$$

$$\tau_{xy} = -y \operatorname{Re} Z \tag{4.2.4}$$

with

$$Z' = \frac{dZ}{dz} = -\frac{Pa}{\pi}\frac{2z^2 - a^2}{z^2(z^2 - a^2)^{3/2}} \tag{4.2.5}$$

For practical use it is of advantage to introduce the coordinates shown in Fig.4.2.1. The following geometric relations hold

$$z = r\exp(i\varphi), \quad z - a = r_1\exp(i\varphi_1), \quad z + a = r_2\exp(i\varphi_2) \tag{4.2.6}$$

$$r = \sqrt{x^2 + y^2}, \quad \tan\varphi = y/x \tag{4.2.7}$$

$$r_1 = \sqrt{(x-a)^2 + y^2}, \quad \tan\varphi_1 = y/(x-a) \tag{4.2.8}$$

$$r_2 = \sqrt{(x+a)^2 + y^2}, \quad \tan\varphi_2 = y/(x+a) \tag{4.2.9}$$

$$\operatorname{Re} Z = \frac{Pa}{\pi r\sqrt{r_1 r_2}}\cos(\varphi + \tfrac{1}{2}\varphi_1 + \tfrac{1}{2}\varphi_2) \tag{4.2.10}$$

$$\operatorname{Im} Z = -\frac{Pa}{\pi r\sqrt{r_1 r_2}}\sin(\varphi + \tfrac{1}{2}\varphi_1 + \tfrac{1}{2}\varphi_2) \tag{4.2.11}$$

$$\operatorname{Re} Z' = -\frac{Pa}{\pi}\left[\frac{2}{(r_1 r_2)^{3/2}}\cos\tfrac{3}{2}(\varphi_1 + \varphi_2) - \frac{a^2}{r^2(r_1 r_2)^{3/2}}\cos(2\varphi + \tfrac{3}{2}\varphi_1 + \tfrac{3}{2}\varphi_2)\right] \tag{4.2.12}$$

$$\operatorname{Im} Z' = \frac{Pa}{\pi}\left[\frac{2}{(r_1 r_2)^{3/2}}\sin\tfrac{3}{2}(\varphi_1 + \varphi_2) - \frac{a^2}{r^2(r_1 r_2)^{3/2}}\sin(2\varphi + \tfrac{3}{2}\varphi_1 + \tfrac{3}{2}\varphi_2)\right] \tag{4.2.13}$$

The stress function Z provides no T-stress term as will be shown in by eq.(6.1.6). Nevertheless, the equilibrium tractions at the circumference act as a normal external load and may produce a T-stress. Radial and tangential stress components along the contour of the disk for a crack with a/R=0.4 are plotted in Fig.4.2.2.

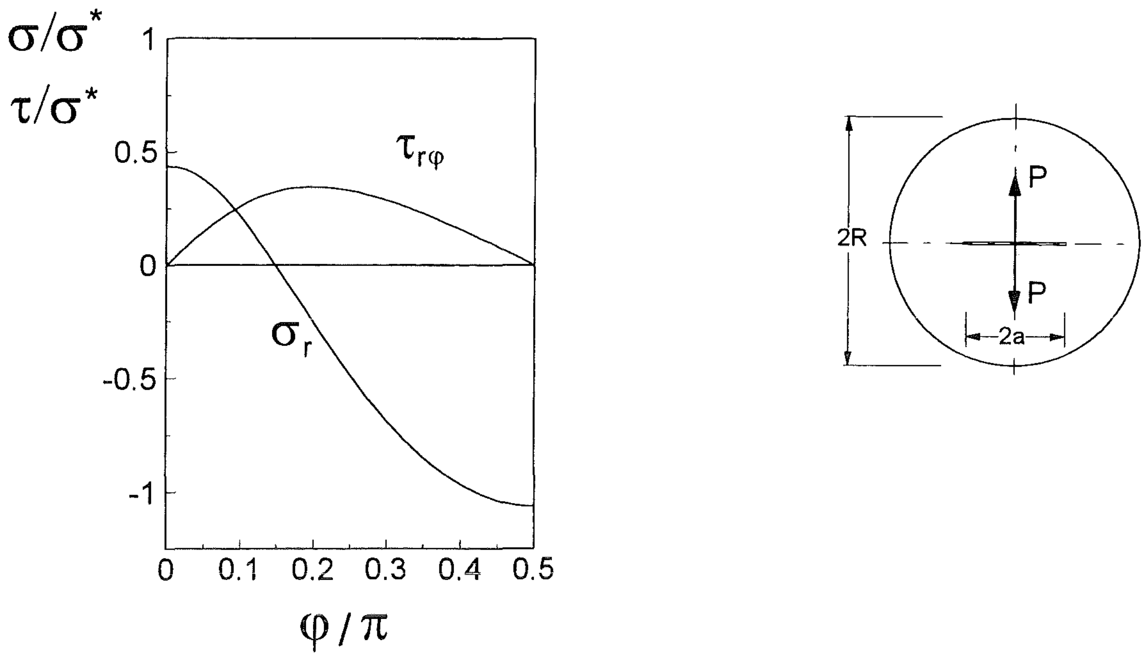

Fig.4.2.2 Normal and shear tractions created by the stress function (4.2.1) along the fictitious disk contour (for φ see Fig. 4.2.1), $\sigma^*=P/(\pi R t)$, t = thickness.

5 Principle of superposition

The procedure necessary for the computations addressed in Section 4.2 is illustrated below. A disk geometry may be chosen. Figure 5.1 explains the principle of superposition for the case of T-stresses. Part a) shows a crack in an infinite body, loaded by a couple of forces P. The T-stress for this case is denoted as T_0. First we compute the normal and shear stresses along a contour (dashed circle) which corresponds to the disk. We cut out the disk along this contour and apply normal and shear tractions at the free boundary which are identical with the stresses computed before (Fig. 5.1b).

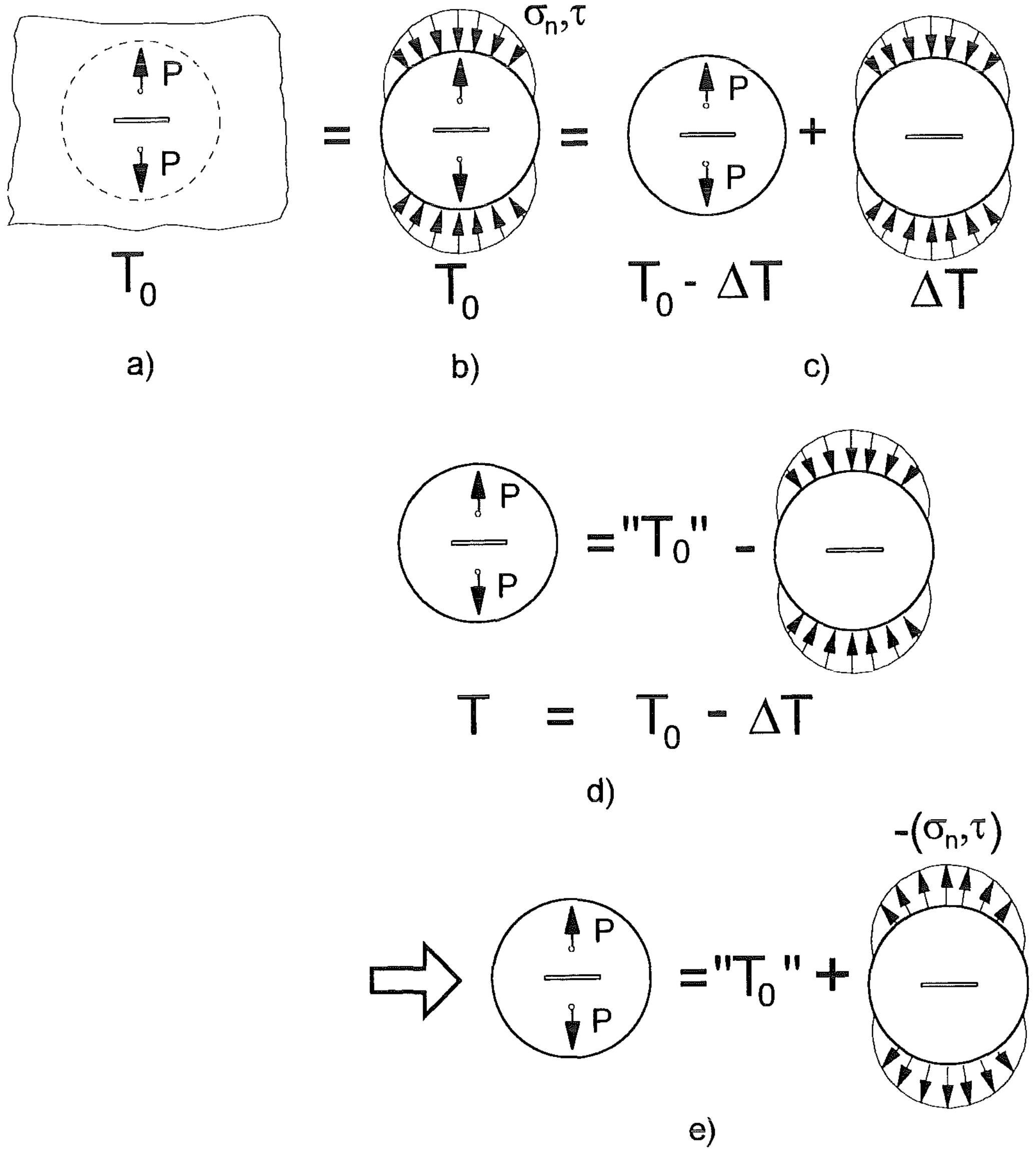

Fig. 5.1 Illustration of the principle of superposition for the computation of T-stresses for single forces.

The disk loaded by the combination of single forces and boundary tractions exhibit the same T-term T_0. Next, we consider the situation b) to be the superposition of the two loading cases shown in part c), namely, the cracked disk loaded by the couple of forces (with T-stress $T-\Delta T$) and a cracked disk loaded by the boundary tractions, having the T-term ΔT. As represented by part d), the T-term of the cracked disk is the difference $T=T_0-\Delta T$. If the sign of the boundary tractions is changed, the equivalent relation is given by part e).

II RESULTS FOR STRESS BOUNDARY CONDITIONS

The following sections contain numerical solutions for the T-stress term and the Green's function under stress boundary conditions. The problems are subdivided in:

- Internally cracked components,
  - cracks in infinite bodies,
  - circular disk with internal crack,
  - rectangular plate with internal crack.
- Edge-cracked components,
  - rectangular plate with edge crack
  - edge-cracked circular disk,
  - cracks ahead of notches.
- Components with multiple edge cracks
  - double-edge-cracked rectangular plate,
  - double-edge-cracked circular disk.

6 Crack in an infinite body

6.1 Couples of forces

The T-stress term resulting from a couple of symmetric point forces (see Fig. 6.1.1) can be derived from the Westergaard stress function [17] which for this special case reads

$$Z = \frac{2P}{\pi} \frac{\sqrt{a^2 - x^2}}{(z^2 - x^2)\sqrt{1-(a/z)^2}} \tag{6.1.1}$$

(note that eq.(3.2.2) is the limit of this relation for $x \to a$). The real part of (6.1.1) gives the x-stress component for $y = 0$

$$\sigma_x \big|_{y=0} = \mathrm{Re}\{Z\} = \frac{2P}{\pi} \frac{\sqrt{a^2 - x^2}\, x'}{(x'^2 - x^2)\sqrt{x'^2 - a^2}} \tag{6.1.2}$$

Its singular part

$$\sigma_{x,\mathrm{sing}} \big|_{y=0} = \frac{2P}{\pi} \frac{\sqrt{a/2}}{\sqrt{a^2 - x^2}\,\sqrt{x'-a}} \tag{6.1.3}$$

provides the well-known stress intensity factor solution

$$K = \lim_{x' \to a} \sqrt{2\pi(x'-a)}\,\sigma_x = \sqrt{\frac{a}{\pi}} \frac{2P}{\sqrt{a^2 - x^2}} \tag{6.1.4}$$

Then, the regular stress term reads

$$\sigma_{x,reg} \big|_{y=0} = \frac{2P}{\pi} \frac{(a^2 - x^2)x' - \sqrt{a/2}\,(x'^2 - x^2)\sqrt{x'+a}}{(x'^2 - x^2)\sqrt{x'^2 - a^2}\,\sqrt{a^2 - x^2}} \tag{6.1.5}$$

and for the T-stress term it results

$$T = \lim_{x' \to a} \sigma_{x,reg} = \begin{cases} 0 & \text{for} \quad x < a \\ \infty & \text{for} \quad x = a \end{cases} \tag{6.1.6}$$

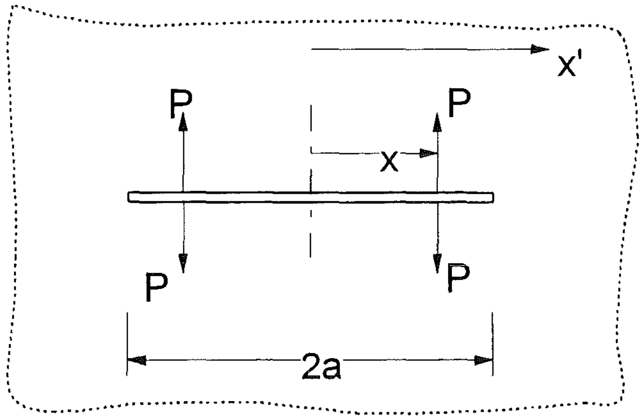

Fig. 6.1.1 Crack in an infinite body loaded by symmetric couples of forces.

6.2 Constant crack-face loading

In the case of a constant crack-face pressure p = const. (Fig. 6.2.1), the stress function reads

$$Z = p\left[\frac{z}{\sqrt{z^2 - a^2}} - 1\right] \tag{6.2.1}$$

resulting in the x-stress of

$$\sigma_x\big|_{y=0} = p\left[\frac{x'}{\sqrt{x'^2 - a^2}} - 1\right] \tag{6.2.2}$$

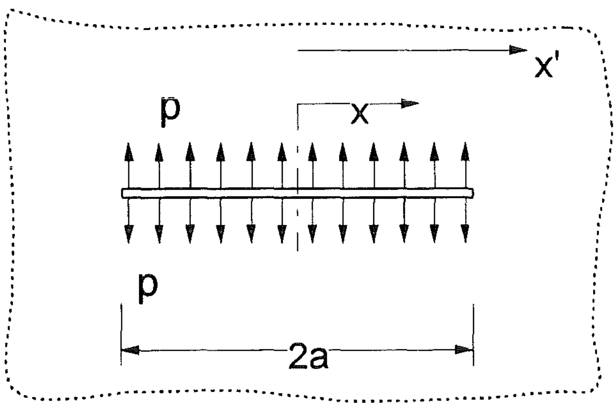

Fig. 6.2.1 Crack in an infinite body under constant crack-face pressure.

The T-stress term results as

$$T = -p \quad . \tag{6.2.3}$$

as found for the small-scale solution (3.2.15).

7 Circular disk with internal crack

7.1 Constant internal pressure

The crack under constant internal pressure (Fig. 7.1.1) has been analyzed with the Boundary Collocation method. T-stress data are shown in Fig. 7.1.2 and Table 7.1.1.

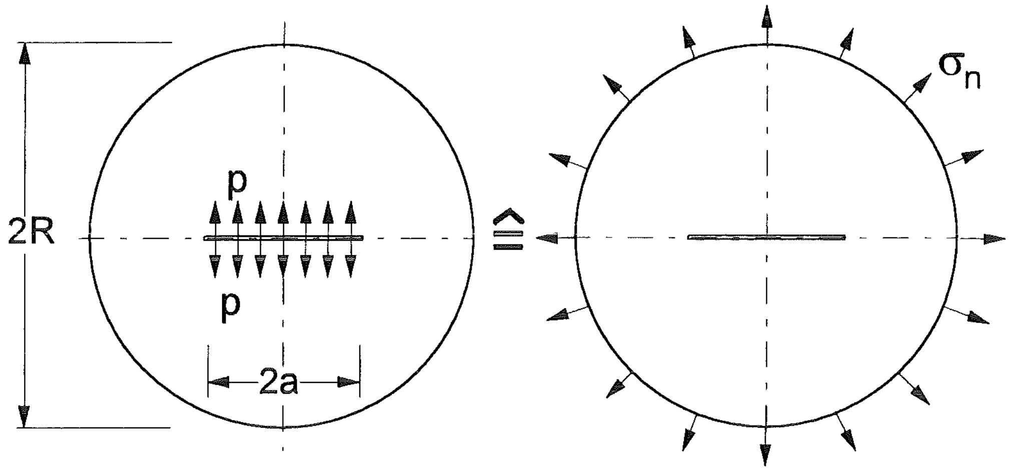

Fig. 7.1.1 Circular disk with internal crack under constant pressure p and equivalent problem of disk loading by normal tractions at the circumference.

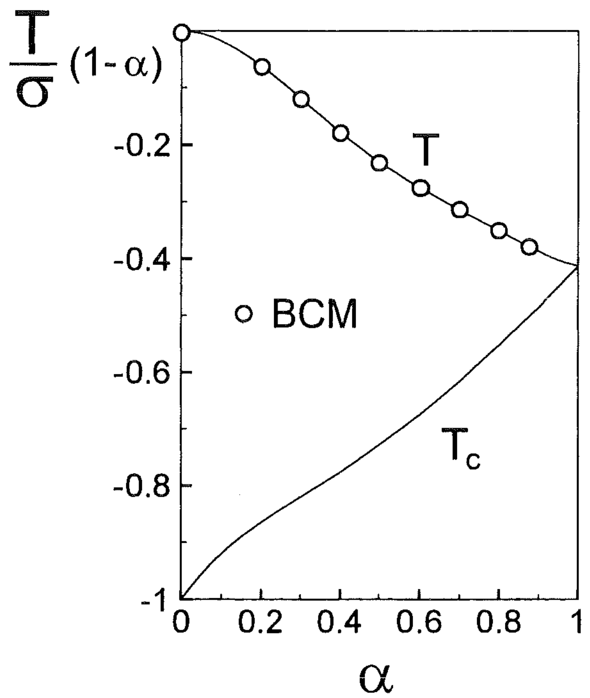

Fig. 7.1.2 T-stress for an internal crack in a circular disk.

$\alpha=a/R$	$T_c/\sigma\cdot(1-\alpha)$	$T/\sigma\cdot(1-\alpha)$	$F\cdot(1-\alpha)^{1/2}$	$\beta\cdot(1-\alpha)^{1/2}$
0	-1.00	0.000	1.000	0.00
0.1	-0.919	-0.019	0.965	-0.020
0.2	-0.864	-0.064	0.951	-0.067
0.3	-0.820	-0.120	0.951	-0.126
0.4	-0.776	-0.176	0.962	-0.183
0.5	-0.728	-0.228	0.979	-0.233
0.6	-0.675	-0.275	0.998	-0.275
0.7	-0.615	-0.315	1.011	-0.311
0.8	-0.552	-0.352	1.004	-0.351
0.9	-0.485	-0.385	0.953	-0.404
1.0	-0.413	-0.413	0.8255	-0.50

Table 7.1.1 T-stress, stress intensity factor and biaxiality ratio for an internally cracked circular disk with constant crack-face pressure (value T for $\alpha=1$ extrapolated); for T and T_c see eqs.(2.9) and (2.11).

The T-values in Table 7.1.1 were extrapolated to $\alpha = 1$. Within the numerical accuracy of the extrapolation, the limit values are

$$\lim_{\alpha\to 1} T/\sigma*(1-\alpha) = \lim_{\alpha\to 1} T_c/\sigma*(1-\alpha) \cong -0.413 = -\frac{1}{\sqrt{\pi^2-4}} \tag{7.1.1}$$

and for the biaxiality ratio

$$\lim_{\alpha\to 1} \beta\sqrt{1-\alpha} \cong \frac{1}{2} \tag{7.1.2}$$

The T-stress terms can be approximated by

$$T_c/\sigma = \frac{-1+\alpha-2.34\alpha^2+4.27\alpha^3-3.326\alpha^4+0.9824\alpha^5}{1-\alpha} \tag{7.1.3}$$

$$T/\sigma = \frac{-2.34\alpha^2+4.27\alpha^3-3.326\alpha^4+0.9824\alpha^5}{1-\alpha} \tag{7.1.4}$$

The stress intensity factor solution (found in the BCM-computations) is in good agreement with the geometric function [10]

$$F = \frac{K}{\sigma_n\sqrt{\pi a}} = \frac{1-0.5\alpha+1.6873\alpha^2-2.671\alpha^3+3.2027\alpha^4-1.8935\alpha^5}{\sqrt{1-\alpha}}. \tag{7.1.5}$$

7.2 Disk partially loaded by normal tractions

A partially loaded disk is shown in Fig.7.2.1a. Constant normal tractions σ_n are applied at the circumference within an angle of 2γ.

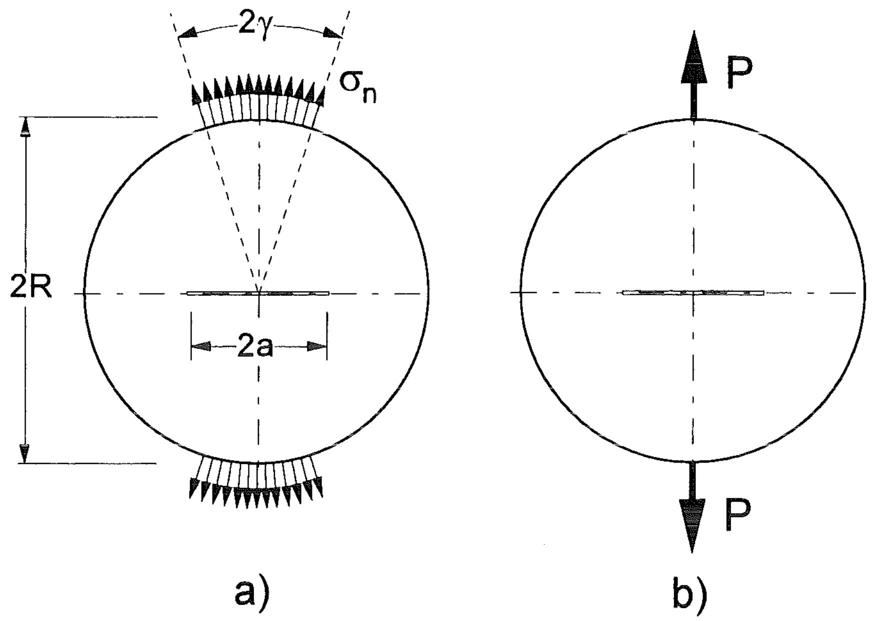

Fig. 7.2.1 a) partially loaded disk, b) diametral loading by a couple of forces (disk thickness: *t*).

The total force in y-direction results from

$$P_y = 2t\sigma_n \int_0^{\gamma} R\cos\gamma' d\gamma' = 2t\sigma_n R\sin\gamma \tag{7.2.1}$$

The x-stress term T, normalised to σ^*, is shown in Fig. 7.2.2. From the limit case $\gamma \to 0$, the solutions for concentrated forces (see Fig. 7.2.1b) are obtained as represented in Fig. 7.2.3.

The T-stress can be fitted by

$$\frac{T}{\sigma^*} = \frac{-4(1-\alpha) + 7.6777\alpha^2 - 16.0169\alpha^3 + 8.7994\alpha^4 - 1.10849\alpha^5}{1-\alpha} \tag{7.2.2}$$

with σ^* defined as

$$\sigma^* = \frac{P_y}{\pi R t}\ , \tag{7.2.3}$$

T_c can be computed from T

$$\frac{T_c}{\sigma^*} = \frac{-3(1-\alpha) + 7.6777\alpha^2 - 16.0169\alpha^3 + 8.7994\alpha^4 - 1.10849\alpha^5}{1-\alpha} - \frac{4\alpha^2}{(1+\alpha^2)^2} \tag{7.2.4}$$

or expressed by a fit relation

$$\frac{T_c}{\sigma^*} \cong \frac{-3(1-\alpha)+2.8996\alpha^2-6.1759\alpha^3+2.5438\alpha^4+0.0841\alpha^5}{1-\alpha} \tag{7.2.5}$$

In this case, the limit values are (at least in very good approximation)

$$\lim_{\alpha\to 1} T/\sigma^*(1-\alpha) = \lim_{\alpha\to 1} T_c/\sigma^*(1-\alpha) \cong -0.648 \cong -\frac{\pi}{2\sqrt{\pi^2-4}} \tag{7.2.6}$$

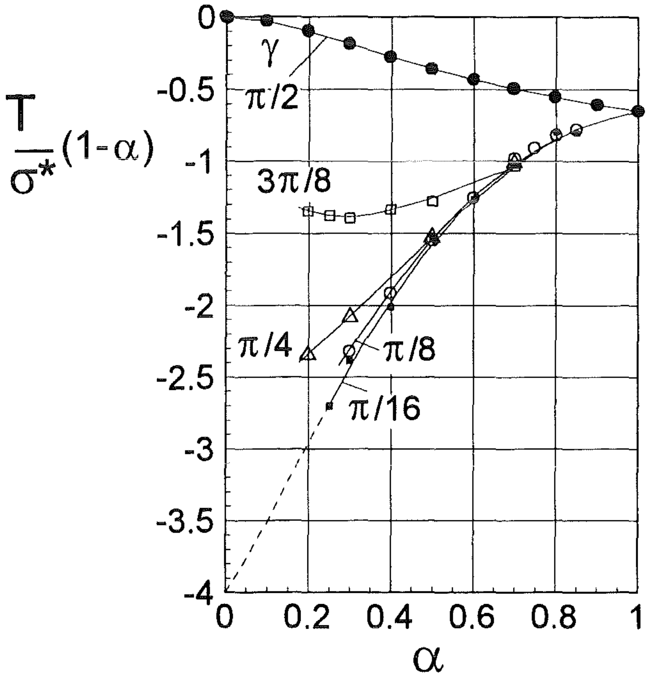

Fig. 7.2.2 T-stress for a circular disk, partially loaded over an angle of 2γ (see Fig. 7.2.1a).

The geometric function F, defined by

$$K_I = \sigma^* \sqrt{\pi a}\, F(a/R) \tag{7.2.7}$$

is plotted in Fig. 7.2.3.

From the limit case $\gamma \to 0$, the solutions for concentrated forces (see Fig. 7.2.1b) are obtained as represented in Fig. 7.2.5. A comparison with the results from literature [22-24] gives good agreement in stress intensity factors. The solution given by Tada et al. [25] (dashed curve in Fig. 7.2.5) deviates by about 20% near a/R=0.8. The results obtained here can be expressed by

$$K_I = \sigma^* \sqrt{\pi a} F_P \ , \quad F_P = \frac{3-1.254\alpha-1.7013\alpha^2+4.0597\alpha^3-2.8059\alpha^4}{\sqrt{1-\alpha}} \tag{7.2.8}$$

with σ* given in (7.2.3).

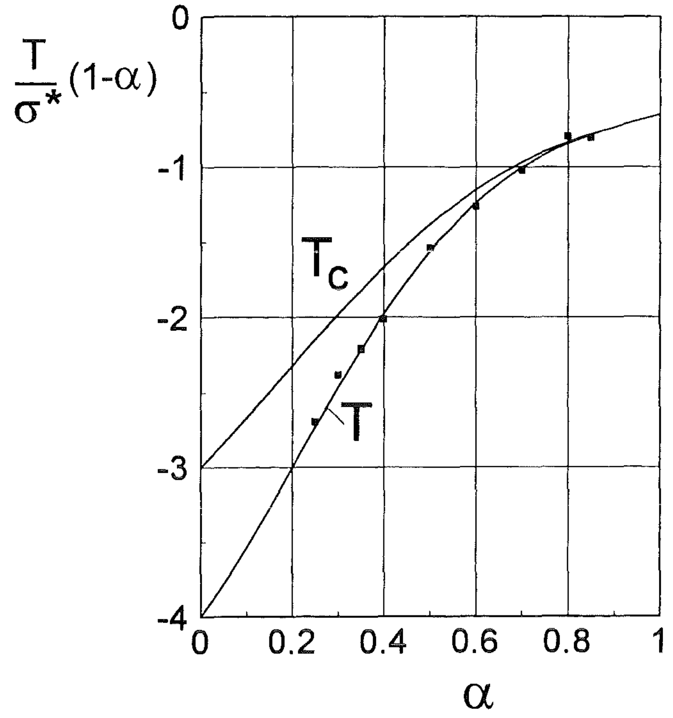

Fig. 7.2.3 T-stress for a circular disk loaded diametrically by concentrated forces (Fig. 7.2.1b). T-stress results including partially distributed stresses with an angle of $\gamma=\pi/16$ (squares) and exact limit cases for $\alpha=0$.

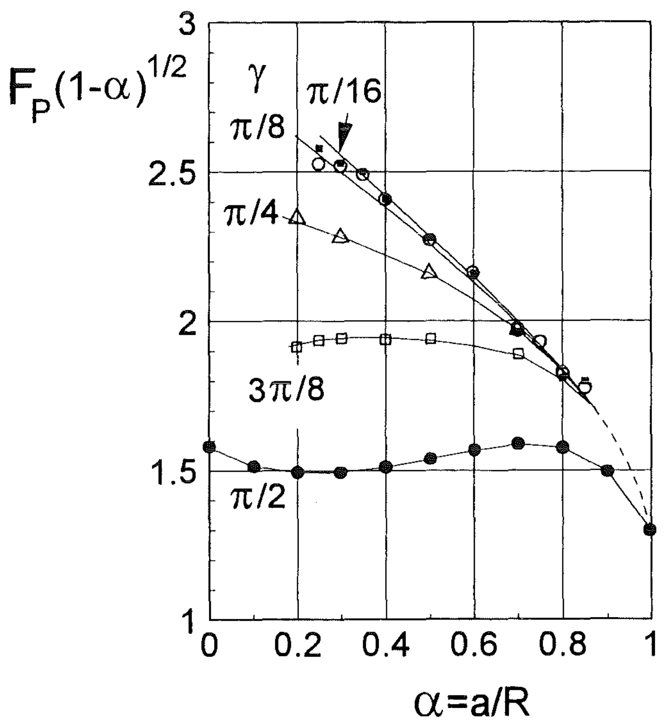

Fig. 7.2.4 Stress intensity factors for a circular disc, partially loaded over an angle of 2γ (see Fig. 7.2.1a).

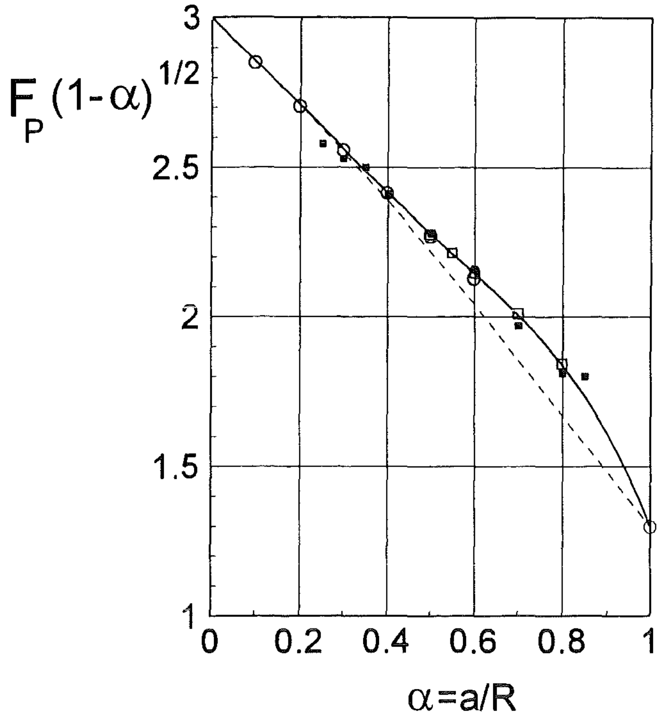

Fig. 7.25 Stress intensity factor and T-stress for a circular disc loaded diametrically by concentrated forces (Fig. 7.2.1b). Comparison of stress intensity factors; solid squares: partially distributed stresses with an angle of $\gamma=\pi/16$, circles: results by Atkinson et al. [22] and Awaji and Sato [23], open squares: results obtained with the weight function technique [24], dashed line: solution proposed by Tada et al.[25].

7.3 Central point force on the crack face

A centrally cracked circular disk, loaded by a couple of forces at the crack center, is shown in Fig.7.3.1. For it, the T-stress was calculated by Boundary Collocation computations.

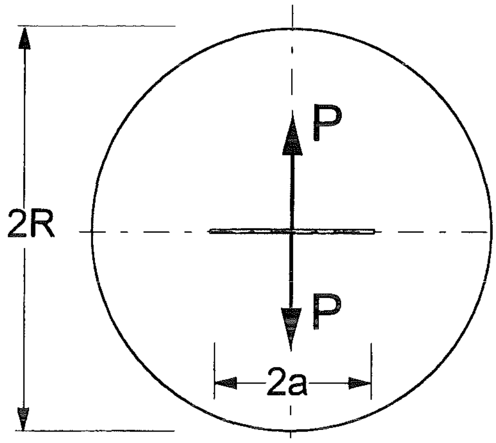

Fig. 7.3.1 Circular disk with a couple of forces acting on the crack faces.

The T-stress data obtained with the BCM-method according to Section 4.2 are plotted in Fig. 7.3.2 as squares. Together with the limit value (7.2.6) the numerically found T-values were fitted by the polynomial

$$\frac{T}{\sigma *} = \frac{-4.19971\alpha + 5.4661\alpha^2 - 1.1497\alpha^3 - 0.7677\alpha^4}{1-\alpha} \tag{7.3.1}$$

This relation is introduced into Fig. 7.3.2 as the solid line.

The stress intensity factor for central point forces is

$$K_I = \frac{P}{\sqrt{\pi a}} F_P \tag{7.3.2}$$

$$F_P = \frac{1 - 1.07884\alpha + 8.24956\alpha^2 - 17.9026\alpha^3 + 20.3339\alpha^4 - 9.305\alpha^5}{\sqrt{1-\alpha}} \tag{7.3.3}$$

Figure 7.3.3 gives a comparison of the BCM-results with results obtained by Tada et al. [25] with an asymptotic extrapolation technique. Maximum differences are in the order of about 10%.

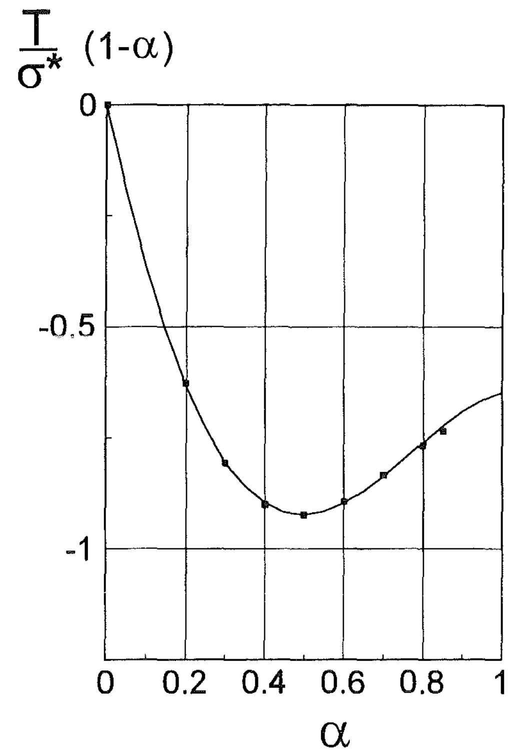

Fig. 7.3.2 T-stress for an internally cracked circular disk with a couple of forces acting in the crack center on the crack faces. Symbols: Numerical results, solid line: fitting curve.

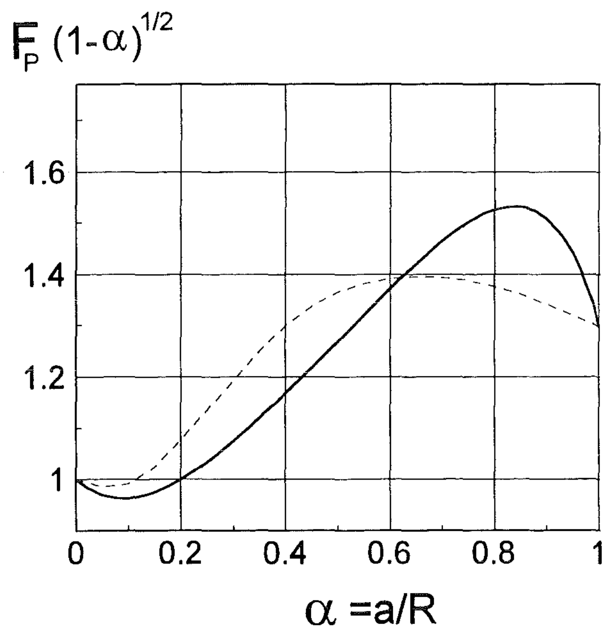

Fig. 7.3.3 Stress intensity factor for a couple of forces P at the crack center, represented by the geometric function F_P. Solid curve: eq.(7.3.3), dashed curve: Tada et al. [25].

8 Estimation of T-terms with a Green's function

8.1 Green's function with one regular term

In order to estimate T-stresses, an approximate Green's function according to eqs.(3.2.22) and (3.2.23) may be applied. A Green's function with only one term was derived according to Section 3.2.2 using the case of constant crack-face pressure σ_0 as the reference loading case which may produce the crack contribution $T_c = T_0$. In this rough approximation the T-term T_c results as

$$T_c = C\int_0^a (1-x^2/a^2)\sigma_y(x)dx - \sigma_y\big|_{x=a} \quad , \quad C = \frac{3}{2a}\left(1+\frac{T_0}{\sigma_0}\right) \tag{8.1.1}$$

This section now deals with a check of the accuracy of the approximate Green's function by comparing the results of the set-up (3.2.22) with T-stress solutions found by application of the Boundary Collocation procedure.

First, the case of concentrated forces at $x = 0$ (see Fig. 7.3.1) is considered. The couple of central forces reads in terms of the Dirac δ-function ($B = 1$)

$$\sigma_y(x) = \frac{P}{2}\delta(x) \tag{8.1.2}$$

Introducing this and (7.1.3) into (8.1.1) leads to

$$T \approx \frac{3P}{4a}\left(1+\frac{T_0}{\sigma_0}\right) \tag{8.1.3}$$

$$\frac{T}{\sigma^*} \approx \frac{3\pi}{4}\,\frac{-2.34\alpha + 4.27\alpha^2 - 3.326\alpha^3 + 0.9824\alpha^4}{1-\alpha} \quad , \quad \sigma^* = \frac{P}{Rt\pi} \tag{8.1.4}$$

The result is plotted in Fig. 8.1.1.

As a second example, the diametral tension test is considered (see Fig. 7.2.1b). Introducing the stress distribution for a diametral tension test,

$$\frac{\sigma_y}{\sigma^*} = \frac{4}{(1+\xi^2)^2} - 1 \quad , \quad \xi = x/R \tag{8.1.5}$$

$$\frac{\sigma_x}{\sigma^*} = -1 + \frac{4\xi^2}{(1+\xi^2)^2} \tag{8.1.6}$$

into (8.1.1) yields, after numerical integration, the T-stress shown in Fig. 8.1.2.

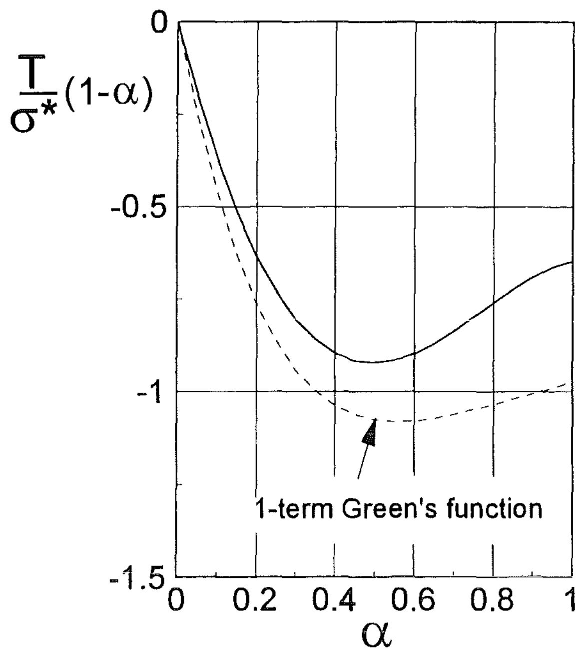

Fig. 8.1.1 T-stresses for an internally cracked circular disk, loaded by a couple of forces at the crack faces (see Fig. 7.3.1) estimated with a 1-term Green's function (dashed curve) compared with results from BCM-computations (solid curve).

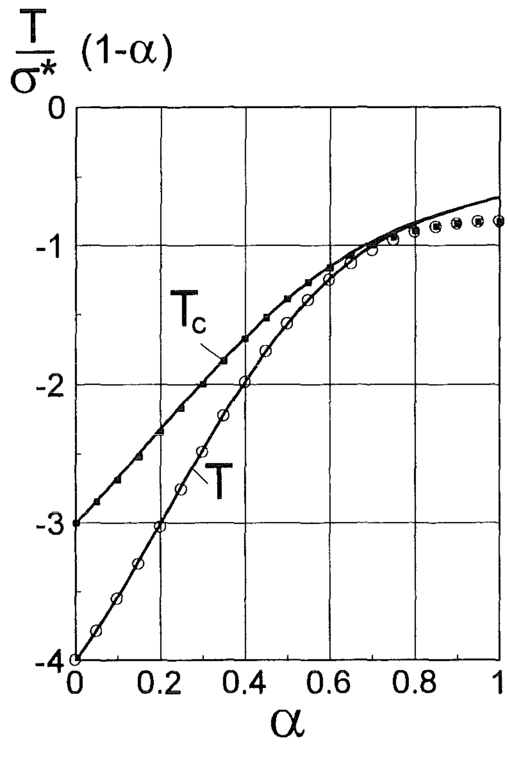

Fig. 8.1.2 T-stresses for an internally cracked circular disk, loaded by a couple of diametral forces at the free boundary (see Fig. 7.2.1b) estimated with a 1-term Green's function (symbols) compared with results from BCM-computations (curves).

From these two examples we can conclude for this first degree of approximation that the application to continuously distributed stresses gives significantly better results than the application to strongly non-homogeneous stresses as in the case of single forces at the crack faces. The reason for this behaviour is the fact that in the reference loading case (constant crack-face pressure) the load was also distributed homogeneously. In both cases the deviations increase with increasing relative crack size α. This makes evident that the Green's function needs higher order terms for larger α.

8.2 Green's function with two regular terms

In order to improve the Green's function, the next regular term is added. Consequently, the Green's function expansion reads

$$t = t_0 + C_1(1 - x^2 / a^2) + C_2(1 - x^2 / a^2)^2 \tag{8.2.1}$$

As a second reference loading case we now use the solution T_P for the internally cracked disk with a pair of single forces P at the crack center (see Fig. 7.3.1).

Introducing the two reference stresses

$$\sigma_1 = const. \quad \sigma_2 = \frac{P}{2}\delta(x) \tag{8.2.2}$$

into eq.(3.1.1) and carrying out the integration provides a system of two equations

$$T_1 / \sigma_1 = -1 + \frac{2a}{3} C_1 + \frac{8a}{15} C_2 \tag{8.2.3}$$

$$T_2 / \sigma^* = \frac{\pi R}{2} C_1 + \frac{\pi R}{2} C_2 \tag{8.2.4}$$

($\sigma^* = P/(Rt\pi)$) from which the coefficients result as

$$C_1 = \frac{15}{2a}\left(1 + \frac{T_1}{\sigma_1}\right) - 8\frac{T_2}{Rt\pi\sigma^*} \tag{8.2.5}$$

$$C_2 = -\frac{15}{2a}\left(1 + \frac{T_1}{\sigma_1}\right) + 10\frac{T_2}{Rt\pi\sigma^*} \tag{8.2.6}$$

or by

$$C_1 = \frac{1}{R}\frac{-6.8622\alpha + 18.1057\alpha^2 - 22.0173\alpha^3 + 9.3229\alpha^4}{1 - \alpha} \tag{8.2.7}$$

$$C_2 = \frac{1}{R}\frac{4.1902\alpha - 14.626\alpha^2 + 21.2854\alpha^3 - 9.8117\alpha^4}{1-\alpha} \tag{8.2.8}$$

With the improved Green's function the diametral tension specimen was computed again using eqs.(8.1.5) and (8.1.6). The result is plotted in Fig. 8.2.1. It becomes obvious that in this approximation the agreement is significantly better for large α.

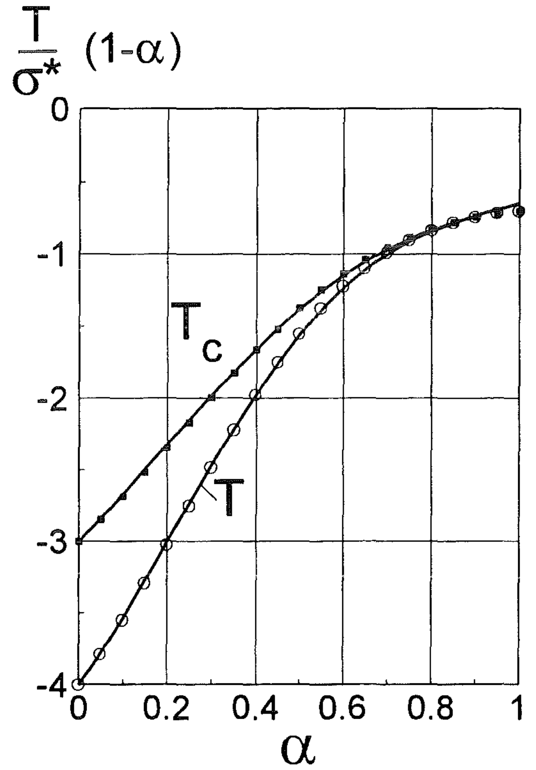

Fig. 8.2.1 T-stresses for an internally cracked circular disk, loaded by a couple of diametral forces at the free boundary (see Fig. 7.2.1b) estimated with a 2-terms Green's function (symbols) compared with results from BCM-computations (curves).

8.3 Brazilian Disk

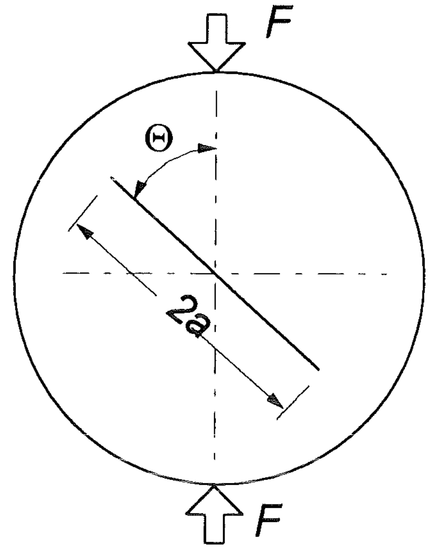

Fig. 8.3.1 Diametral compression test with internal crack (disk thickness: t).

Stress intensity factors K_{I}, K_{II} and related geometric functions F_{I}, F_{II}

$$K_I = \sigma_0 F_I \sqrt{\pi a} = \int_0^a \sigma(x) h_I(x,a)\,dx \tag{8.3.1}$$

$$K_{II} = \sigma_0 F_{II} \sqrt{\pi a} = \int_0^a \tau(x) h_{II}(x,a)\,dx \tag{8.3.2}$$

Characteristic stress:

$$\sigma_0 = \frac{F}{\pi a t}\ , \tag{8.3.3}$$

(identical with the maximum tensile stress in the center of the disk).

The circumferential stress component in an uncracked Brazilian disk has been given by Erdlac (quoted in [22]) as

$$\sigma_\varphi = \sigma_n = \frac{2P}{\pi t R}\left[\frac{1}{2} - \frac{(1-\rho\cos\Theta)\sin^2\Theta}{(1+\rho^2-2\rho\cos\Theta)^2} - \frac{(1+\rho\cos\Theta)\sin^2\Theta}{(1+\rho^2+2\rho\cos\Theta)^2}\right],\quad \rho = r/R \tag{8.3.4}$$

$$\sigma_r = \frac{2P}{\pi t R}\left[\frac{1}{2} - \frac{(1-\rho\cos\Theta)(\cos\Theta-\rho)^2}{(1+\rho^2-2\rho\cos\Theta)^2} - \frac{(1+\rho\cos\Theta)(\cos\Theta+\rho)^2}{(1+\rho^2+2\rho\cos\Theta)^2}\right] \tag{8.3.5}$$

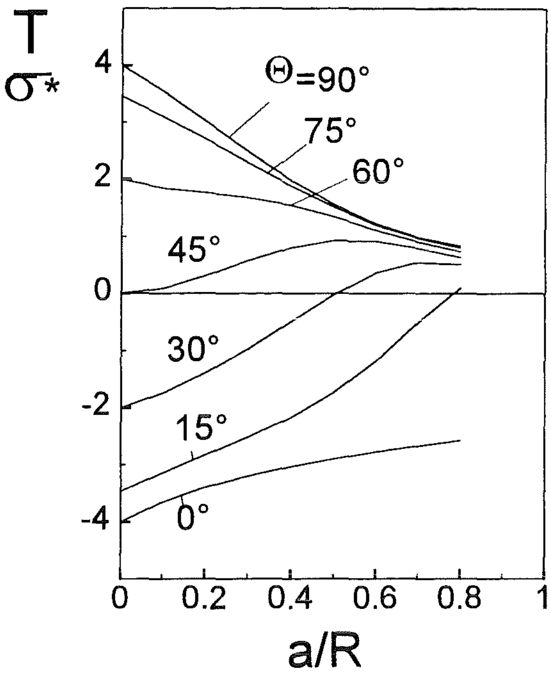

Fig. 8.3.2 T-stress for the Brazilian disk as a function of the angle Θ.

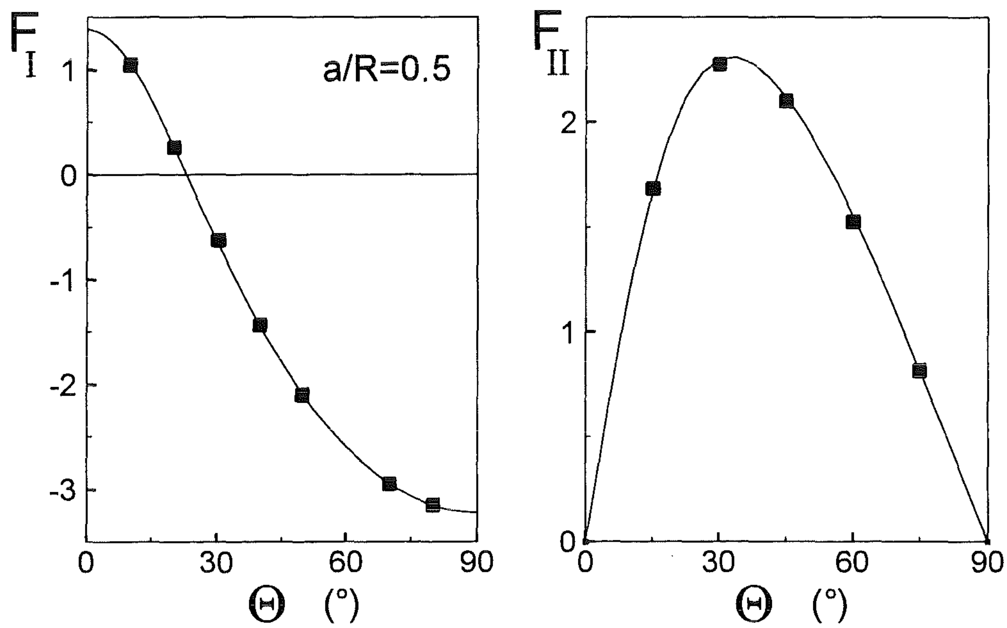

Fig. 8.3.3 Geometric functions for a/R=0.5 as a function of the angle Θ. Curves: obtained with the weight function procedure; squares: Results from Atkinson et al. [22] and Awaji and Sato [23].

a/R	$\Theta=0°$	15°	30°	45°	60°	75°	90°
0	-4.000	-3.464	-2.000	0.000	2.000	3.464	4.000
0.1	-3.656	-3.136	-1.745	0.091	1.855	3.104	3.552
0.2	-3.398	-2.829	-1.396	0.312	1.773	2.711	3.029
0.3	-3.197	-2.515	-0.969	0.581	1.684	2.294	2.485
0.4	-3.033	-2.163	-0.492	0.812	1.543	1.883	1.980
0.5	-2.895	-1.733	-0.015	0.935	1.344	1.509	1.555
0.6	-2.775	-1.183	0.369	0.919	1.116	1.201	1.227
0.7	-2.668	-0.510	0.553	0.795	0.906	0.971	0.993
0.8	-2.574	0.106	0.513	0.643	0.746	0.815	0.839

Table 8.3.1 T-stress $T(1\text{-}a/R)$ for the Brazilian disk test.

a/R	$\Theta=0°$	15°	30°	45°	60°	75°	90°
0	0.	1.000	1.732	2.000	1.732	1.000	0.
0.1	0.	1.023	1.758	2.010	1.724	0.988	0.
0.2	0.	1.092	1.835	2.036	1.698	0.955	0.
0.3	0.	1.214	1.957	2.069	1.656	0.907	0.
0.4	0.	1.400	2.116	2.097	1.603	0.856	0.
0.5	0.	1.670	2.299	2.119	1.554	0.813	0.
0.6	0.	2.053	2.491	2.146	1.530	0.792	0.
0.7	0.	2.578	2.697	2.220	1.564	0.808	0.
0.8	0.	3.260	3.009	2.441	1.720	0.889	0.

Table 8.3.2 Geometric function F_{II} for the Brazilian disk tests.

a/R	$\Theta=0°$	15°	30°	45°	60°	75°	90°
0	1.000	0.732	0	-1.000	-2.000	-2.732	-3.000
0.1	1.017	0.737	-0.020	-1.037	-2.033	-2.750	-3.016
0.2	1.063	0.746	-0.084	-1.141	-2.120	-2.793	-3.031
0.3	1.137	0.752	-0.200	-1.308	-2.248	-2.854	-3.062
0.4	1.241	0.742	-0.379	-1.527	-2.406	-2.940	-3.118
0.5	1.384	0.693	-0.635	-1.789	-2.594	-3.065	-3.220
0.6	1.578	0.562	-0.973	-2.083	-2.819	-3.250	-3.393
0.7	1.846	0.263	-1.381	-2.413	-3.108	-3.525	-3.665
0.8	2.244	-0.302	-1.843	-2.824	-3.530	-3.965	-4.112

Table 8.3.2 Geometric function F_{I} for the Brazilian disk tests.

9 Rectangular plate with internal crack

The geometric data of the rectangular plate with an internal crack are illustrated in Fig.9.1.1.

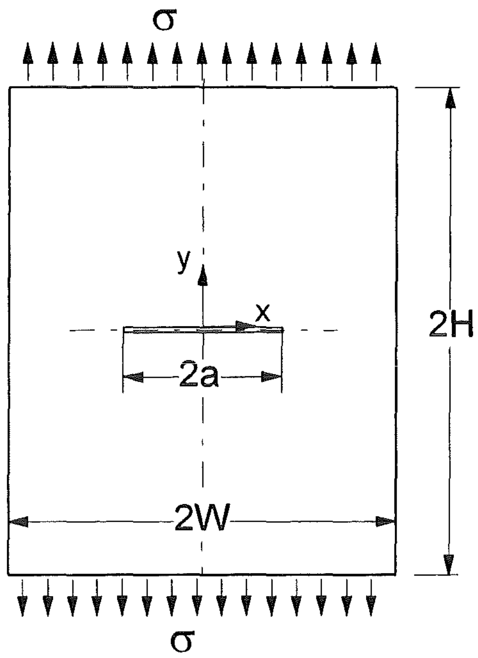

Fig. 9.1 Rectangular plate with a central internal crack (geometric data).

The plate under uniaxial load (tensile stresses at the ends $y=\pm H$) shows no σ_x-component in the uncracked structure. Consequently, the quantities T and T_c are identical. T-stress results obtained by BCM-computations are shown in Fig. 9.2a and entered into Table 9.1.

$\alpha=a/W$	H/W=0.35	0.50	0.75	1.00	1.25
0	-1.0	-1.0	-1.0	-1.0	-1.0
0.1	-0.97	-0.96	-0.92	-0.91	-0.9
0.2	-0.95	-0.92	-0.88	-0.85	-0.83
0.3	-0.766	-0.855	-0.85	-0.809	-0.777
0.4	-0.455	-0.745	-0.805	-0.756	-0.716
0.5	-0.110	-0.616	-0.738	-0.692	-0.656
0.6	0.145	-0.502	-0.647	-0.620	-0.596
0.7	0.215	-0.400	-0.543	-0.55	-0.53
0.8	0.13	-0.291	-0.45	-0.46	-0.47
0.9	-0.10	-0.25	-0.38	-0.41-	-0.43
1.0	-0.413	-0.413	-0.413	-0.413	-0.413

Table 9.1 T-stress term, normalized as $T/\sigma(1-\alpha)$, for different crack and plate geometries.

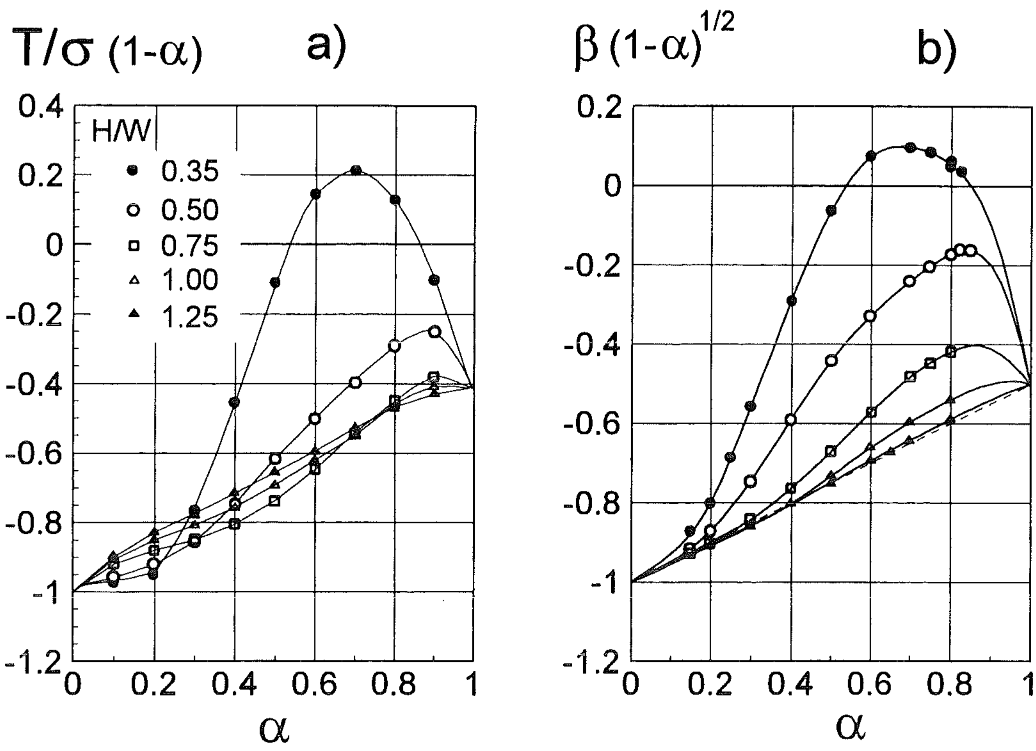

Fig.9.2 Internal crack in rectangular plate, a) T-stress, b) biaxiality ratio.

	H/W=1.5	1.25	1.00	0.75	0.5	0.35
α=0	1.00	1.00	1.00	1.00	1.00	1.00
0.2	0.916	0.924	0.940	0.977	1.051	1.182
0.3	0.888	0.905	0.940	1.008	1.147	1.373
0.4	0.869	0.890	0.942	1.053	1.262	1.562
0.5	0.851	0.877	0.943	1.099	1.391	1.742
0.6	0.827	0.856	0.937	1.130	1.533	1.938
0.7	0.816	0.826	0.914	1.125	1.668	2.197
0.8	0.814	0.818	0.840	1.088	1.689	2.41
1.0	0.826	0.826	0.826	0.826	0.826	0.826

Table 9.2 Geometric function for tension $F{\cdot}(1-a/W)^{1/2}$.

The biaxiality ratio, defined by eq.(2.9), is plotted in Fig. 9.2b and additionally given in Table 9.3.

For a long plate (H/W> 1.5) the biaxiality ratio β can be expressed by

$$\beta \cong -\frac{1-0.5\alpha}{\sqrt{1-\alpha}} \qquad (9.1)$$

$\alpha = a/W$	H/W=0.35	0.50	0.75	1.00	1.25
0	-1.0	-1.0	-1.0	-1.0	-1.0
0.1	-0.93	-0.95	-0.955	-0.955	-0.95
0.2	-0.801	-0.872	-0.90	-0.91	-0.905
0.3	-0.558	-0.746	-0.843	-0.860	-0.858
0.4	-0.291	-0.591	-0.764	-0.803	-0.805
0.5	-0.063	-0.443	-0.672	-0.734	-0.749
0.6	0.075	-0.328	-0.573	-0.661	-0.693
0.7	0.098	-0.241	-0.483	-0.598	-0.645
0.8	0.055	-0.173	-0.418	-0.54	-0.59
0.9	-0.1	-0.2	-0.41	0.5	-0.54
1.0	-0.5	-0.5	-0.5	-0.5	-0.5

Table 9.3 Biaxiality ratio, normalized as $\beta\,(1-\alpha)^{1/2}$, for different crack and plate geometries.

Figure 9.3 shows results for the biaxiality ratio β. The open symbols are results reported in [10] and the solid ones represent data from Table 9.3. Very good agreement can be concluded from this illustration with maximum deviations of about 1%.

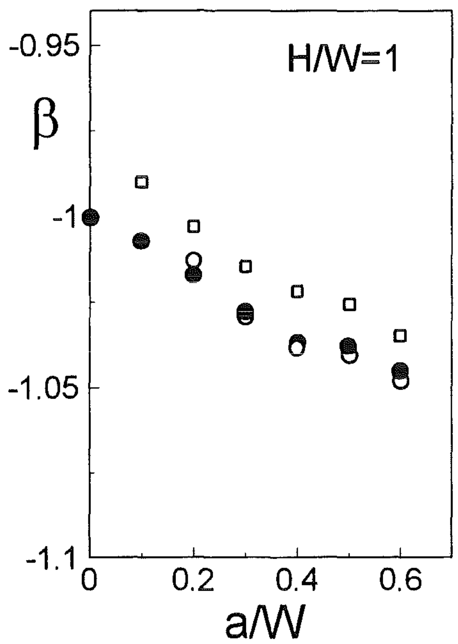

Fig. 9.3 Comparison of results compiled in Tables 1 and 2 with data reported in [12]. Open symbols: open circles Leevers and Radon [5], squares: Kfouri [6], solid circles: Table 9.3.

The Williams coefficients A_1, A_1*, A_2 and A^*_2, defined by eq.(2.2), are entered in Tables 9.4- and 9.7.

α=a/W	H/W=0.35	0.50	0.75	1.00	1.25
0.2	-0.0651	-0.0817	-0.0837	-0.0824	-0.0817
0.3	0.0117	-0.0508	-0.0674	-0.0685	-0.0686
0.4	0.1223	-0.0074	-0.0493	-0.0575	-0.0603
0.5	0.2665	0.0557	-0.022	-0.0452	-0.0549
0.6	0.4560	0.1584	0.0216	-0.0300	-0.0485
0.7	0.7797	0.3607	0.0893	-0.0133	-0.1178
0.8	0.7242	0.7987	0.1645	-0.3734	-0.2886

Table 9.4 Coefficient A_1 for different crack and plate geometries.

α=a/W	H/W=0.35	0.50	0.75	1.00	1.25
0.2	-0.2608	-0.0792	-0.0180	-0.0064	-0.0019
0.3	-0.5306	-0.1920	-0.0527	-0.0197	-0.0053
0.4	-0.7606	-0.3129	-0.1065	-0.0409	-0.0089
0.5	-0.9124	-0.4263	-0.1787	-0.0655	-0.0086
0.6	-0.9652	-0.5736	-0.2694	-0.0812	-0.0041
0.7	-1.096	-0.9091	-0.3629	-0.0555	0.333
0.8	-1.429	-1.709	-0.3075	1.154	0.8425

Table 9.5 Coefficient A^*_1 for different crack and plate geometries.

α=a/W	H/W=0.50	0.75	1.25
0.2	0.1977	0.136	0.113
0.3	0.2126	0.118	0.070
0.4	0.2372	0.139	0.057
0.5	0.2797	0.188	0.057
0.6	0.4367	0.278	0.079
0.65	0.6322	0.352	0.119
0.7	0.9848	0.462	-0.079
0.8	2.748	0.911	-0.463

Table 9.6 Coefficient A_2.

$\alpha=a/W$	H/W=0.50	0.75	1.25
0.2	-0.06174	-0.023	-0.003
0.3	0.0133	-0.032	-0.005
0.4	0.1697	-0.031	-0.003
0.5	0.3255	-0.032	0.000
0.6	0.3194	-0.063	-0.004
0.65	0.1475	-0.104	-0.022
0.7	-0.2523	-0.190	0.025
0.8	-2.747	-0.816	0.092

Table 9.7 Coefficient A^*_2.

For the evaluation of arbitrarily distributed stresses in the uncracked plate the application of the Green's function procedure is recommended. An approximative computation of T is possible by

$$T = \frac{3}{2a}(1+T_t/\sigma_0)\int_0^a (1-x^2/a^2)\sigma_y(x)\,dx - \sigma_y\Big|_{x=a} \tag{9.2}$$

with T_t given by the data in Table 9.1. The related stress intensity factor (necessary for the computation of the biaxiality ratio β) can be calculated with eq.(3.1.1a). Weight functions are given in handbooks (see e.g. [10]). A rough approximation reads

$$h \cong \sqrt{\frac{1+x/a}{\pi a}}\left[\frac{1}{\sqrt{1-x/a}} + 2(F-1)\sqrt{1-x/a}\right] \tag{9.3}$$

with the geometric function for constant stress as given in Table 9.2.

10 Edge-cracked rectangular plate

10.1 Rectangular plate under tension

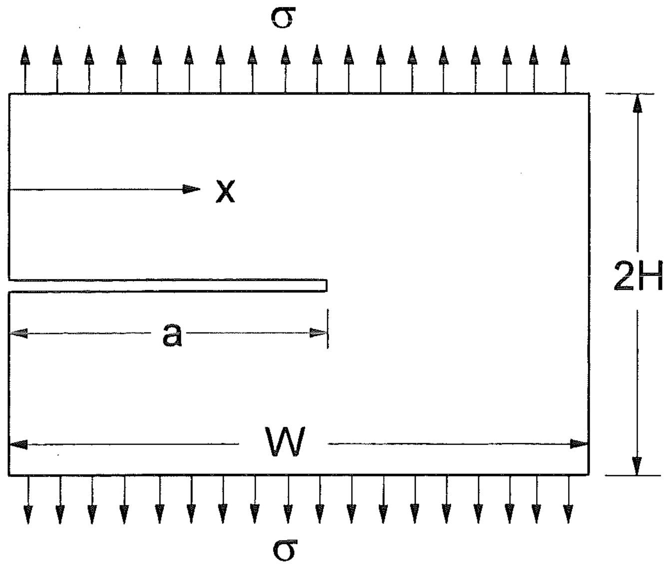

Fig. 10.1.1 Edge-cracked rectangular plate under tensile loading.

$\alpha = a/W$	H/W=1.5	1.00	0.75	0.50	0.40	0.30	0.25
0	-0.526	-0.526	-0.526	-0.526	-0.526	-0.526	-0.526
0.1	-0.452	-0.452	-0.452	-0.444	-0.432	-0.416	-0.400
0.2	-0.374	-0.376	-0.373	-0.334	-0.270	-0.084	0.143
0.3	-0.299	-0.298	-0.282	-0.148	0.030	0.449	0.890
0.4	-0.208	-0.205	-0.175	0.040	0.310	0.912	1.526
0.5	-0.106	-0.102	-0.070	0.167	0.473	1.165	1.858
0.6	0.006	0.008	0.032	0.220	0.490	1.142	1.812
0.7	0.122	0.123	0.134	0.234	0.404	0.869	1.387
0.8	0.232	0.234	0.240	0.268	0.324	0.524	0.760
0.9	0.352	0.353	0.356	0.364	0.372	0.376	0.380
1.0	0.474	0.474	0.474	0.474	0.474	0.474	0.474

Table 10.1.1 T-stress for a plate under tension $T/\sigma\cdot(1-a/W)^2$.

For a long plate (H/W= 1.5) the T-stress is

$$\frac{T}{\sigma} = \frac{-0.526 + 0.641\alpha + 0.2049\alpha^2 + 0.755\alpha^3 - 0.7974\alpha^4 + 0.1966\alpha^5}{(1-\alpha)^2} \qquad (10.1.1)$$

The biaxiality ratio reads in this case

$$\beta = \frac{-0.469 + 0.1456\alpha + 1.3394\alpha^2 + 0.4369\alpha^3 - 2.1025\alpha^4 + 1.0726\alpha^5}{\sqrt{1-\alpha}} \qquad (10.1.2)$$

The stress intensity factor is entered in Table 10.1.2 in form of the geometric function eq.(2.8).

	H/W=1.5	1.00	0.75	0.5	0.4	0.3	0.25
α=0	1.1215	1.1215	1.1215	1.1215	1.1215	1.1215	1.1215
0.1	1.0170	1.0174	1.0182	1.0352	1.0649	1.1455	1.2431
0.2	0.9800	0.9798	0.9877	1.0649	1.1625	1.3619	1.5358
0.3	0.9722	0.9729	0.9840	1.0821	1.2134	1.4892	1.7225
0.4	0.9813	0.9819	0.9915	1.0819	1.2106	1.5061	1.7819
0.5	0.9985	0.9989	1.0055	1.0649	1.1667	1.4298	1.7013
0.6	1.0203	1.0204	1.0221	1.0496	1.1073	1.2898	1.5061
0.7	1.0440	1.0441	1.0442	1.0522	1.0691	1.1498	1.2685
0.8	1.0683	1.0683	1.0690	1.0691	1.0734	1.0861	1.1201
1.0	1.1215	1.1215	1.1215	1.1215	1.1215	1.1215	1.1215

Table 10.1.2 Geometric function for tension $F\cdot(1-a/W)^{3/2}$.

$\alpha = a/W$	H/W=1.5	1.00	0.75	0.50	0.40	0.30	0.25
0	-0.469	-0.469	-0.469	-0.469	-0.469	-0.469	-0.469
0.1	-0.444	-0.444	-0.444	-0.429	-0.406	-0.363	-0.322
0.2	-0.382	-0.384	-0.377	-0.314	-0.232	-0.062	0.093
0.3	-0.308	-0.306	-0.287	-0.137	0.025	0.302	0.517
0.4	-0.212	-0.209	-0.176	0.037	0.256	0.606	0.856
0.5	-0.106	-0.102	-0.070	0.157	0.405	0.815	1.092
0.6	0.006	0.008	0.031	0.210	0.443	0.885	1.203
0.7	0.117	0.118	0.128	0.222	0.378	0.756	1.093
0.8	0.217	0.219	0.225	0.251	0.302	0.482	0.679
1.0	0.423	0.423	0.423	0.423	0.423	0.423	0.423

Table 10.1.3 Biaxiality ratio $\beta(1-a/W)^{1/2}$.

In Fig. 10.1.2 the biaxiality ratios for $H/W = 0.5$ and 1.0 are compared with a solution in tension [5] available for these geometries. The agreement is very good.

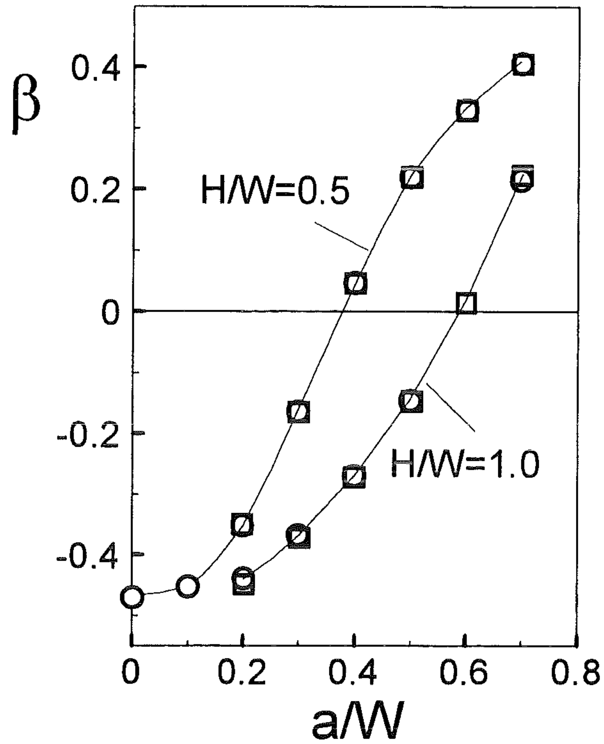

Fig. 10.1.2 Biaxiality ratios β (Table 10.1.3, circles) compared with data reported by Leevers and Radon [5] (squares).

Tables 10.1.4 and 10.1.5 represent some values for the coefficients A_1 and A^*_1 of the Williams series expansion

	H/W=1.00	0.75	0.5	0.4	0.3	0.25
α=0.2	-0.0459	-0.0440	-0.0251	0.0061	0.0907	
0.3	-0.0140	-0.0084	0.0436	0.1219	0.3205	0.5414
0.4	0.0438	0.0537	0.1431	0.2782	0.6248	1.011
0.5	0.1655	0.1770	0.2933	0.4836	1.0043	1.595
0.6	0.4513	0.4606	0.5774	0.8001	1.477	2.294
0.7	1.254	1.257	1.335	1.5314	2.240	3.195
0.8	3.768	4.284	4.346	4.440	4.81	

Table 10.1.4 Coefficients A_1 for tension.

	1.00	0.75	0.5	0.4	0.3	0.25
α=0.2	0.2473	0.2379	0.1574	0.0561	-0.1510	
0.3	0.1453	0.1223	-0.0188	-0.1640	-0.4022	-0.5714
0.4	0.0551	0.0328	-0.1050	-0.2557	-0.4886	-0.5957
0.5	-0.0807	-0.0815	-0.1247	-0.2257	-0.4073	-0.4062
0.6	-0.3932	-0.3563	-0.1838	-0.0893	-0.0277	0.1377
0.7	-1.383	-1.313	-0.821	-0.2534	0.7099	1.446
0.8	-5.22	-5.90	-5.26	-4.04	0.866	

Table 10.1.5 Coefficients A^*_1 for tension.

For long plates ($H/W \geq 1.5$) the coefficients A_1 and A^*_1 can be approximated by [9]

$$A_1 \cong \frac{-0.02279 + 0.04107\alpha + 0.03231\alpha^2 + 0.2470\alpha^3 - 0.3241\alpha^4 + 0.1358\alpha^5}{(1-\alpha)^{5/2}\sqrt{\alpha}} \tag{10.1.3}$$

$$A^*_1 \cong \frac{0.04813 - 0.1062\alpha - 0.08187\alpha^2 + 0.3276\alpha^3 - 0.4092\alpha^4 + 0.1511\alpha^5}{(1-\alpha)^3\alpha} \tag{10.1.4}$$

	1.00	0.5	0.25
α=0.3	0.0111	0.0328	-0.7476
0.4	0.0888	-0.0130	-1.8675
0.5	0.2546	-0.0451	-3.4075
0.6	0.7246	0.1850	-5.415
0.7	2.4535	1.7412	-7.471
0.8	10.61	11.55	

Table 10.1.6 Coefficients A_2 for tension.

	1.00	0.5	0.25
α=0.3	-0.2882	-0.0631	3.368
0.4	-0.2302	0.2938	5.898
0.5	-0.3278	0.5297	8.845
0.6	-0.8237	0.3264	12.513
0.7	-3.088	-1.981	16.688
0.8	-16.39	-18.47	

Table 10.1.7 Coefficients A^*_2 for tension.

10.2 Rectangular plate under bending load

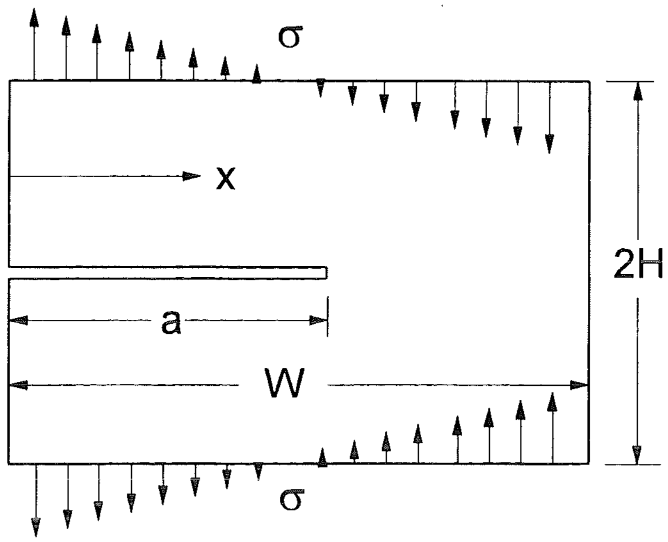

Fig. 10.2.1 Edge-cracked rectangular plate under bending loading.

α=a/W	H/W=1.5	0.75	0.50	0.40	0.30	0.25
0	-0.526	-0.526	-0.526	-0.526	-0.526	-0.526
0.2	-0.150	-0.148	-0.114	-0.061	0.099	0.292
0.3	-0.039	-0.024	0.080	0.222	0.559	0.920
0.4	0.044	0.067	0.224	0.424	0.873	1.333
0.5	0.099	0.124	0.283	0.493	0.964	1.439
0.6	0.133	0.150	0.269	0.438	0.840	1.251
0.7	0.151	0.158	0.217	0.314	0.574	0.857
0.8	0.158	0.158	0.174	0.204	0.302	0.426
0.9	0.140	0.142	0.150	0.162	0.169	0.186
1.0	0.113	0.113	0.113	0.113	0.113	0.113

Table 10.2.1 T-stress for a plate under bending $T/\sigma\cdot(1-a/W)^2$.

For a long plate ($H/W \geq 1.5$) the T-stress is

$$\frac{T}{\sigma_b} = \frac{-0.526 + 2.481\alpha - 3.553\alpha^2 + 2.6384\alpha^3 - 0.9276\alpha^4}{(1-\alpha)^2} \tag{10.2.1}$$

with the bending stress σ_b defined by

$$\sigma(x) = \sigma_b(1 - 2x/W) \tag{10.2.2}$$

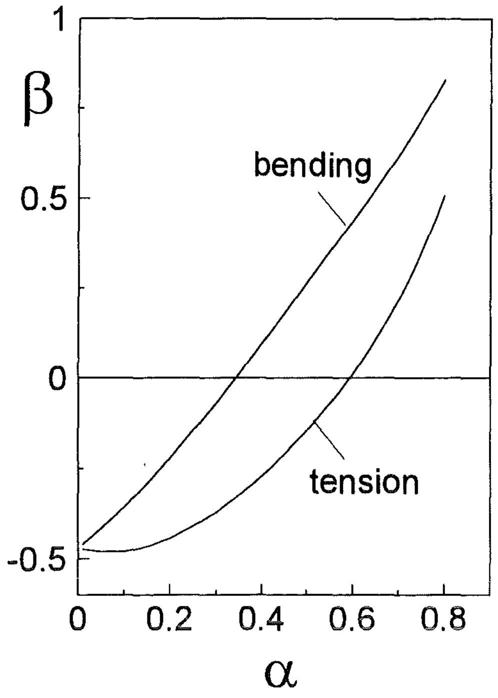

Fig. 10.2.2 Biaxiality ratio for an edge-cracked plate or bar in tension and bending

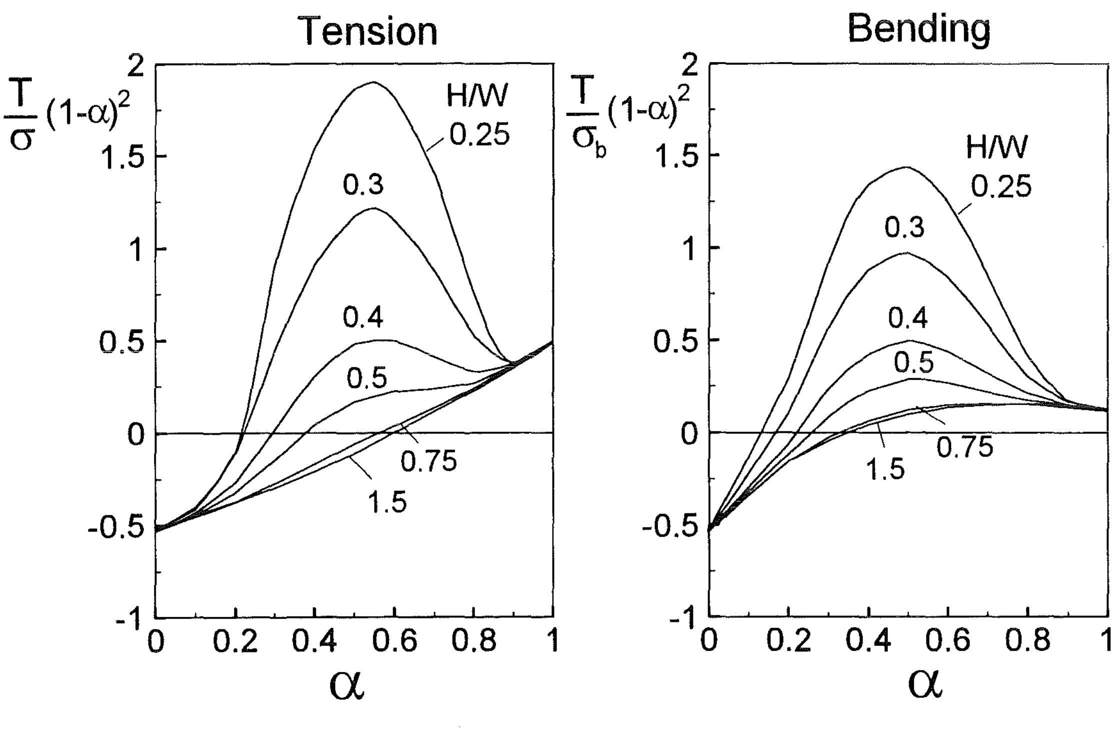

Fig. 10.2.3 T-stress under tensile and bending loadings.

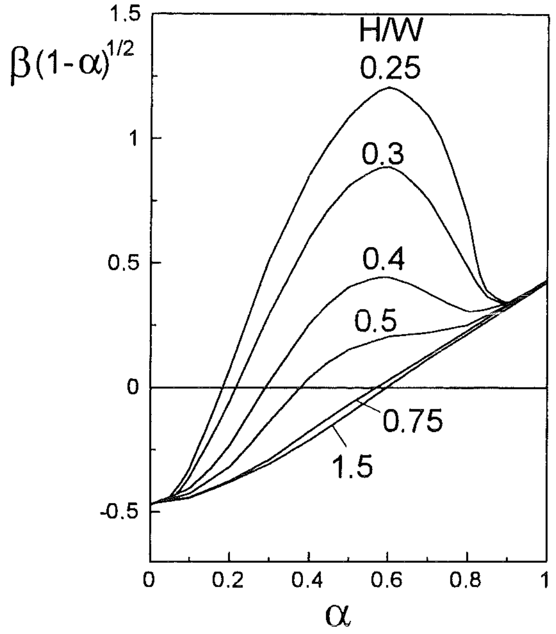

Fig. 10.2.4 Biaxiality ratio in the form $\beta(1-\alpha)^{1/2}$

	H/W=1.5	1.25	1.00	0.75	0.5	0.4
α=0	1.1215	1.1215	1.1215	1.1215	1.1215	1.1215
0.2	0.7561	0.7561	0.7562	0.7628	0.8279	0.9130
0.3	0.6583	0.6583	0.6589	0.6677	0.7444	0.8475
0.4	0.5861	0.5861	0.5865	0.5930	0.6567	0.7505
0.5	0.5293	0.5293	0.5296	0.5332	0.5717	0.6388
0.6	0.4842	0.4842	0.4842	0.4852	0.5022	0.5367
0.7	0.4481	0.4479	0.4478	0.4478	0.4514	0.4621
0.8	0.4203	0.4188	0.4191	0.4185	0.4180	0.4185
1.0	0.374	0.374	0.374	0.374	0.374	0.374

Table 10.2.2 Geometric function for bending $F_b \cdot (1-a/W)^{3/2}$.

The biaxiality ratio for a long plate (H/W=1.5) is approximated by

$$\beta = \frac{-0.469 + 1.2825\alpha + 0.6543\alpha^2 - 1.2415\alpha^3 + 0.07568\alpha^4}{\sqrt{1-\alpha}} \qquad (10.2.3)$$

	H/W=1.5	0.75	0.5	0.4
α=0	-0.469	-0.469	-0.469	-0.469
0.2	-0.198	-0.194	-0.138	-0.067
0.3	-0.059	-0.036	0.107	0.262
0.4	0.075	0.113	0.341	0.565
0.5	0.187	0.233	0.495	0.772
0.6	0.275	0.309	0.536	0.816
0.7	0.337	0.353	0.481	0.679
0.8	0.376	0.378	0.416	0.487
1.0	0.302	0.302	0.302	0.302

Table 10.2.3 Biaxiality ratio for bending $\beta\cdot(1-a/W)^{1/2}$.

In Fig. 10.2.5 the biaxiality ratios for $H/W = 1.5$ are compared with a solution from the literature [8]. It should be noted that the results given by Sham [8] were determined for a very long plate with $H/W=6$. Nevertheless, this solution (squares) is very close to the BCM-results of Table 10.2.3 (curve: interpolated by application of cubic splines). This excellent agreement indicates that the plates are represented in both cases by the limit case of an "infinitely long plate".

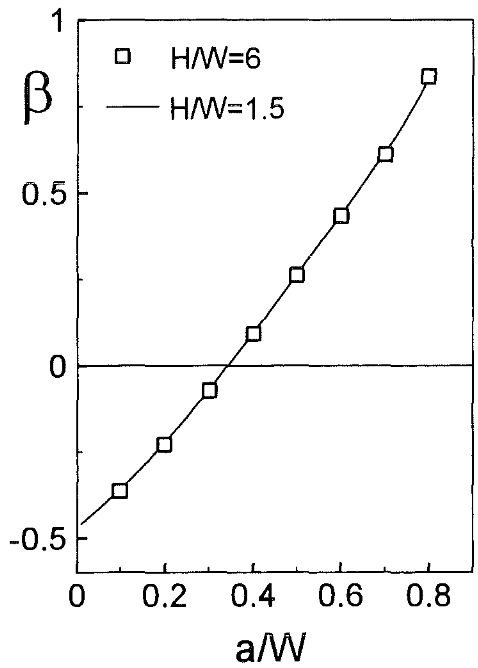

Fig. 10.2.5 Biaxiality ratios β (Table 10.2.3, curve) compared with data reported by Sham [8] (squares).

Higher order coefficients of the Williams stress function for bending are compiled in Tables 10.2.4 and 10.2.5.

α	H/W=1.5	1.25	1.00	0.75	0.5	0.4
0.2	0.021	0.023	0.0233	0.0249	0.0409	0.0672
0.3	0.06	0.06	0.0652	0.0696	0.1104	0.1722
0.4	0.116	0.118	0.1185	0.1257	0.1906	0.2887
0.5	0.201	0.201	0.2023	0.2104	0.2885	0.4148
0.6	0.362	0.362	0.3623	0.3684	0.4409	0.5751
0.7	0.720	0.742	0.745	0.7472	0.7922	0.900
0.8	-0.713	0.771	1.785	2.030	2.049	2.088

Table 10.2.4 Coefficient A_1 for bending.

α	H/W=1.5	1.25	1.00	0.75	0.5	0.4
0.2	-0.034	-0.028	-0.025	-0.033	-0.102	-0.188
0.3	-0.1216	-0.127	-0.123	-0.141	-0.251	-0.363
0.4	-0.1944	-0.1958	-0.197	-0.213	-0.310	-0.408
0.5	-0.2884	-0.2872	-0.289	-0.289	-0.308	-0.348
0.6	-0.4666	-0.4668	-0.464	-0.440	-0.315	-0.213
0.7	-0.9162	-0.951	-0.952	-0.907	-0.598	-0.230
0.8	1.369	-1.08	-2.62	-2.924	-2.521	-1.84

Table 10.2.5 Coefficient A^*_1 for bending.

For long plates (H/W=1.5) the coefficients A_1 and A^*_1 can be approximated by [9]

$$A_1 \cong \frac{-0.02279 + 0.19661\alpha - 0.30552\alpha^2 + 0.247618\alpha^3 - 0.08037\alpha^4}{(1-\alpha)^{5/2}\sqrt{\alpha}} \qquad 10.2.4)$$

$$A^*_1 \cong \frac{0.04813 - 0.4224\alpha + 1.0005\alpha^2 - 1.0269\alpha^3 + 0.3799\alpha^4}{(1-\alpha)^3\alpha} \qquad (10.2.5)$$

10.3 Green's function for single-edge-cracked plates

A Green's function for single-edge-cracked plates can be given by

$$t(x) = t_0 + C_1(1 - x/a) + C_2(1 - x/a)^2 \tag{10.3.1}$$

or

$$T_c = -\sigma_y\big|_{x=a} + C_1\int_0^a \sigma_y(x)(1 - x/a)\,dx + C_2\int_0^a \sigma_y(x)(1 - x/a)^2 dx \tag{10.3.2}$$

with the coefficients C_1 and C_2 given in the following tables.

α=a/W	H/W=1.5	0.75	0.50	0.40	0.30
0.2	2.531	2.015	2.53	4.78	8.16
0.3	1.456	1.306	4.00	6.53	11.74
0.4	1.167	1.792	4.93	8.33	15.13
0.5	1.728	2.112	5.71	9.46	18.67
0.6	3.167	3.417	6.04	10.21	21.60
0.7	6.204	6.422	8.05	11.73	23.31

Table 10.3.1 Coefficient $C_1 \cdot W$ for the Green's function, eq.(10.3.1).

α=a/W	H/W=1.5	0.75	0.50	0.40	0.30
0.2	2.438	3.234	3.37	1.50	0.80
0.3	1.714	2.286	0.980	0.82	1.55
0.4	1.417	1.167	0.925	1.46	3.81
0.5	0.864	1.152	1.44	3.17	5.95
0.6	0.437	0.875	2.81	5.00	8.28
0.7	0.789	1.034	3.35	5.93	10.71

Table 10.3.2 Coefficient $C_2 \cdot W$ for the Green's function, eq.(10.3.1).

In order to determine the biaxiality ratio for any stress distribution one has to compute also the stress intensity factor for these stresses. Therefore, the fracture mechanics weight function h is necessary from which the stress intensity factor results as

$$K_I = \int_0^a \sigma(x) h(x,a)\, dx \qquad (10.3.3)$$

where $\sigma(x)$ is the normal stress distribution in the uncracked component along the prospective crack line of an edge crack. An approximate weight function for the edge-cracked rectangular plate is

$$h = \sqrt{\frac{2}{\pi a}} \left[\frac{1}{\sqrt{1-\rho}} + D_0\sqrt{1-\rho} + D_1(1-\rho)^{3/2} \right], \quad \rho = x/a \qquad (10.3.4)$$

α	H/W=1.5	1.25	1.00	0.75	0.5	0.4
0.2	1.001	1.001	1.003	1.010	1.249	1.347
0.3	1.298	1.302	1.326	1.317	1.539	1.816
0.4	1.581	1.581	1.598	1.616	1.836	2.036
0.5	1.827	1.829	1.835	1.859	1.973	2.122
0.6	1.996	1.996	1.998	2.001	2.027	2.110
0.7	2.070	2.071	2.071	2.079	2.104	2.094
0.8	2.015	2.015	2.017	2.054	2.064	2.094

Table 10.3.3 Coefficient $D_0(1-\alpha)^{3/2}$ for weight function (10.3.4).

α	H/W=1.5	1.25	1.00	0.75	0.5	0.4
0.2	0.1963	0.200	0.210	0.2245	0.255	0.634
0.3	0.3072	0.301	0.2641	0.3422	0.516	0.784
0.4	0.4909	0.4909	0.4661	0.4887	0.624	1.006
0.5	0.7329	0.7300	0.7213	0.7183	0.857	1.170
0.6	1.074	1.074	1.072	1.077	1.186	1.368
0.7	1.526	1.525	1.525	1.513	1.516	1.629
0.8	2.128	2.128	2.128	2.066	2.050	2.018

Table 10.3.4 Coefficient $D_1(1-\alpha)^{3/2}$ for weight function (10.3.4).

10.4 Edge-cracked bar in 3-point bending

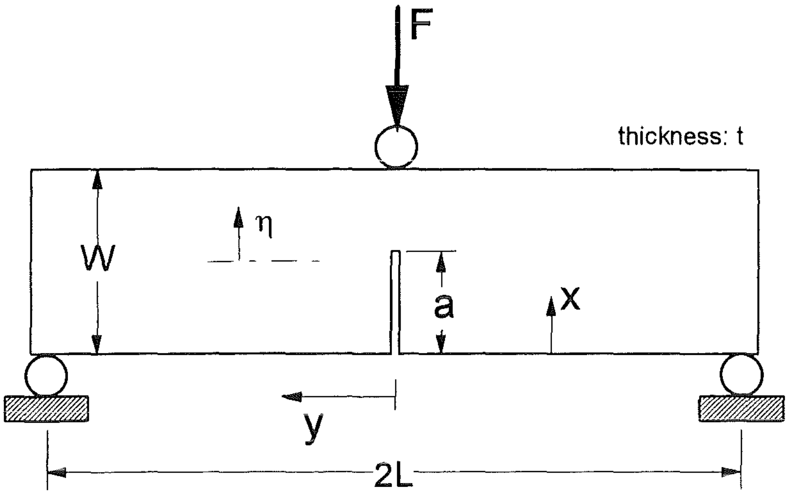

Fig. 10.4.1 3-point bending test.

The T-stresses for the 3-point bending test were computed by application of the Green's function method, using an expansion with two regular terms, eqs.(10.3.1) and (10.3.2). The stresses normal to the crack plane are given by Filon [26]

$$\sigma_n = -\frac{3\eta PL}{tW^3} - \frac{2P}{tL}\sum_{n=1}^{\infty}\frac{\sinh(mW/2) - \frac{1}{2}mW\cosh(mW/2)}{mW + \sinh(mW)}\cos(my)\cosh(m\eta)$$

$$-\frac{2P}{tL}\sum_{0}^{\infty}\frac{m\eta\sinh(mW/2)}{mW + \sinh(mW)}\cos(my)\sinh(m\eta)$$

$$-\frac{2P}{tL}\sum_{n=1}^{\infty}\frac{\cosh(MW/2) - \frac{1}{2}MW\sinh(MW/2)}{\sinh(MW) - MW}\cos(My)\sinh(M\eta)$$

$$-\frac{2P}{tL}\sum_{0}^{\infty}\frac{M\eta\cosh(MW/2)}{\sinh(MW) - MW}\cos(My)\cosh(M\eta) \qquad (10.4.1)$$

$$m = \frac{2n\pi}{L}, \quad M = \frac{(2n+1)\pi}{L} \qquad (10.4.2)$$

$$\sigma^* = \frac{3PL}{W^2 t} \qquad (10.4.3)$$

The stress intensity factors were computed with the weight function technique using eq.(3.1.1a) and the weight function given in [10].

$\alpha = a/W$	L/W=10	5	4	3	2.5	2
0.2	-0.2280	-0.2217	-0.2185	-0.2133	-0.2090	-0.2027
0.3	-0.0776	-0.0756	-0.0746	-0.0730	-0.0717	-0.0697
0.4	0.1174	0.1125	0.1101	0.106	0.1027	0.0977
0.5	0.3822	0.3683	0.3614	0.3499	0.3406	0.3267
0.6	0.8063	0.7813	0.7688	0.7479	0.7313	0.7062
0.7	1.6380	1.5983	1.5784	1.5453	1.5189	1.4791

Table 10.4.1 T-stress T_c/σ^* for the edge-cracked bar in 3-point bending.

The constant stress component in the uncracked body along the crack line, σ_y, is given by [26]

$$\sigma_x = -\frac{P}{2tL} - \frac{2P}{tL}\sum_{n=1}^{\infty}\frac{\sinh(mW/2)+\frac{1}{2}mW\cosh(mW/2)}{mW+\sinh(mW)}\cosh(m\eta)$$

$$+\frac{2P}{tL}\sum_{0}^{\infty}\frac{m\eta\sinh(mW/2)}{mW+\sinh(mW)}\sinh(m\eta)$$

$$-\frac{2P}{tL}\sum_{n=1}^{\infty}\frac{\cosh(MW/2)-\frac{1}{2}MW\sinh(MW/2)}{\sinh(MW)-MW}\sinh(M\eta)$$

$$+\frac{2P}{tL}\sum_{0}^{\infty}\frac{M\eta\cosh(MW/2)}{\sinh(MW)-MW}\cosh(M\eta) \qquad (10.4.4)$$

and, consequently, the T-term T results as

$$T = T_c + \sigma_x\big|_{\eta=a-W/2} \qquad (10.4.5)$$

The stresses resulting from (10.4.4) are nearly independent by L/W for $L/W \geq 2$. This gives rise for an approximative relation

$$\sigma_x \cong -\frac{2P}{\pi tW}\frac{\xi}{1-\xi} + \frac{P}{tW}(0.474\xi - 3.159\xi^2 + 2.149\xi^3)\ , \quad \xi = x/W \qquad (10.4.6)$$

The T-stress according to eq.(10.4.5) is entered in Table 10.4.2. The geometric function is given in Table 10.4.3 and the related biaxiality ratios are entered in Table 10.4.4 and plotted in Fig.10.4.2.

α=a/W	L/W=10	5	4	3	2.5	2
0	-0.526	-0.526	-0.526	-0.526	-0.526	-0.526
0.1	-0.291	-0.292	-0.291	-0.290	-0.289	-0.288
0.2	-0.150	-0.149	-0.149	-0.149	-0.149	-0.149
0.3	-0.044	-0.049	-0.054	-0.056	-0.058	-0.063
0.4	0.035	0.026	0.022	0.014	0.008	-0.001
0.5	0.088	0.077	0.071	0.061	0.054	0.044
0.6	0.122	0.111	0.105	0.096	0.088	0.077
0.7	0.141	0.132	0.127	0.119	0.113	0.103
0.8	0.143	0.137	0.132	0.125	0.120	0.112
0.9	0.132	0.128	0.126	0.122	0.119	0.115
1	0.113	0.113	0.113	0.113	0.113	0.113

Table 10.4.2 T-stress in the form of $T/\sigma^*(1\text{-}a/W)^2$ for the edge-cracked bar in 3-point bending.

α=a/W	L/W=10	5	4	3	2.5	2
0.1	0.8964	0.8849	0.8791	0.8694	0.8616	0.8504
0.2	0.7493	0.7381	0.7325	0.7231	0.7156	0.7046
0.3	0.6485	0.6387	0.6337	0.6255	0.6188	0.6091
0.4	0.5774	0.5690	0.5651	0.5582	0.5527	0.5447
0.5	0.5242	0.5177	0.5145	0.5091	0.5048	0.4985
0.6	0.4816	0.4770	0.4744	0.4704	0.4672	0.4626
0.7	0.4458	0.4430	0.4408	0.4381	0.4359	0.4328
0.8	0.4154	0.4140	0.4124	0.4108	0.4094	0.4076

Table 10.4.3 Geometric function $F(1\text{-}a/W)^{3/2}$.

α=a/W	L/W=10	5	4	3	2.5	2
0	-0.469	-0.469	-0.469	-0.469	-0.469	-0.469
0.1	-0.325	-0.330	-0.331	-0.334	-0.335	-0.339
0.2	-0.200	-0.202	-0.203	-0.206	-0.208	-0.211
0.3	-0.068	-0.077	-0.085	-0.090	-0.094	0.103
0.4	0.061	0.046	0.039	0.025	0.014	-0.002
0.5	0.168	0.149	0.138	0.120	0.107	0.088
0.6	0.253	0.233	0.221	0.204	0.188	0.166
0.7	0.316	0.298	0.288	0.272	0.259	0.238
0.8	0.344	0.331	0.320	0.304	0.293	0.259
0.9	0.332	0.327	0.321	0.314	0.309	0.301
1	0.302	0.302	0.302	0.302	0.302	0.302

Table 10.4.4 Biaxiality ratio in the form of $\beta(1\text{-}a/W)^{1/2}$ for the edge-cracked bar in 3-point bending.

A comparison with literature data is given in Fig. 10.4.3 for L/W=2. Data from Leevers and Radon [5] (squares) and Kfouri [6] (circles) are plotted together with the data of Table 10.4.4 (curve). Whereas the data of Leevers and Radon differ significantly the agreement with the data provided by Kfouri is very good.

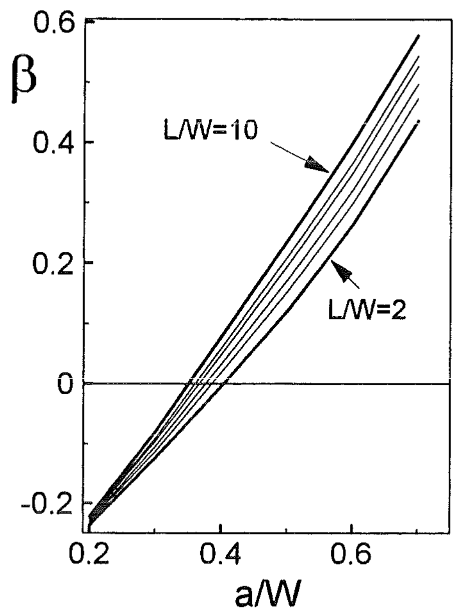

Fig. 10.4.2 Biaxiality ratio β for edge-cracked 3-point bending specimens with different ratios L/W.

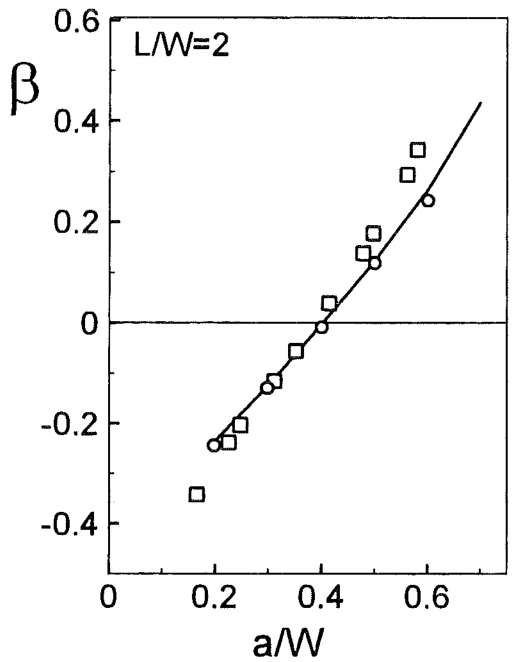

Fig. 10.4.3 Comparison between Table 10.4.4 (curve) and results of Leevers and Radon [5] (squares) and Kfouri [6] (circles).

10.5 The Double Cantilever Beam (DCB) specimen

The Double-Cantilever Beam (DCB) specimen is illustrated in Fig. 10.5.1. Concentrated forces P are applied at the ends of the cantilevers.

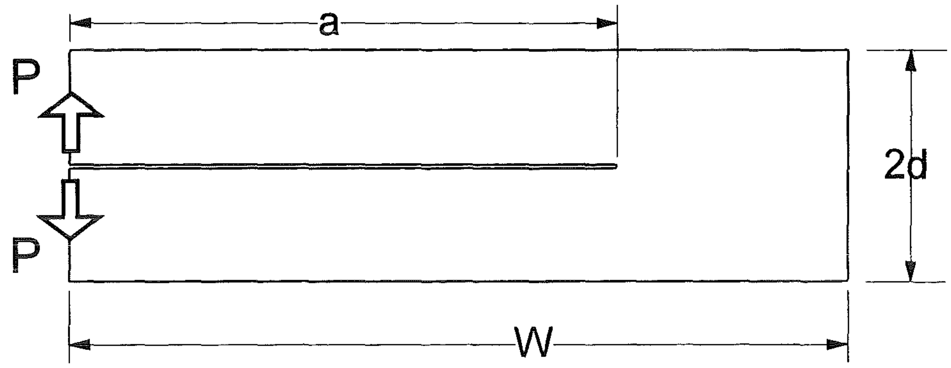

Fig. 10.5.1 Double-Cantilever-Beam specimen.

The biaxiality ratio β obtained for the DCBis found to be independent of a/W if $a/W < 0.55$. For d/a< 0.5 the biaxiality ratio can be described by the relation [13]

$$\frac{1}{\beta} \cong 0.681\frac{d}{a} + 0.0685 \tag{10.5.1}$$

Using the stress intensity factor solution

$$K_I = \sqrt{\frac{12}{d}}\,\frac{P}{B}\left(\frac{a}{d} + 0.68\right) \tag{10.5.2}$$

(B= specimen thickness) yields for the T-stress

$$T = \frac{\beta K_I}{\sqrt{\pi a}} \cong \sqrt{\frac{12}{\pi a d}}\,\frac{P}{B}\,\frac{\frac{a}{d} + 0.68}{0.681\frac{d}{a} + 0.0685} \tag{10.5.3}$$

The approximate relation (10.5.1) is represented in Fig. 10.5.2 together with results reported by Leevers and Radon [5] (symbols). The agreement of the plotted data is sufficient for $0.1 < d/a < 0.5$ and $a/W \geq 0.4$. Maximum deviations are less than 10%.

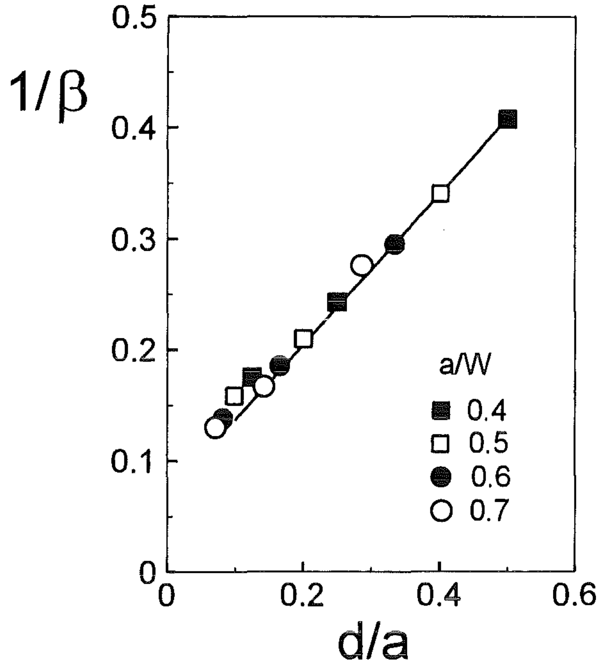

Fig. 10.5.2 Biaxiality ratio for the DCB specimen. Line: eq.(10.5.1), symbols: Leevers and Radon [5].

10.6 Couple of opposite point forces

An infinitely long strip with a single edge crack is considered (Fig. 10.6.1). A pair of opposite point forces generates stresses in the plane of the crack.

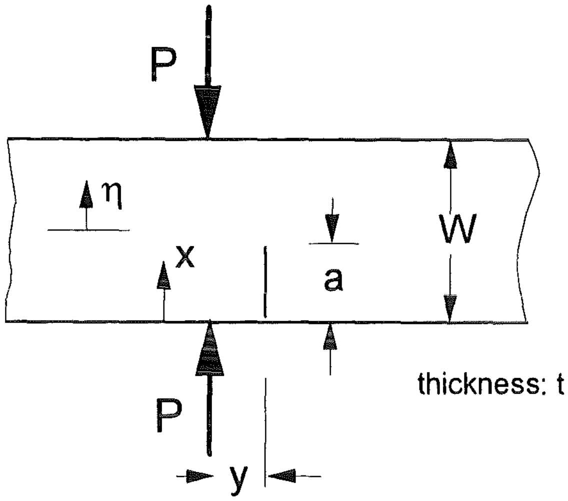

Fig. 10.6.1 Edge cracked strip with opposite concentrated forces.

The T-stresses for the edge crack affected by two opposite concentrated forces P were computed by application of the Green's function method, using an expansion with two regular terms, eqs.(10.3.1) and (10.3.2).

The stresses normal to the plane of the crack, σ_n, are given by [26]

$$\sigma_n = -\frac{4P}{\pi W t}\int_0^\infty \frac{\sinh u - u\cosh u}{\sinh 2u + 2u}\cos\frac{2uy}{W}\cosh\frac{2u\eta}{W}\,du -$$

$$-\frac{4P}{\pi W t}\int_0^\infty \frac{2uy}{W}\frac{\sinh u}{\sinh 2u + 2u}\cos\frac{2uy}{W}\sinh\frac{2u\eta}{W}\,du \qquad (10.6.1)$$

with $\eta = x - W/2$. The characteristic stress is chosen as

$$\sigma^* = \frac{P}{Wt} \qquad (10.6.2)$$

resulting in the T-term T_c/σ^* according to eq.(2.11). Table 10.6.1 shows the results. For the computation of the total constant stress term, the related stress in the uncracked body has to be computed from

$$\sigma_x = -\frac{4P}{\pi W t}\int_0^\infty \frac{\sinh u + u\cosh u}{\sinh 2u + 2u}\cos\frac{2uy}{W}\cosh\frac{2u\eta}{W}\,du$$

$$+\frac{8P}{\pi W t}\int_0^\infty \frac{u\eta}{W}\frac{\sinh u}{\sinh 2u + 2u}\cos\frac{2uy}{W}\sinh\frac{2u\eta}{W}\,du \tag{10.6.3}$$

and it then results

$$T = T_c + \sigma_x\big|_{\eta=a-W/2} \tag{10.6.4}$$

α=a/W	x/W=0.1	0.2	0.5	0.7	1.0	1.5
0.2	-0.355	0.273	0.143	0.054	0.009	0.00
0.3	-0.541	-0.027	0.209	0.119	0.034	0.001
0.4	-0.561	-0.169	0.226	0.159	0.053	0.002
0.5	-0.558	-0.213	0.226	0.171	0.060	0.003
0.6	-0.565	-0.180	0.225	0.160	0.053	0.002
0.7	-0.576	-0.046	0.219	0.127	0.037	0.001

Table 10.6.1 T-stress T_c/σ^* for the edge-cracked strip under opposite concentrated forces.

α=a/W	x/W=0.1	0.2	0.5	0.7	1.0	1.5
0.2	-2.48	-0.584	0.1044	0.0713	0.026	0.002
0.3	-2.44	-1.169	0.1064	0.1386	0.063	0.006
0.4	-2.28	-1.390	0.0660	0.1758	0.090	0.008
0.5	-2.22	-1.448	0.0438	0.1859	0.100	0.010
0.6	-2.28	-1.401	0.0650	0.1768	0.090	0.008
0.7	-2.47	-1.188	0.1804	0.1466	0.066	0.006

Table 10.6.2 T-stress T/σ^* for the edge-cracked strip under opposite concentrated forces.

The stress intensity factors K_{I} and K_{II} with the geometric functions F_{I} and F_{II} are defined by

$$K_{\mathrm{I}} = \sigma^*\sqrt{\pi a}F_{\mathrm{I}}\ , \qquad K_{\mathrm{II}} = \sigma^*\sqrt{\pi a}F_{\mathrm{II}} \tag{10.6.3}$$

For their calculation the weight function method was used. The results are entered in Tables 10.6.3 and 10.6.4

a/W	x/W=0.1	0.20	0.50	0.75	1.0	1.5
0.1	-1.175	-0.238	0.054	0.040	0.017	0.005
0.2	-1.210	-0.495	0.056	0.060	0.029	0.004
0.3	-0.969	-0.522	0.038	0.064	0.032	0.004
0.4	-0.781	-0.455	0.025	0.057	0.030	0.004
0.5	-0.649	-0.366	0.021	0.046	0.024	0.003
0.6	-0.549	-0.270	0.023	0.033	0.017	0.002
0.7	-0.453	-0.163	0.023	0.020	0.009	0.001
0.8	-0.316	-0.050	0.016	0.008	0.003	0.001

Table 10.6.2 Geometric function F_{II}.

a/W	x/W=0.1	0.20	0.50	0.75	1.0	1.5
0.1	-0.959	0.048	0.346	0.173	0.060	0.000
0.2	-0.579	-0.163	0.220	0.129	0.048	0.001
0.3	-0.347	-0.121	0.142	0.091	0.036	0.001
0.4	-0.238	-0.056	0.098	0.061	0.024	0.000
0.5	-0.173	-0.003	0.072	0.039	0.013	-0.001
0.6	-0.116	0.044	0.050	0.022	0.006	-0.001
0.7	-0.046	0.080	0.028	0.011	0.002	-0.002
0.8	0.047	0.083	0.009	0.008	0.001	-0.003

Table 10.6.3 Geometric function F_I.

10.7 Rectangular plate with thermal stresses

A long rectangular plate with a parabolically distributed temperature Θ

$$\Theta = 4\Theta_0\left[\frac{x}{W} - \left(\frac{x}{W}\right)^2\right] \tag{10.7.1}$$

(with the maximum temperature Θ_0) is considered, which causes a stress distribution

$$\sigma_y = \sigma^*\left(\frac{2}{3} - 4\frac{x}{W} + 4\frac{x^2}{W^2}\right)\ ,\quad \sigma^* = \alpha_T\Theta_0 E \tag{10.7.2}$$

with E = Young's modulus and α_T = thermal expansion coefficient. The stress distribution is shown in Fig. 10.7.1a. Introducing this stress distribution into eq.(10.3.2) and using the approximate Green's function (3.2.18), (3.2.20) yields the T-stress

$$\frac{T}{\sigma^*} = \frac{2}{3}(1-\alpha)^2\left(1 + \frac{T_t}{\sigma_0}\right) + 4\alpha(1-\alpha) - \frac{2}{3} \tag{10.7.3}$$

where T_t is the reference T-stress solution for pure tension with tensile stress σ_0 taken from Table 10.1.1 or from eq.(10.1.1). The related stress intensity factor solution K, obtained with the weight function given in [10], has been entered additionally in Fig. 10.7.1b.

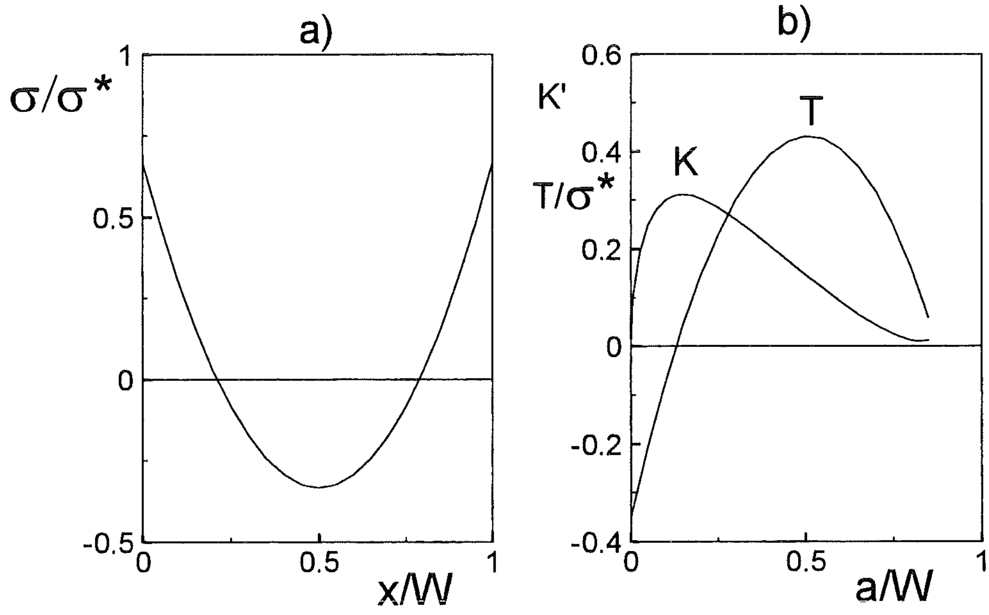

Fig. 10.7.1 a) thermal stresses in a rectangular plate, b) stress intensity factor and T-stress, $K' = K/(\sigma^* W^{1/2})$.

The biaxiality ratio represented in Fig. 10.7.2 was computed from the T-stress solution eq.(10.7.2) and the stress intensity factor solution K. Large positive biaxiality ratios are obvious for deep cracks. This is the consequence of the low stress intensity factors near $a/W = 0.8$.

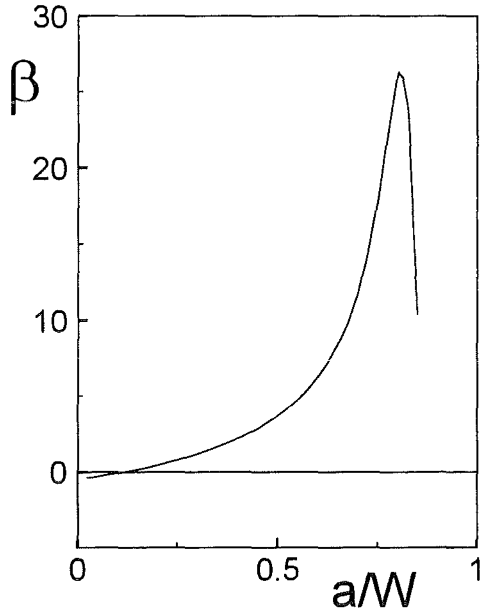

Fig. 10.7.2 Biaxiality ratio for thermal stresses given by eq.(10.7.1).

10.8 Partially loaded rectangular plate

A plate loaded by a constant stress over a range d is shown in Fig. 10.8.1. The related T-stress terms T_d and the biaxiality ratios are entered into Tables 10.8.1-10.8.8.

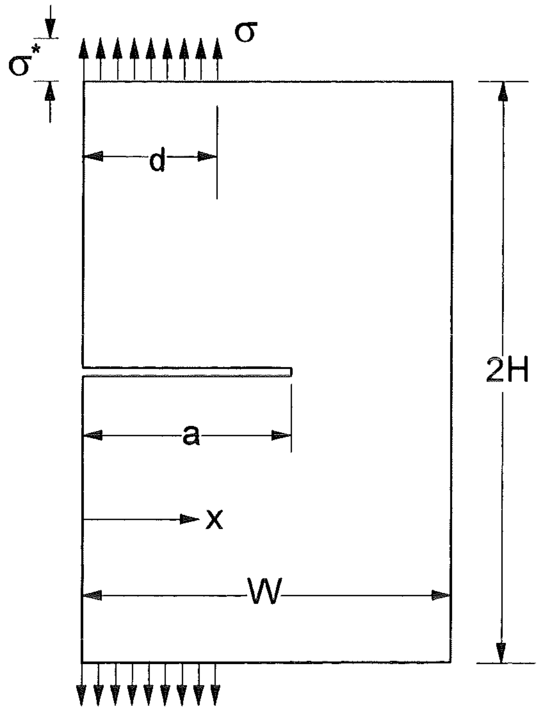

Fig. 10.8.1 Partially loaded edge-cracked rectangular plate.

Due to the nonhomogeneous tractions at the plate ends already in the uncracked component a stress component σ_x will be generated along the crack line. Consequently, the T-term resulting from the coefficient A_0* of the Williams expansion and T_c in the sense of eq.(2.11) must be different. In this Section only the total T-terms are reported.

$\alpha=a/W$	$d/W=0$	0.25	0.5	0.75	1.0
0.3	0	-0.196	-0.362	-0.501	-0.608
0.4	0	-0.072	-0.197	-0.372	-0.577
0.5	0	0.123	0.092	-0.102	-0.419
0.6	0	0.461	0.660	0.468	0.040
0.7	0	1.199	1.90	1.806	1.337

Table 10.8.1 T-stress T_d/σ^* for $H/W=1.25$.

$\alpha = a/W$	d/W=0	0.25	0.5	0.75	1.0
0.3	0	-0.174	-0.360	-0.515	-0.606
0.4	0	-0.042	-0.193	-0.383	-0.570
0.5	0	0.157	0.117	-0.409	-0.409
0.6	0	0.522	0.680	0.474	0.051
0.7	0	1.329	1.959	1.917	1.366

Table 10.8.2 T-stress T_d/σ^* for H/W=1.00.

$\alpha = a/W$	d/W=0	0.25	0.5	0.75	1.0
0.3	0	-0.094	-0.333	-0.524	-0.571
0.4	0	0.098	-0.115	-0.369	-0.485
0.5	0	0.348	0.251	-0.039	-0.277
0.6	0	0.703	0.808	0.560	0.199
0.7	0	1.456	2.052	2.011	1.485

Table 10.8.3 T-stress T_d/σ^* for H/W=0.75.

$\alpha = a/W$	d/W=0	0.25	0.5	0.75	1.0
0.3	0	0.257	-0.119	-0.317	-0.299
0.4	0	0.722	0.457	0.136	0.110
0.5	0	1.157	1.195	0.783	0.666
0.6	0	1.614	2.007	1.668	1.372
0.7	0	2.250	3.174	3.007	2.593

Table 10.8.4 T-stress T_d/σ^* for H/W=0.50.

$\alpha = a/W$	d/W=0.25	0.5	0.75	1.0
0.3	-0.156	-0.184	-0.225	-0.311
0.4	-0.045	-0.077	-0.124	-0.213
0.5	0.056	0.026	-0.024	-0.105
0.6	0.142	0.122	0.073	0.006
0.7	0.209	0.213	0.160	0.116

Table 10.8.5 Biaxiality ratio $\beta(1\text{-}a/W)^{1/2}$ for H/W=1.25.

$\alpha=a/W$	d/W=0.25	0.5	0.75	1.0
0.3	-0.138	-0.181	-0.230	-0.306
0.4	-0.026	-0.074	-0.129	-0.209
0.5	0.071	0.032	0.026	-0.102
0.6	0.154	0.124	0.073	0.008
0.7	0.227	0.205	0.167	0.118

Table 10.8.6 Biaxiality ratio $\beta(1\text{-}a/W)^{1/2}$ for H/W=1.00.

$\alpha=a/W$	d/W=0.25	0.5	0.75	1.0
0.3	-0.071	-0.164	-0.235	-0.284
0.4	0.059	-0.044	-0.125	-0.176
0.5	0.153	0.068	-0.009	-0.069
0.6	0.209	0.149	0.086	0.031
0.7	0.251	0.216	0.175	0.128

Table 10.8.7 Biaxiality ratio $\beta(1\text{-}a/W)^{1/2}$ for H/W=0.75.

$\alpha=a/W$	d/W=0.25	0.5	0.75	1.0
0.3	0.166	-0.054	-0.135	-0.136
0.4	0.378	0.158	0.043	0.037
0.5	0.488	0.329	0.177	0.157
0.6	0.466	0.355	0.248	0.209
0.7	0.386	0.332	0.261	0.222

Table 10.8.8 Biaxiality ratio $\beta(1\text{-}a/W)^{1/2}$ for H/W=0.50.

An example of application of this loading case may be demonstrated for a plate with H/W = 1.25 loaded by a couple of point forces P at several locations d/W as illustrated in Fig. 10.8.2a. The evaluation of the related T-stress term is explained in Fig. 10.8.2b.

First, we determine the T_d/σ^*-values for two values d_1 and d_2 with $d_1 = d\text{-}\varepsilon$ and $d_2 = d\text{+}\varepsilon$ ($\varepsilon \ll d$) by interpolation of the tabulated results applying cubic splines. The normal force P is given by

$$P = \sigma^* (d_2 - d_1) t \qquad (10.8.1)$$

(t = thickness). The T-stress for this case is and for the case of d_1, $d_2 \rightarrow d$ ($\varepsilon \rightarrow 0$)

$$T_P = \frac{\partial(T_d / \sigma^*)}{\partial(d/W)} \frac{P}{Wt} \tag{10.8.3}$$

In Fig. 10.8.3 the T-stresses are plotted as a function of the relative crack length a/W.

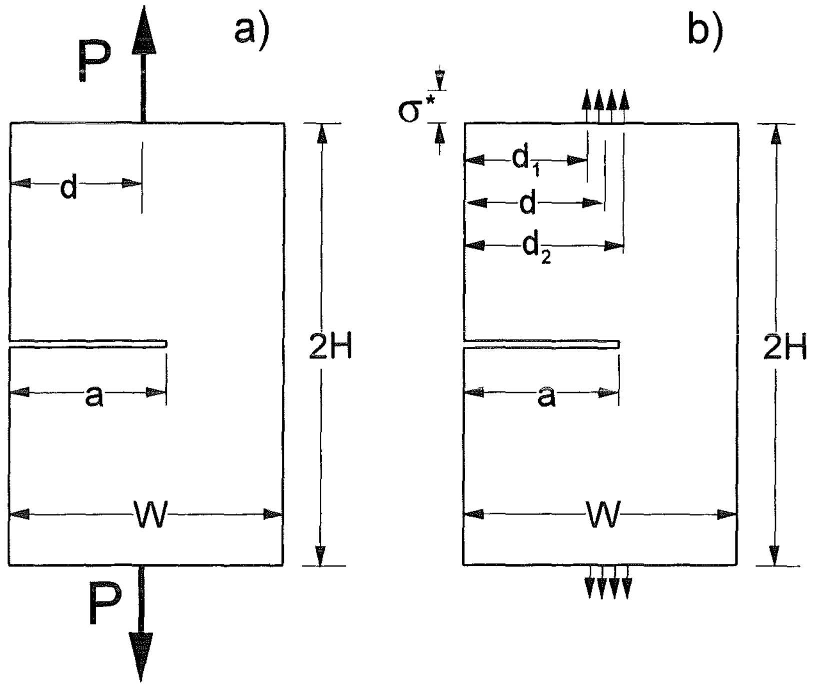

Fig. 10.8.2 Computation of T-stresses in plates loaded by a couple of point forces.

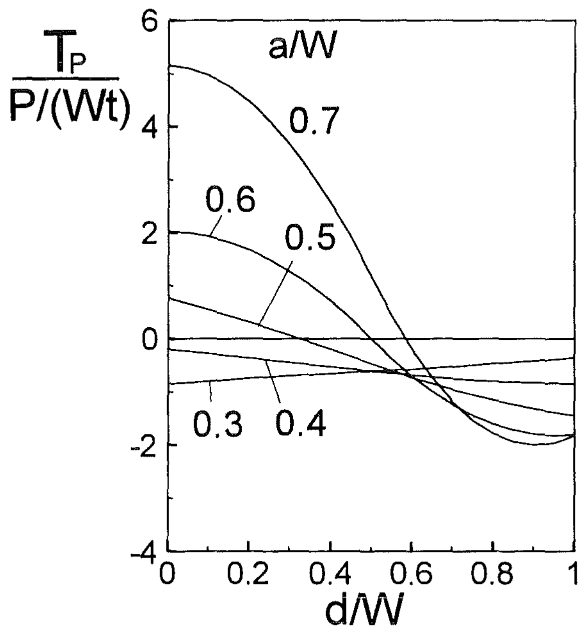

Fig. 10.8.3 T-stress caused by a couple of forces acting at location d ($H/W = 1.25$).

T-stresses for couples of point forces obtained with eq.(10.8.3) are entered into Tables 10.8.9-10.8.12. These results can be used to compute the T-stress for any given distribution of normal tractions σ_n at the ends of the plate

$$T = \frac{1}{W}\int_0^W \frac{T_P}{\sigma *}\sigma_n(x)dx \quad , \quad \sigma * = \frac{P}{Wt}. \tag{10.8.4}$$

If a smooth distribution of normal tractions acts at the ends of the plate it is of advantage to rewrite eq.(10.8.4) and to apply integration by parts. This leads to

$$T = \frac{T_d}{\sigma *}\sigma_n\Big|_{x=d=W} - \int_0^W \frac{T_d}{\sigma *}\frac{\mathrm{d}\sigma}{\mathrm{d}x}\mathrm{d}x. \tag{10.8.5}$$

As an example the T-stress for bending was computed from (10.8.5). The results for two values of H/W are shown in Fig. 10.8.4 (circles) together with the data of Table 10.2.1 (curves) which were obtained directly from BCM-computations. The agreement is good.

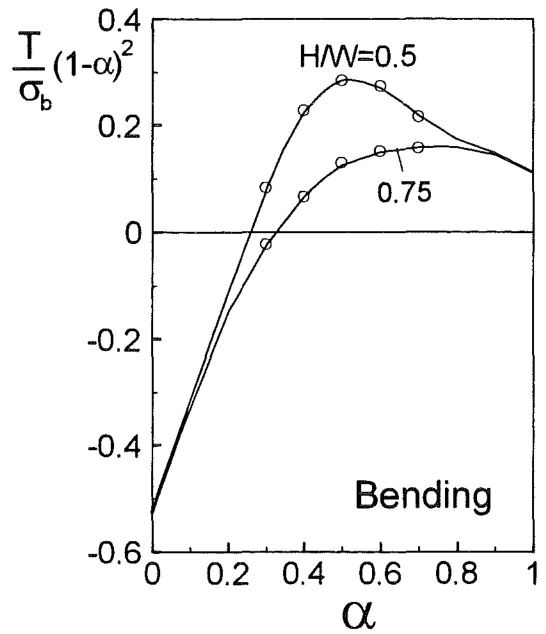

Fig. 10.8.4 Comparison of bending results obtained with eq.(10.8.5) (circles) and with BCM (curves).

Geometric function for stress intensity factor defined by

$$K_I = \sigma * F\sqrt{\pi a} \tag{10.8.6}$$

$\alpha=a/W$	d/W=0	0.25	0.5	0.75	1.0
0.3	0	1.049	1.643	1.859	1.637
0.4	0	1.245	1.990	2.318	2.103
0.5	0	1.546	2.538	2.968	2.825
0.6	0	2.054	3.472	4.080	4.034
0.7	0	3.138	5.274	6.191	6.327

Table 10.8.9 Geometric function F for H/W=1.25.

$\alpha=a/W$	d/W=0	0.25	0.5	0.75	1.0
0.3	0	1.056	1.668	1.871	1.656
0.4	0	1.280	2.009	2.296	2.112
0.5	0	1.568	2.599	2.982	2.824
0.6	0	2.139	3.483	4.101	4.035
0.7	0	3.207	5.229	6.280	6.353

Table 10.8.10 Geometric function F for H/W=1.00.

$\alpha=a/W$	d/W=0	0.25	0.5	0.75	1.0
0.3	0	1.100	1.697	1.864	1.681
0.4	0	1.302	2.038	2.295	2.135
0.5	0	1.614	2.612	3.012	2.842
0.6	0	2.129	3.435	4.099	4.043
0.7	0	3.174	5.209	6.284	6.357

Table 10.8.11 Geometric function F for H/W=0.75.

$\alpha=a/W$	d/W=0	0.25	0.5	0.75	1.0
0.3	0	1.296	1.862	1.961	1.847
0.4	0	1.479	2.242	2.422	2.323
0.5	0	1.676	2.752	3.126	3.007
0.6	0	2.193	3.575	4.249	4.146
0.7	0	3.190	5.240	6.307	6.386

Table 10.8.12 Geometric function F for H/W=0.50.

Similar to the T-term, the stress intensity factor can be computed

$$K = \frac{K_d}{\sigma *}\sigma_n\Big|_{x=d=W} - \int_0^W \frac{K_d}{\sigma *}\frac{\mathrm{d}\sigma}{\mathrm{d}x}\mathrm{d}x \qquad (10.8.7)$$

10.9 Compact Tension specimen

The Compact Tension (CT) specimen is illustrated in Fig. 10.9.1.

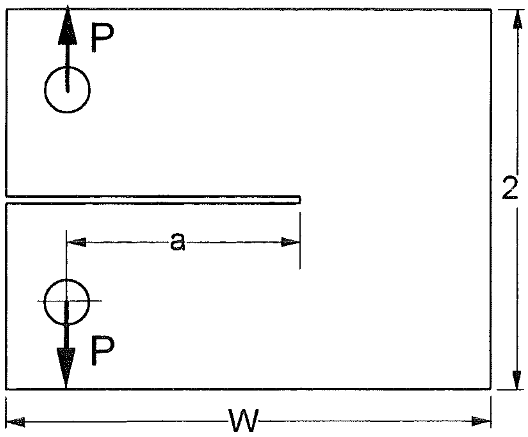

Fig. 10.9.1 Compact Tension specimen.

Results from the literature are entered in Fig. 10.9.2 for the biaxiality ratio β together with limit cases ($\alpha \to 0$ and $\alpha \to 1$) taken from Table 10.2.3. The curve introduced in Fig. 10.9.2 can be described by

$$\beta = \frac{-0.469 + 4.2327\alpha - 5.0162\alpha^2 - 2.3707\alpha^3 + 6.1866\alpha^4 - 2.2613\alpha^5}{\sqrt{1-\alpha}} \qquad (10.9.1)$$

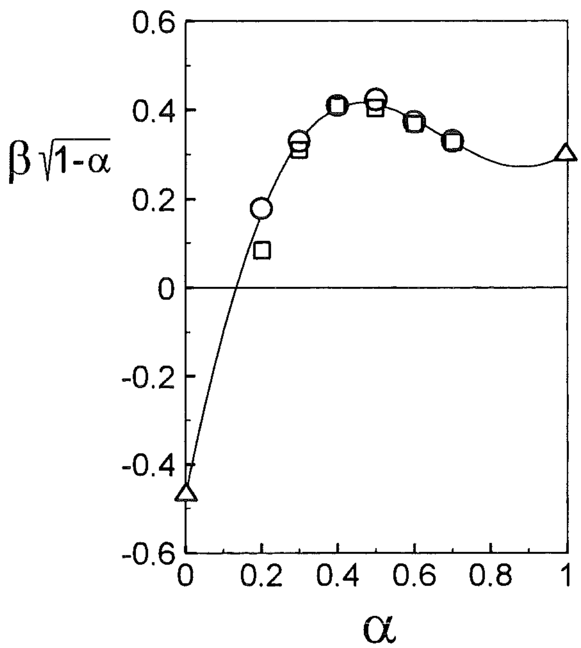

Fig. 10.9.2 Biaxiality ratio for the CT-specimen; curve: eq.(10.9.1), squares: Leevers and Radon [5], circles: Cotterell [27], triangles: limit cases from Table 10.2.3.

11 Edge-cracked circular disk

Edge-cracked circular disks are often used as fracture mechanics test specimens, especially in case of ceramic materials [28][29]. Figure 11.1 shows the geometric data.

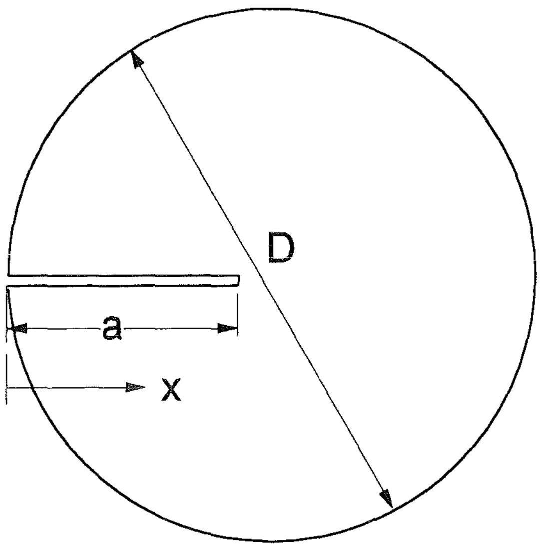

Fig. 11.1 Geometric data of an edge-cracked circular disk.

11.1 Circumferentially loaded disk

A circular disk is loaded by constant normal tractions σ_n along the circumference (loading as in Fig.7.1.1)

$$\sigma_n = \text{const}\,, \quad \tau = 0 \tag{11.1.1}$$

In this case it holds [10]

$$A^*_0 (1-\alpha)^2 = -0.11851 = C^*_0 \quad , \quad \alpha = a/W \tag{11.1.2}$$

and, from eqs.(2.9) and (2.11)

$$\begin{aligned} \frac{T}{\sigma_n} &= -4A^*_0 = \frac{0.474}{(1-\alpha)^2} \\ \frac{T_c}{\sigma_n} &= \frac{0.474}{(1-\alpha)^2} - 1 \end{aligned} \tag{11.1.3}$$

The value C^*_0, occurring in eq.(11.1.2) is identical with the coefficient of Wigglesworth's [30] expansion for the edge-cracked semi-infinite body.

With the stress intensity factor solution

$$K_I = \sigma_n F\sqrt{\pi a}\ , \quad F = \frac{1.1215}{(1-\alpha)^{3/2}} \tag{11.1.4}$$

the biaxiality ratio results as

$$\beta = \frac{0.4227}{\sqrt{1-\alpha}} \tag{11.1.5}$$

Further coefficients of the Williams stress function are [10]

$$A_1 = \frac{-0.02279 + 0.1322\alpha}{(1-\alpha)^{5/2}\sqrt{\alpha}} \tag{11.1.6}$$

$$A^*_1 = \frac{0.04812 - 0.1185\alpha}{(1-\alpha)^3\alpha} \tag{11.1.7}$$

$$A_2 = \frac{-0.00680 - 0.03416\alpha + 0.0991\alpha^2}{(1-\alpha)^{7/2}\alpha^{3/2}} \tag{11.1.8}$$

$$A^*_2 = \frac{-0.01787 + 0.09627\alpha - 0.11851\alpha^2}{(1-\alpha)^4\alpha^2} \tag{11.1.9}$$

11.2 Diametrically loaded disk

11.2.1 Load perpendicular to the crack

The Green's function method may be applied here to the diametrically loaded edge-cracked disk (Fig. 11.2.1).

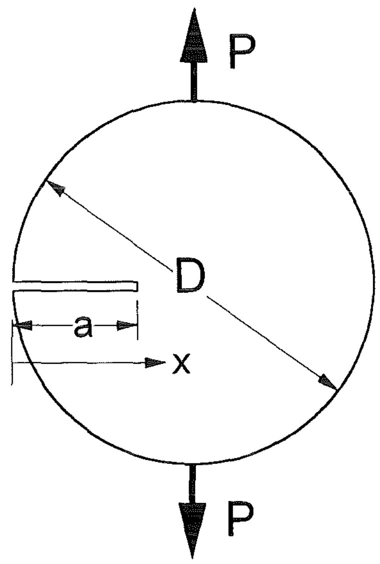

Fig. 11.2.1 Diametrically loaded circular disk.

Using eq.(11.1.3) as the reference T-stress solution the coefficient C for the Green's function, represented by eqs.(3.2.19) and (3.2.20), follows as

$$C = \frac{0.9481}{a(1-\alpha)^2}, \quad \alpha = a/D \tag{11.2.1}$$

Consequently, the T-stress can be computed from

$$T = \frac{0.9481}{(1-\alpha)^2}\int_0^1 (1-\rho)\sigma_y(\rho)d\rho - \sigma_y\big|_{x=a}, \quad \rho = x/a \tag{11.2.2}$$

As an application a disk of unit thickness is considered, which is diametrically loaded by a pair of forces P. The forces may act perpendiculary to the crack plane. In this case the stresses are given by

$$\frac{\sigma_y}{\sigma^*} = \frac{4}{[1+(1-\xi)^2]^2} - 1, \quad \xi = x/R, R = D/2 \tag{11.2.3}$$

$$\frac{\sigma_x}{\sigma^*} = \frac{4(1-\xi)^2}{[1+(1-\xi)^2]^2} - 1, \quad \sigma^* = \frac{P}{\pi R t} \tag{11.2.4}$$

as illustrated in Fig. 11.2.2. Introducing σ_y in eq.(3.22) yields the T-stress term

$$T \cong \frac{0.9481\sigma^*}{2(1-\alpha)^2(a/R)^2}\left[4\left(1-\frac{a}{R}\right)\arctan\left(1-\frac{a}{R}\right)+2\frac{a}{R}-\frac{a^2}{R^2}-\pi\left(1-\frac{a}{R}\right)\right]-\sigma_y\Big|_{x=a} \tag{11.2.5}$$

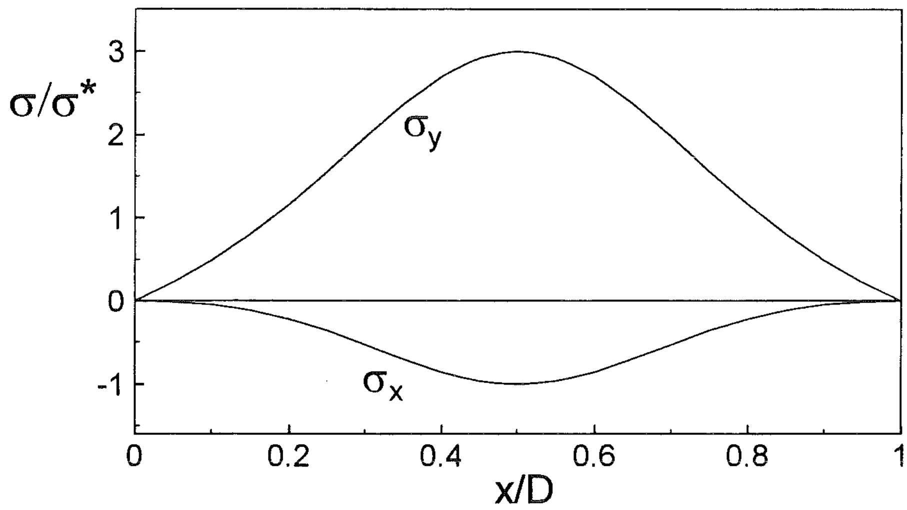

Fig. 11.2.2 Stresses along the x-axis in a diametrically loaded disk.

The stress intensity factor results from [16] as

$$K_I = \int_0^a h(x,a)\sigma_y \, dx \tag{11.2.6}$$

where h is the fracture mechanics weight function. In case of an edge-cracked disk a representation is given in [10], i.e.

$$h(x,a) = \sqrt{\frac{2}{\pi a}}\left[\frac{\rho}{\sqrt{1-\rho}} + D_0\sqrt{1-\rho} + D_1(1-\rho)^{3/2} + D_2(1-\rho)^{5/2}\right] \tag{11.2.7}$$

with the coefficients

$$\begin{aligned} D_0 &= (1.5721 + 2.4109\alpha - 0.8968\alpha^2 - 1.4311\alpha^3)/(1-\alpha)^{3/2} \\ D_1 &= (0.4612 + 0.5972\alpha + 0.7466\alpha^2 + 2.2131\alpha^3)/(1-\alpha)^{3/2} \\ D_2 &= (-0.2537 + 0.4353\alpha - 0.2851\alpha^2 - 0.5853\alpha^3)/(1-\alpha)^{3/2} \end{aligned} \tag{11.2.8}$$

By consideration of the total x-stress (crack contribution and x-stress component in the un-cracked body), one can compute the biaxiality ratio according to eq.(2.12)

The T-stress and the stress intensity factor result in the biaxiality ratio β which is shown as curve in Fig. 11.2.3.

In addition to the Green's function computations, the biaxiality ratios were directly determined with the Boundary Collocation method (BCM) which provides the coefficients A_0, A^*_0 and by eq.(2.13) the quantity β for the situation of diametrical loading. The results are entered as circles. An excellent agreement is obvious between the BCM results and those obtained from the Green's function representation. This is an indication of an adequate description of the Green's function by the set-up eq.(3.2.19) using only one regular term.

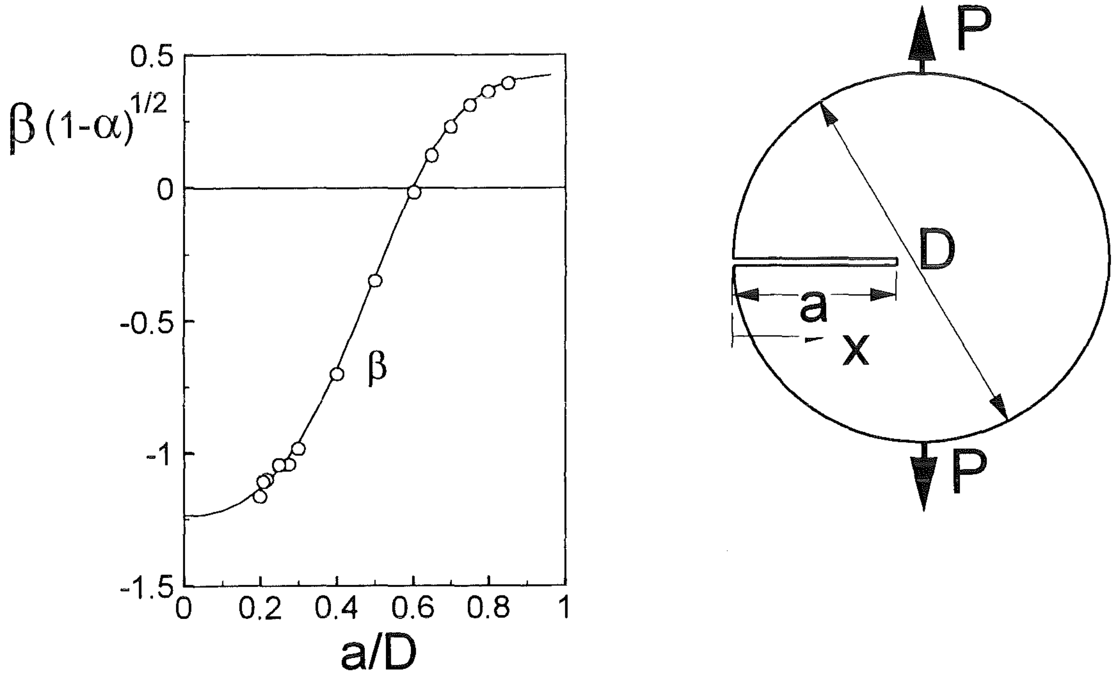

Fig. 11.2.3 Biaxiality ratio for an edge-cracked circular disk diametrically loaded by a pair of forces; lines: eq.(11.2.5), circles: BCM-results.

a/D	$T(1-a/D)^2$	$\beta(1-a/D)^{1/2}$
0	0	-1.236
0.1	-0.364	-1.216
0.2	-0.732	-1.134
0.3	-0.970	-0.960
0.4	-0.915	-0.682
0.5	-0.526	-0.333
0.6	0.007	0.004
0.7	0.430	0.245
0.8	0.652	0.370

Table 11.2.1 T-stress and biaxiality ratio for Fig 11.2.3.

11.2.2 Brazilian disk (edge-cracked)

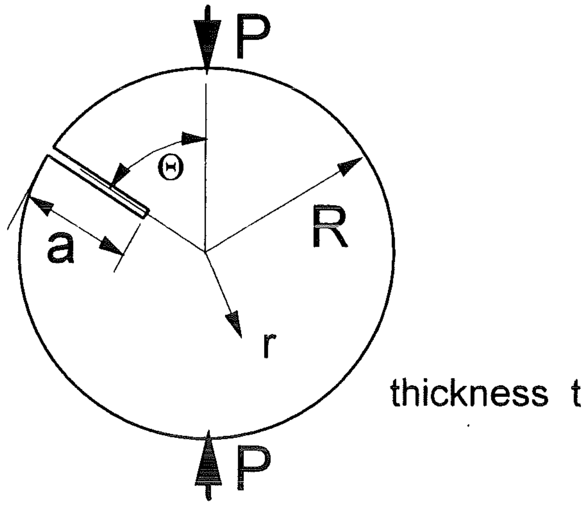

Fig. 11.2.4 Brazilian disk test with edge-cracked disk.

The circumferential stress component in an uncracked Brazilian disk (Fig.11.2.4) has been given by Erdlac (quoted in [22]) as

$$\sigma_\varphi = \sigma_n = \frac{2P}{\pi t R}\left[\frac{1}{2} - \frac{(1-\rho\cos\Theta)\sin^2\Theta}{(1+\rho^2-2\rho\cos\Theta)^2} - \frac{(1+\rho\cos\Theta)\sin^2\Theta}{(1+\rho^2+2\rho\cos\Theta)^2}\right], \quad \rho = r/R \qquad (11.2.9)$$

Using eq.(11.2.2) the T-stress can be determined. The T-stress term, evaluated for several relative crack depths a/W and several angles Θ is compiled in Tables 11.2.1 and 11.2.2 and the biaxiality ratio in Table 11.2.3.

$\alpha=a/2R$	$\Theta=\pi/16$	$\pi/8$	$\pi/4$	$3\pi/8$	$7\pi/16$	$\pi/2$
0	0	0	0	0	0	0
0.05	2.671	1.086	0.359	0.215	0.191	0.184
0.1	0.933	1.466	0.715	0.460	0.415	0.401
0.2	-1.687	0.194	1.068	0.979	0.937	0.922
0.3	-2.319	-1.099	0.691	1.328	1.428	1.456
0.4	-2.546	-1.824	-0.078	1.235	1.577	1.691
0.5	-2.744	-2.310	-0.896	0.518	0.952	1.104
0.6	-3.050	-2.814	-1.906	-1.153	-0.959	-0.894
0.65	-3.290	-3.163	-2.727	-2.637	-2.662	-2.675
0.7	-3.637	-3.683	-4.085	-4.911	-5.196	-5.297

Table 11.2.1 T-stress T_c/σ^* for the Brazilian disk test ($\sigma^*=P/(\pi Rt)$).

For the determination of the total x-stress at the crack tip (i.e. the determination of T from T_c) the radial stress component has to be included, which was also derived by Erdlac

$$\sigma_r = \frac{2P}{\pi t R}\left[\frac{1}{2} - \frac{(1-\rho\cos\Theta)(\cos\Theta-\rho)^2}{(1+\rho^2-2\rho\cos\Theta)^2} - \frac{(1+\rho\cos\Theta)(\cos\Theta+\rho)^2}{(1+\rho^2+2\rho\cos\Theta)^2}\right] \tag{11.2.10}$$

$\alpha = a/2R$	$\Theta = \pi/16$	$\pi/8$	$\pi/4$	$3\pi/8$	$7\pi/16$	$\pi/2$
0	0.000	0.000	0.000	0.000	0.000	0.000
0.05	1.858	1.067	0.376	0.227	0.203	0.195
0.1	-1.979	1.097	0.760	0.511	0.464	0.449
0.15	-4.587	-0.044	1.015	0.837	0.784	0.766
0.2	-5.482	-1.470	1.020	1.172	1.152	1.143
0.25	-5.669	-2.610	0.743	1.467	1.543	1.561
0.3	-5.633	-3.383	0.252	1.670	1.910	1.981
0.35	-5.556	-3.888	-0.337	1.737	2.192	2.337
0.4	-5.508	-4.231	-0.922	1.643	2.317	2.543
0.45	-5.515	-4.493	-1.445	1.380	2.210	2.497
0.5	-5.592	-4.725	-1.896	0.932	1.799	2.104
0.55	-5.752	-4.959	-2.305	0.257	1.017	1.282
0.6	-6.012	-5.221	-2.750	-0.746	-0.219	-0.042
0.65	-6.399	-5.539	-3.389	-2.251	-2.041	-1.979
0.7	-6.950	-5.968	-4.524	-4.569	-4.714	-4.773
0.75	-7.735	-6.663	-6.746	-8.316	-8.844	-9.029

Table 11.2.2 T-stress T/σ^* for the Brazilian disk test ($\sigma^* = P/(\pi t R)$).

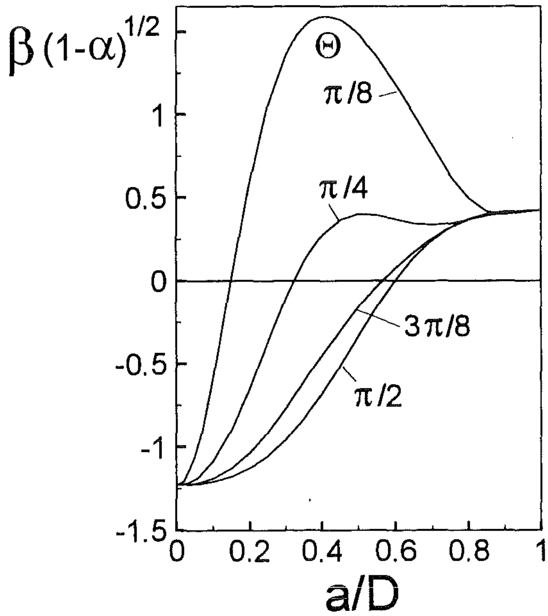

Fig. 11.2.5 Brazilian disk test with an edge-cracked disk and biaxiality ratio $\beta(1-\alpha)^{1/2}$, $\alpha = a/D$.

$\alpha = a/2R$	$\Theta = \pi/16$	$\pi/8$	$\pi/4$	$3\pi/8$	$7\pi/16$	$\pi/2$
0	-1.228	-1.228	-1.228	-1.228	-1.228	-1.228
0.05	-0.608	-1.062	-1.196	-1.220	-1.224	-1.225
0.1	0.549	-0.594	-1.087	-1.188	-1.204	-1.209
0.15	1.446	0.019	-0.900	-1.127	-1.166	-1.178
0.2	1.995	0.600	-0.651	-1.036	-1.106	-1.128
0.25	2.301	1.053	-0.372	-0.914	-1.021	-1.054
0.3	2.455	1.358	-0.104	-0.769	-0.910	-0.955
0.35	2.510	1.529	0.118	-0.610	-0.776	-0.830
0.4	2.500	1.591	0.276	-0.449	-0.622	-0.679
0.45	2.440	1.570	0.367	-0.297	-0.457	-0.510
0.5	2.342	1.486	0.400	-0.158	-0.289	-0.332
0.55	2.209	1.354	0.394	-0.034	-0.127	-0.156
0.6	2.043	1.190	0.369	0.076	0.021	0.004
0.65	1.843	1.005	0.345	0.173	0.147	0.139
0.7	1.608	0.814	0.334	0.255	0.247	0.245
0.75	1.337	0.636	0.343	0.320	0.320	0.321
1	0.423	0.423	0.423	0.423	0.423	0.423

Table 11.2.3 Biaxiality ratio $\beta(1\text{-}a/D)^{1/2}$ for the Brazilian disk test.

11.2.3 Disk with thermal stresses

In a thermally loaded circular disk the stresses in the absence of a crack consist of the circumferential stress component σ_φ and of the radial stress distribution σ_r. The two stress components can be computed from the temperature distribution $\Theta(r)$ with $r = D/2\text{-}x$ (see e.g. [31])

$$\sigma_r = \alpha_T E \left(\frac{1}{R^2} \int_0^R \Theta\, r\, dr - \frac{1}{r^2} \int_0^r \Theta\, r\, dr \right) \tag{11.2.11}$$

$$\sigma_\varphi = \alpha_T E \left(\frac{1}{R^2} \int_0^R \Theta\, r\, dr + \frac{1}{r^2} \int_0^r \Theta\, r\, dr - \Theta \right) \tag{11.2.12}$$

with the thermal expansion coefficient α_T. The temperatures found e.g. in [29] can be expressed by

$$\Theta(r) = \Theta_0 \left[1 + B_2 \left(\frac{r}{R} \right)^2 + B_4 \left(\frac{r}{R} \right)^4 \right] \tag{11.2.13}$$

with the maximum temperature occurring in the centre of the disk ($r = 0$). The related stresses are given by

$$\sigma_\varphi = \alpha_T E \Theta_0 \left[\frac{1}{4} B_2 + \frac{1}{6} B_4 - \frac{3}{4} B_2 \left(\frac{r}{R} \right)^2 - \frac{5}{6} B_4 \left(\frac{r}{R} \right)^4 \right] \tag{11.2.14}$$

$$\sigma_r = \alpha_T E \Theta_0 \left[\frac{1}{4} B_2 \left(1 - \frac{r^2}{R^2} \right) + \frac{1}{6} B_4 \left(1 - \frac{r^4}{R^4} \right) \right] \tag{11.2.15}$$

For a typical stress distribution in a thermally heated disk one can conclude from curves plotted in [29]

$$\sigma_\varphi = -\sigma^* \left[1 - \frac{9}{2} \left(\frac{r}{R} \right)^2 + \frac{5}{2} \left(\frac{r}{R} \right)^4 \right] \tag{11.2.16}$$

$$\sigma_r = -\sigma^* \left[1 - \frac{3}{2} \left(\frac{r}{R} \right)^2 + \frac{1}{2} \left(\frac{r}{R} \right)^4 \right] \tag{11.2.17}$$

where σ^* is the circumferential tensile stress at $r = R$. The stresses are and shown in Fig. 11.2.6.

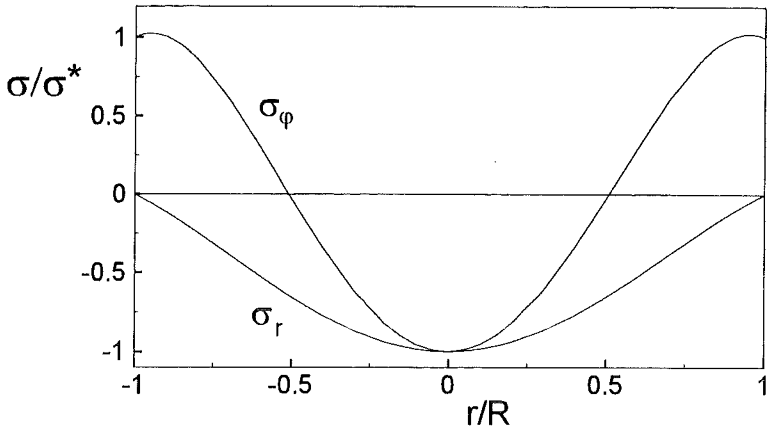

Fig. 11.2.6 Stress distributions in a thermally heated disk.

When eq.(11.2.2) is used, the thermal stresses result in the T-stress

$$T_c \cong -0.15801\sigma^* \left[2\left(\frac{a}{R}\right)^2 - 4\frac{a}{R} - 3\right] - \sigma_y\Big|_{x=a} \tag{11.2.18}$$

Including the σ_x-stress, present already in the uncracked disk, it results with eq.(2.11)

$$\frac{T}{\sigma^*} = \frac{T_c}{\sigma^*} + \frac{\sigma_r}{\sigma^*}\Big|_{x=a} \tag{11.2.19}$$

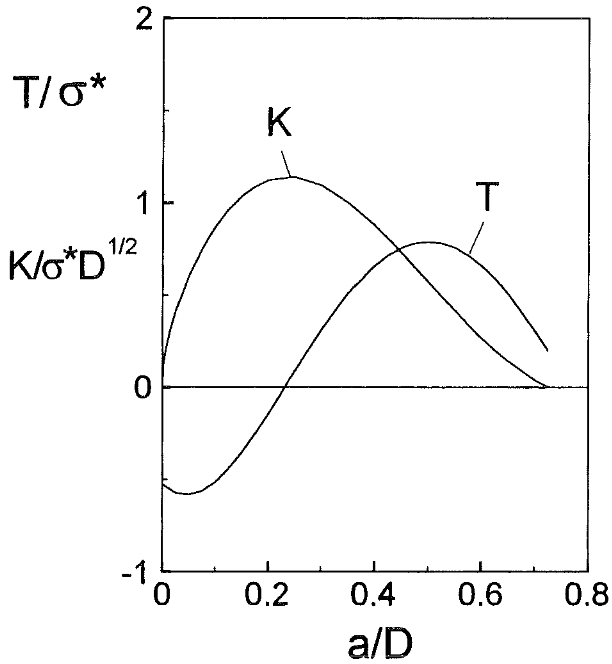

Fig. 11.2.7 Stress intensity factor and T-stress for a disk under thermal loading.

The two T-stresses are plotted in Fig. 11.2.7 together with the stress intensity factor computed with the weight function for the edge-cracked disk.

The biaxiality ratio β, defined by eq.(2.12), is plotted in Fig. 11.2.8. Very high β-values occur for $a/D > 0.6$. The main reason is the very small stress intensity factor which disappears at approximately $a/D = 0.7$.

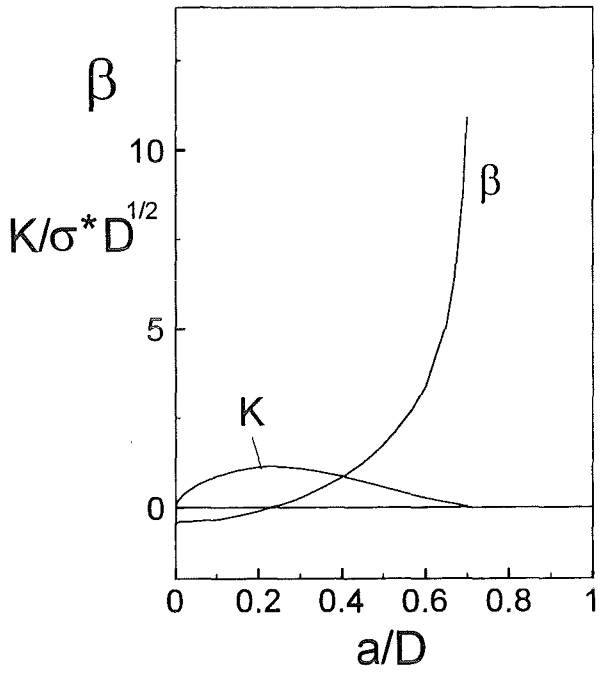

Fig. 11.2.8 Stress intensity factor K and biaxiality ratio β for the edge-cracked disk under thermal loading.

12 Cracks ahead of notches

Special specimens contain narrow notches which are introduced in order to simulate a starter crack. This is for instance the case in fracture toughness experiments carried out on ceramics. A plate with a slender edge notch of depth a_0 is considered. A small crack of length ℓ is assumed to occur directly at the notch root with the radius R. The geometrical data are illustrated in Fig. 12.1.

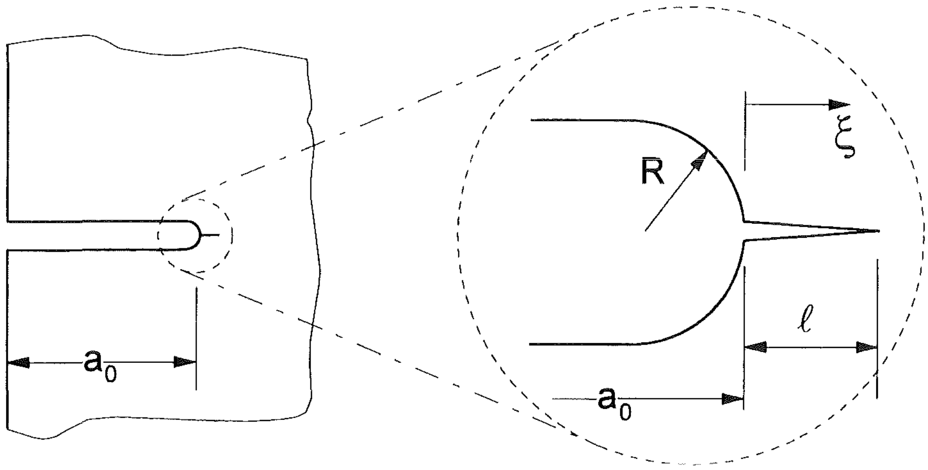

Fig. 12.1 A small crack emanating from the root of a notch.

In the absence of a crack the stresses near the notch root are given by

$$\sigma_y = \frac{2K(a_0)}{\sqrt{\pi(R+2\xi)}}\frac{R+\xi}{R+2\xi} \tag{12.1}$$

$$\sigma_x = \frac{2K(a_0)}{\sqrt{\pi(R+2\xi)}}\frac{\xi}{R+2\xi} \tag{12.2}$$

(for ξ see Fig. 12.1) as shown by Creager and Paris [32]. The quantity $K(a_0)$ is the stress intensity factor of a crack with same length a_0 as the notch under identical external load

$$K(a_0) = \sigma^* F(a_0)\sqrt{\pi a_0} \tag{12.3}$$

with the characteristic stress σ^* and the geometric function F. The stresses resulting from eqs.(12.1) and (12.2) are plotted in Fig. 12.2. The solid parts of the curves represent the region ($0 \le \xi \le R/2$) where higher order terms are negligible. A small crack of length ℓ is considered which emanates from the notch root (Fig. 12.1).

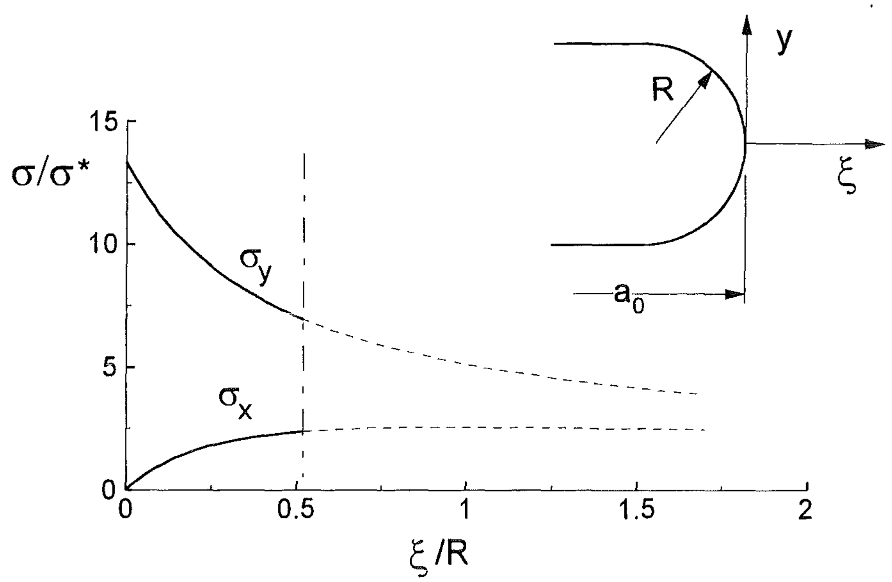

Fig. 12.2 Stresses ahead of a slender notch computed according to Creager and Paris [32] for $a_0/W = 0.5$ and $R/W = 0.025$.

Under externally applied load the coefficients of the stress function were calculated with BCM applying the outer fiber bending stress as the reference stress, i.e.

$$\sigma^* = \sigma_b = \frac{6M}{W^2 t} \tag{12.4}$$

with specimen width W, thickness t and bending moment M. The coefficient A_0 is related to the stress intensity factor K_I by

$$K_I = \sigma^* F(\ell)\sqrt{\pi \ell}\,, \quad F(\ell) = \sqrt{18W/\ell}\, A_0 \tag{12.5}$$

with the geometric function F. The T-term T, eq.(2.11), results directly from the coefficient A^*_0. In Fig. 12.3 the term T is plotted versus a/W the relative for several notch depths a_0. Additionally, the "long crack solution" given by eq.(10.2.1) is introduced as solid curve. This curve represents the T-stress for an edge crack of total length $a = a_0 + \ell$.

Results obtained under tensile loading are plotted in Fig. 12.4. In this case the characteristic stress is identical with the remote tensile stress σ_0, i.e. $\sigma^* = \sigma_0$. In this representation the solid line is described by eq.(10.1.1).

For the limit case $\ell/R \to 0$ the T-stress can be determined from the solution for a small crack in a semi-infinite plate with a tensile stress identical with the maximum normal stress σ_{max} occurring directly at the notch root

$$\sigma_{max} = 2\sigma^* F(a_0)\sqrt{\frac{a_0}{R}} \tag{12.6}$$

Directly at the free surface ($\xi = 0$) it holds $\sigma_x = 0$ and, therefore, $T_c = T$ for $\ell/R \to 0$. It can be concluded

$$T_0 = T_{\ell/R\to 0} = \left.\frac{T_{plate}}{\sigma^*}\right|_{\alpha\to 0} \sigma_{max} \tag{12.7}$$

$$\left.\frac{T_{plate}}{\sigma^*}\right|_{\alpha\to 0} = -4(A^*_0)_{plate,\alpha\to 0} = -0.526 \tag{12.8}$$

and, consequently,

$$\frac{T_0}{\sigma^*} = -1.052\,F(a_0)\sqrt{\frac{a_0}{R}} \tag{12.9}$$

It becomes obvious from eq.(12.9) that for slender notches very strong compressive T-stresses occur in the limit case $\ell/R \to 0$. The limit values T_0 for tension and bending, indicated by the arrows in Figs. 12.3 and 12.4, are entered in Table 12.1.

In Fig. 12.5 both the bending and the tensile results are plotted in a normalised representation. From Fig. 12.5b we can conclude that the deviation between the T-stress term for the crack/notch configuration and the long-crack solution T^* (with the crack assumed to have the total length $a_0+\ell$) is negligible for $\ell/R > 1$. The drastic decrease in T for $\ell/R \to 0$ must occur within the range $0 < \ell/R < 0.2$.

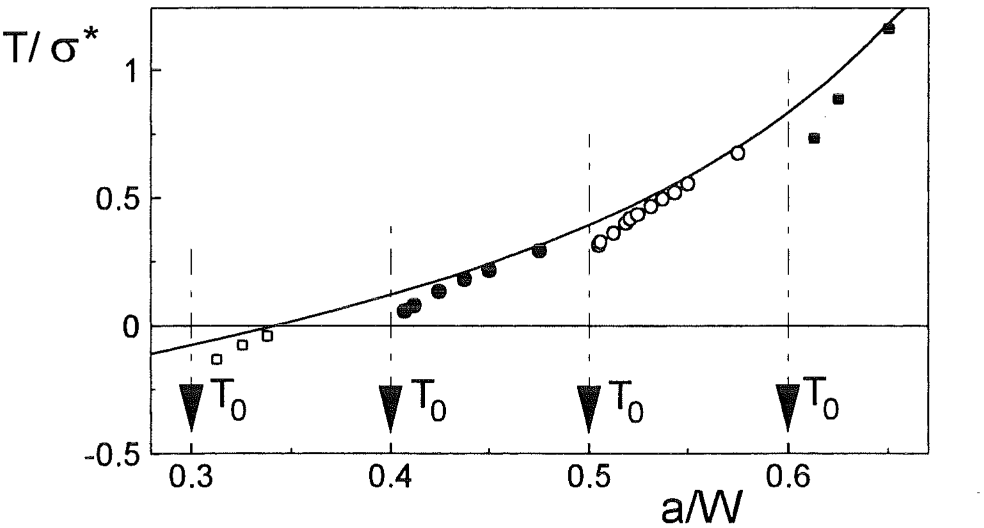

Fig. 12.3 T-stress for a small crack ahead of a slender notch in bending, computed with the Boundary Collocation Method for $R/W = 0.025$. Solid line: long-crack solution.

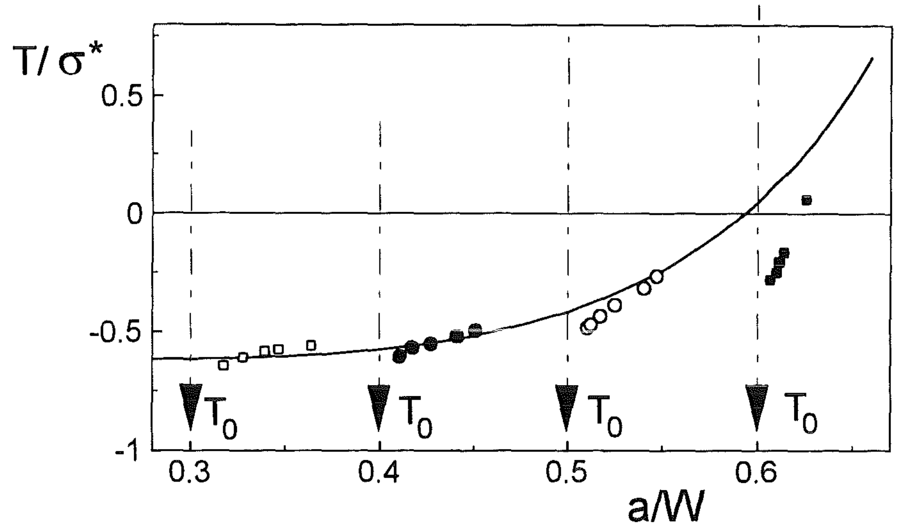

Fig. 12.4 T-stress for a small crack ahead of a slender notch in tension, computed with the Boundary Collocation Method for $R/W = 0.025$. Solid line: long-crack solution.

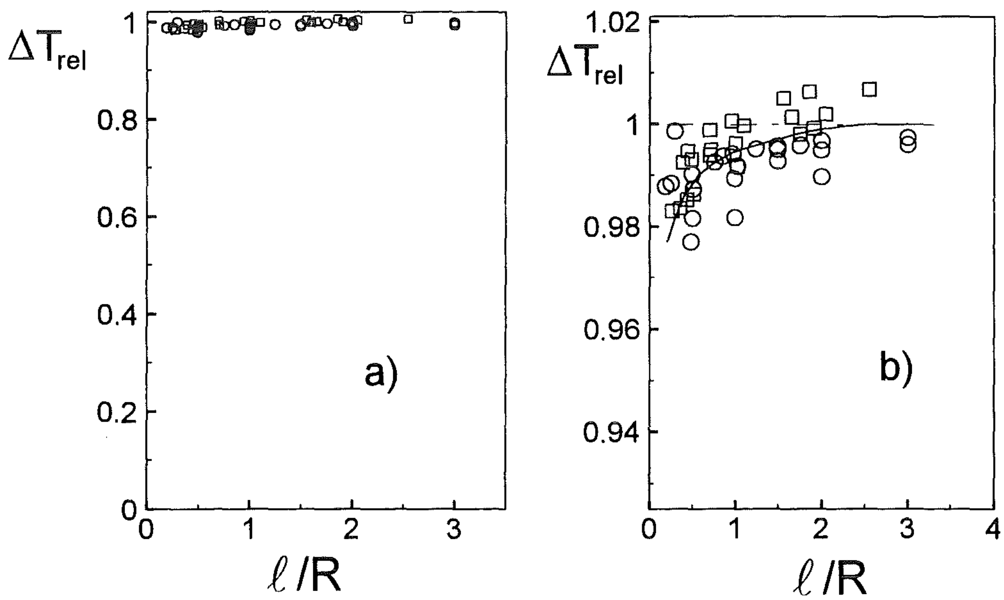

Fig. 12.5 T-stress in a normalised representation $\Delta T_{rel} = (T-T_0)/(T^*-T_0)$, T^* = long-crack solution; circles: tension, squares: bending.

a/W	T_0/σ^* (bending)	T_0/σ^* (tension)
0.3	-4.11	-6.05
0.4	-5.28	-8.91
0.5	-7.01	-13.31
0.6	-9.86	-20.74

Table 12.1 Limit values for the T-stress term ($\ell/R \to 0$).

13 Double-edge-cracked plate

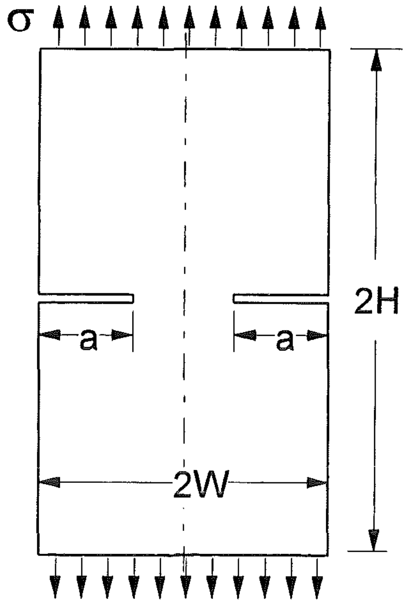

Fig. 13.1 Double-edge-cracked rectangular plate

T-stresses for the Double-edge notched rectangular plate (Fig. 13.1) are compiled in Table 13.1.

α=a/W	H/W=1.5	1.25	1.00	0.75	0.50	0.35
0.0	-0.526	-0.526	-0.526	-0.526	-0.526	-0.526
0.1	-0.530	-0.530	-0.530			
0.2	-0.532	-0.528	-0.527			
0.3	-0.532	-0.520	-0.512	-0.473	-0.257	0.293
0.4	-0.528	-0.504	-0.440	-0.282	0.256	1.546
0.5	-0.522	-0.464	-0.316	0.045	1.058	3.135
0.6	-0.510	-0.409	-0.153	0.483	2.202	5.24
0.7	-0.4932	-0.32	0.023	0.969	3.68	8.13

Table 13.1 T-stress T/σ for the Double-edge-cracked plate in tension.

Stress intensity factors, defined by

$$K_I = \sigma F \sqrt{\pi a}\ , \quad F' = F(1 - a/W)^{1/2} \tag{13.1}$$

are compiled in Table 13.2 and the biaxiality ratios β are given in Table 13.3.

a/W	L/W=1.5	1.25	1.0	0.75	0.50	0.35
0	1.1215	1.1215	1.1215	1.1215	1.1215	1.1215
0.3	0.94	0.96	1.029	1.18	1.496	1.891
0.4	0.8891	0.9197	0.9946	1.1926	1.646	2.196
0.5	0.8389	0.8659	0.9427	1.1537	1.719	2.437
0.6	0.7900	0.8135	0.8760	1.0597	1.6529	2.535
0.7	0.7420	0.7492	0.8029	0.9297	1.4142	2.46
1.0	0.6366	0.6366	0.6366	0.6366	0.6366	0.6366

Table 13.2 Geometric function F_I'.

For a long plate (H/W=1.5) the T-stress term and the biaxiality ratio may be approximated by

$$\frac{T}{\sigma} = \frac{-0.526 + 0.4672\alpha + 0.1844\alpha^2 - 0.1153\alpha^3}{1-\alpha} \tag{13.2}$$

$$\beta = \frac{-0.469 + 0.14067\alpha + 0.35646\alpha^2 - 0.00986\alpha^3}{\sqrt{1-\alpha}} \tag{13.3}$$

and for the quadratic plate (H/W=1)

$$T/\sigma = -0.526 + 0.1804\alpha - 2.7241\alpha^2 + 9.5966\alpha^3 - 6.3883\alpha^4 \tag{13.4}$$

$$\beta = -0.469 + 0.1229\alpha - 1.2256\alpha^2 + 6.0628\alpha^3 - 4.4983\alpha^4 \tag{13.5}$$

α=a/W	H/W=1.5	1.25	1.00	0.75	0.50	0.35
0.0	-0.469	-0.469	-0.469	-0.469	-0.469	-0.469
0.1	-0.475	-0.470	-0.464			
0.2	-0.476	-0.465	-0.451			
0.3	-0.472	-0.453	-0.416	-0.336	-0.144	0.174
0.4	-0.460	-0.425	-0.343	-0.183	0.120	0.545
0.5	-0.440	-0.379	-0.237	0.028	0.435	0.910
0.6	-0.408	-0.318	-0.110	0.288	0.842	1.307
0.7	-0.364	-0.228	0.016	0.571	1.424	1.903

Table 13.3 Biaxiality ratio β for the double-edge-cracked plate in tension.

Results of Table 13.2 are compared in Fig. 13.2 with data from the literature (Kfouri [6]). Differences of less than 0.01 were found, i.e. an excellent agreement can be stated. Further coefficients of the Williams stress function are listed in Tables 13.4 and 13.5.

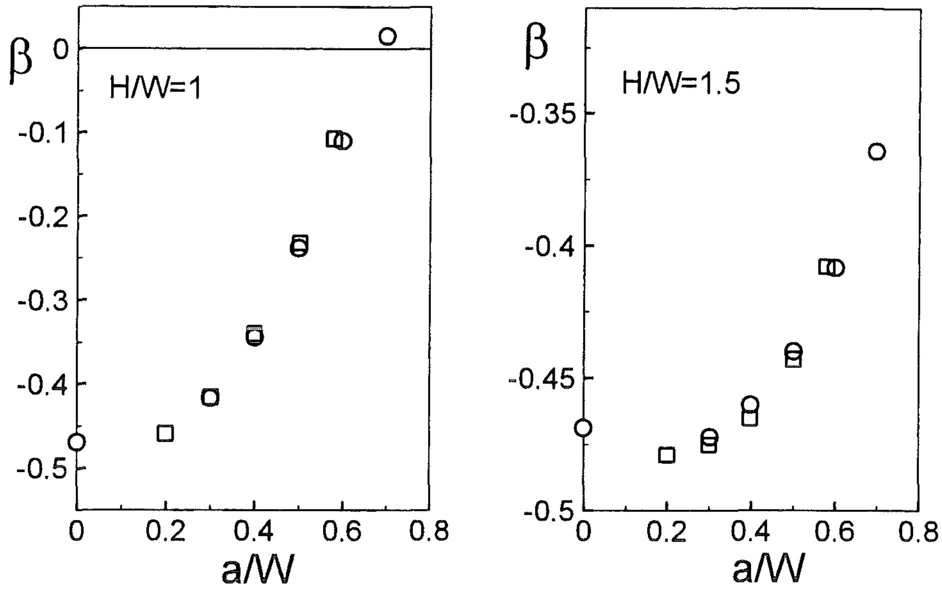

Fig. 13.2 Comparison of results with available data from literature. Circles: Table 13.2, squares: Kfouri [6].

$\alpha=a/W$	H/W=1.5	1.25	1.00	0.75	0.50
0.3	-0.045	-0.043	-0.0362	-0.0192	0.0441
0.4	-0.0416	-0.0371	-0.0237	0.0147	0.1395
0.5	-0.0414	-0.0339	-0.0118	0.0522	0.2591
0.6	-0.0454	-0.0277	-0.0053	0.0840	0.3936
0.7	-0.0591	-0.0457	-0.0110	0.0956	0.5074

Table 13.4 Coefficient A_1 for the Double-edge-cracked plate in tension.

$\alpha=a/W$	H/W=1.5	1.25	1.00	0.75	0.50
0.3	0.1555	0.148	0.1208	0.0771	-0.0509
0.4	0.1086	0.0911	0.0489	-0.0382	-0.1991
0.5	0.0759	0.0505	-0.0099	-0.1384	-0.3478
0.6	0.0515	0.0014	-0.0496	-0.2157	-0.5472
0.7	0.0356	0.0039	-0.0671	-0.2510	-0.7722

Table 13.5 Coefficient A^*_1 for the Double-edge-cracked plate in tension.

In order to evaluate arbitrary stress distributions in the uncracked plate a weight function for stress intensity factors, see eq.(3.1.1a), is given according to the representation

$$h=\sqrt{\frac{2}{\pi a}}\left(\frac{1}{\sqrt{1-\rho}}+D_0\sqrt{1-\rho}+D_1(1-\rho)^{3/2}\right),\quad \rho=x/a \tag{13.6}$$

with the coefficients D_0, D_1 listed in Tables 13.8 and 13.9.

α=a/W	0.25	0.50	1.00
0.3	0.541	0.0447	-0.0173
0.4	-1.867	0.007	0.0026
0.5	-3.24	-0.061	0.0023
0.6	-4.43	-0.158	-0.022
0.7	-5.54	-0.372	-0.083

Table 13.5 Coefficient A_2.

α=a/W	0.25	0.50	1.00
0.3	3.37	-0.096	-0.244
0.4	5.90	0.203	-0.142
0.5	8.50	0.390	-0.075
0.6	10.48	0.497	-0.017
0.7	11.45	0.661	0.036

Table 13.6 Coefficient A^*_2.

a/W	L/W=0.35	0.50	0.75	1.00	1.50
0	0.585	0.584	0.584	0.584	0.584
0.3	3.75	2.43	1.403	0.932	0.614
0.4	4.91	3.26	1.777	1.085	0.720
0.5	6.46	3.93	2.004	1.252	0.879
0.6	8.14	4.29	2.12	1.478	1.160
0.7	9.62	4.05	2.33	1.88	1.494

Table 13.8 Coefficient D_0 for eq.(13.6).

a/W	L/W=0.35	0.50	0.75	1.00	1.50
0	0.256	0.256	0.256	0.256	0.256
0.3	1.303	0.953	0.552	0.302	0.216
0.4	2.56	1.48	0.624	0.335	0.178
0.5	3.37	2.05	0.739	0.325	0.134
0.6	3.71	2.43	0.787	0.243	0.01
0.7	3.95	2.83	0.557	0.024	0.034

Table 13.9 Coefficient D_1 for eq.(13.6).

14 Double-edge-cracked circular disk

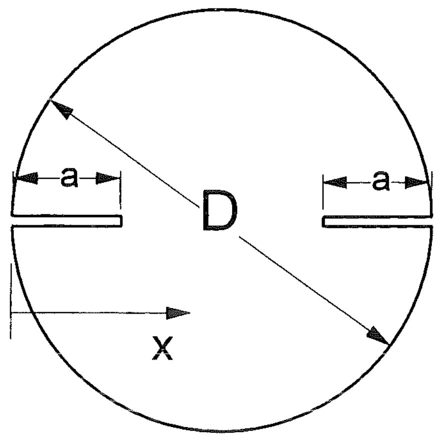

Fig. 14.1 Double-edge-cracked disk.

Figure 14.1 shows the double-edge-cracked disk. The T-stress under loading by constant circumferential normal tractions σ_n is shown in Fig. 14.2 together with the biaxiality ratio β. In contrast to the single-edge-cracked disk the relative crack length is defined here by $\alpha = a/R$ ($R = D/2$).

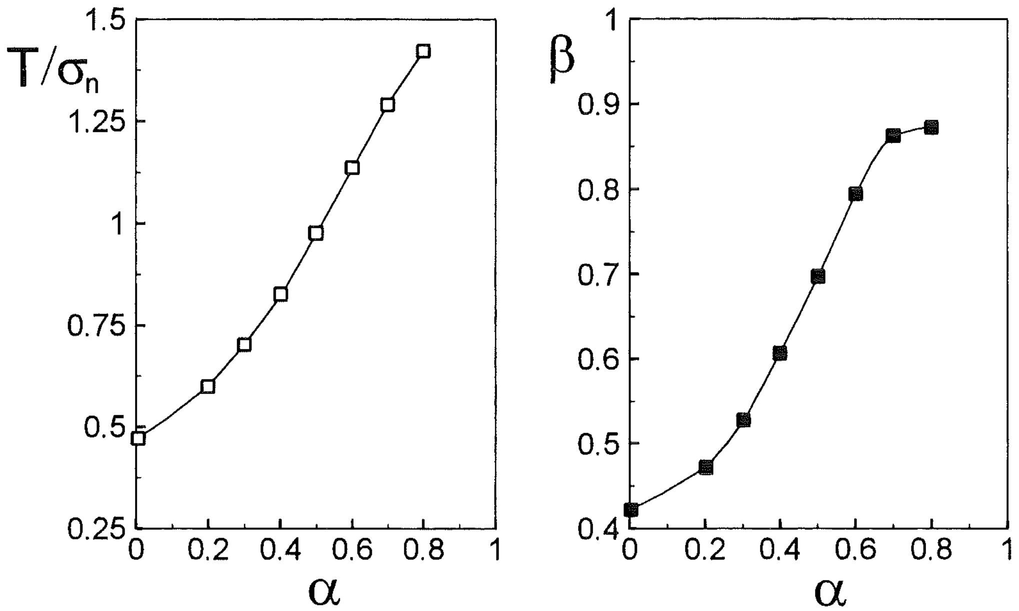

Fig. 14.2 T-stress and biaxiality ratio for the double-edge-cracked circular disk under circumferential normal tractions.

α	T/σ_n	β	$a \cdot C$
0	0.474	0.423	0.9481
0.2	0.599	0.472	1.199
0.3	0.702	0.528	1.405
0.4	0.829	0.604	1.658
0.5	0.977	0.698	1.954
0.6	1.136	0.795	2.273
0.7	1.290	0.865	2.580
0.8	1.425	0.873	2.850

Table 14.1 T-stress, biaxiality ratio and coefficient for the Green's function. Loading: constant circumferential normal tractions.

The T-stress, entered into Table 14.1, can be expressed by

$$\frac{T}{\sigma_n} = 0.474 + 0.4022\alpha + 0.9104\alpha^2 + 1.4406\alpha^3 - 1.6874\alpha^4 \tag{14.1}$$

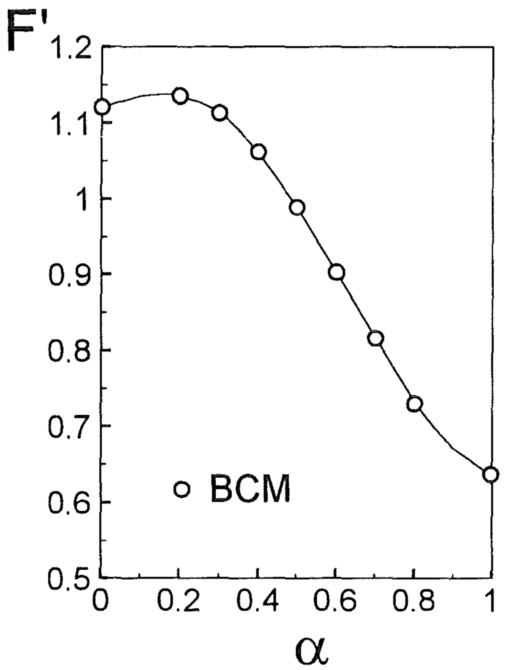

Fig. 14.3 Geometric function F' for the Double-edge-cracked disk.

The geometric function F for the stress intensity factor is

$$K = \sigma_n F\sqrt{\pi a} \quad , \quad F' = F\sqrt{1-\alpha} \; , \tag{14.2}$$

with the geometric function shown in Fig. 14.3 and approximated by

$$F = \frac{1.1215 + 0.2746\alpha - 0.7959\alpha^2 - 1.1411\alpha^3 + 1.1776\alpha^4}{\sqrt{1-\alpha}} \tag{14.3}$$

For the Green's function under symmetrical loading the same set-up is chosen as used for single-edge-cracked components, namely, expressed in the integrated form

$$T = C\int_0^a (1 - x/a)\sigma_y(x)dx - \sigma_y\Big|_{x=a} \tag{14.4}$$

with the parameter C entered into Table 14.1 and fitted for $\alpha \le 0.8$ by the polynomial

$$C = \frac{1}{a}(0.9481 + 0.8043\alpha + 1.8207\alpha^2 + 2.8813\alpha^3 - 3.3747\alpha^4) \tag{14.5}$$

A weight function for the computation of related stress intensity factors according to eq.(3.1.1a) is given by

$$h = \sqrt{\frac{2}{\pi a}}\left(\frac{1}{\sqrt{1-\rho}} + D_0\sqrt{1-\rho} + D_1(1-\rho)^{3/2} + D_2(1-\rho)^{5/2}\right), \quad \rho = x/a \tag{14.6}$$

with coefficients compiled in Table 14.2. This weight function is appropriate for symmetric loading at both single edge cracks.

α	D_0	D_1	D_2
0	0.4501	0.7000	-0.3100
0.1	0.7167	0.6860	-0.2894
0.2	0.9396	0.6932	-0.2760
0.3	1.1157	0.7058	-0.2668
0.4	1.2549	0.6998	-0.2563
0.5	1.3890	0.6344	-0.2343
0.6	1.5957	0.4227	-0.1782
0.7	2.0673	-0.1587	-0.0304

Table 14.2 Coefficients for weight function eq.(14.6).

15 Double-edge-cracked Brazilian disk

The Brazilian disk test with a double-edge-cracked circular disk is illustrated by Fig. 15.1.

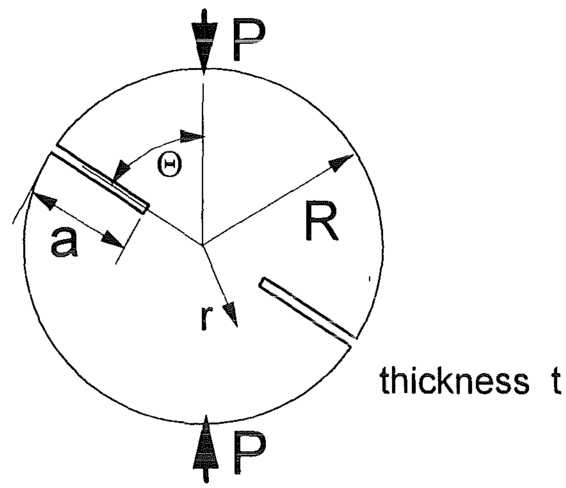

Fig. 15.1 Brazilian disk test with double-edge-cracked specimen.

Using the Green's function and the stress distribution given by eqs.(11.2.20) and (11.2.11) the T-stress was computed for the Brazilian disk test with double-edge-cracked disks. Tables 15.1 and 15.2 contain the data for several angles Θ (see Fig. 15.1).

$\alpha=a/R$	$\Theta=\pi/32$	$\pi/16$	$\pi/8$	$\pi/4$	$3\pi/8$	$7\pi/16$	$\pi/2$
0	0	0	0	0	0	0	0
0.1	2.400	2.671	1.086	0.359	0.215	0.191	0.184
0.2	-1.946	0.900	1.453	0.711	0.458	0.413	0.399
0.3	-2.951	-0.917	0.0942	0.958	0.711	0.656	0.639
0.4	-3.185	-1.884	0.081	1.018	0.946	0.907	0.893
0.5	-3.226	-2.370	-0.716	0.867	1.129	1.142	1.143
0.6	-3.190	-2.610	-1.317	0.557	1.229	1.336	1.367
0.7	-3.100	-2.703	-1.72	0.177	1.232	1.459	1.531
0.8	-2.955	-2.688	-1.95	-0.179	1.148	1.493	1.608

Table 15.1 T-stress T_c/σ^* for the Brazilian disk test ($\sigma^*=P/(\pi R t)$).

$\alpha=a/R$	$\Theta=\pi/32$	$\pi/16$	$\pi/8$	$\pi/4$	$3\pi/8$	$7\pi/16$	$\pi/2$
0	0	0	0	0	0	0	0
0.1	-3.075	1.859	1.076	0.376	0.227	0.203	0.195
0.2	-8.879	-2.012	1.084	0.756	0.509	0.462	0.447
0.3	-8.773	-4.696	-0.096	0.995	0.825	0.773	0.756
0.4	-8.009	-5.678	-1.584	0.969	1.139	1.123	1.114
0.5	-7.348	-5.934	-2.788	0.649	1.403	1.484	1.504
0.6	-6.833	-5.924	-3.601	0.118	1.571	1.818	1.891
0.7	-6.42	-5.81	-4.10	-0.484	1.62	2.08	2.23
0.8	-6.07	-5.65	-4.36	-1.02	1.56	2.23	2.46

Table 15.2 T-stress T/σ^* for the Brazilian disk test ($\sigma^*=P/(\pi Rt)$).

Mode-I stress intensity factors computed with the weight function eq.(14.6) and expressed by the geometric function F are entered in Table 15.3. The geometric function F is defined by

$$K=\sigma^* F\sqrt{\pi a} \quad , \quad \sigma^*=P/(\pi Rt) \tag{15.1}$$

$\alpha=a/R$	$\Theta=\pi/32$	$\pi/16$	$\pi/8$	$\pi/4$	$3\pi/8$	$7\pi/16$	$\pi/2$
0	0	0	0	0	0	0	0
0.1	-6.189	-2.953	-0.970	-0.304	-0.180	-0.160	-0.154
0.2	-4.105	-3.312	-1.709	-0.648	-0.399	-0.357	-0.344
0.3	-2.728	-2.680	-1.989	-0.987	-0.652	-0.590	-0.571
0.4	-1.901	-2.044	-1.927	-1.274	-0.927	-0.854	-0.832
0.5	-1.343	-1.541	-1.713	-1.479	-1.212	-1.145	-1.127
0.6	-0.934	-1.153	-1.469	-1.607	-1.500	-1.459	-1.445
0.7	-0.615	-0.855	-1.263	-1.705	-1.809	-1.817	-1.817

Table 15.3 Stress intensity factor represented by geometric function F for the Brazilian disk test.

III RESULTS FOR MIXED BOUNDARY CONDITIONS

The following sections contain numerical solutions for the T-stress term for plates which are loaded at the ends by prescribed displacements. The problems are subdivided in:

- Single-edge-cracked components,
  - rectangular plates under constant displacement v
  - rectangular plates under bending displacement v
  - rectangular plates under constant displacements u and v.
- Double-edge-cracked plate,
  - rectangular plate under constant displacement v
  - rectangular plate under constant displacements u and v.
- Internally cracked plate,
  - rectangular plate under constant displacement v
  - rectangular plate under constant displacements u and v.

16 Array of deep edge cracks

Figure 16.1 shows an array of periodical edge cracks. BCM-computations were performed for an element of periodicity for the special case of a constant remote tensile stress σ. The boundary conditions are given by constant displacements v and disappearing shear stresses along the symmetry lines, i.e.

$$v = \frac{\sigma}{E'}\frac{d}{2}\,; \quad \tau_{xy} = 0 \text{ for } y = \pm d/2 \tag{16.1}$$

($E' = E$ for plane stress and $E' = E/(1-\nu^2)$ for plane strain, E = Young's modulus, ν = Poisson's ratio) as illustrated in Fig. 16.2. The coefficient A^*_0 is shown in Fig. 16.3a as a function of the ratio d/a for different relative crack lengths $\alpha = a/W$. The result can be summarised as

$$A^*_0 = 0.148\ , \quad d/a \le 1.5 \tag{16.2}$$

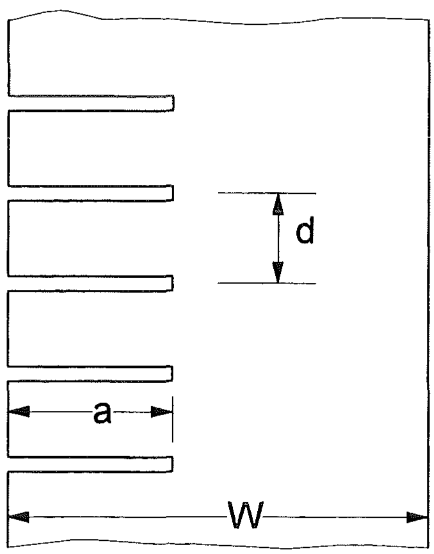

Fig. 16.1 Periodical edge cracks in an endless strip.

The coefficient A_0 is plotted in Fig. 16.3b in the normalised form

$$\tilde{A}_0 = 6A_0\sqrt{\pi W/d} \tag{16.3}$$

For all values $\alpha = a/W$ investigated it was found

$$\tilde{A}_0 = 1.000 \pm 0.002 \tag{16.4}$$

resulting in the stress intensity factor solution

$$K_I = \sigma\sqrt{d/2} \tag{16.5}$$

(see e.g. [33]). The T-stress term is

$$T = -0.592\sigma \tag{16.6}$$

and the biaxiality ratio β according to eq.(2.12) results as

$$\beta = -1.484\sqrt{a/d} \tag{16.7}$$

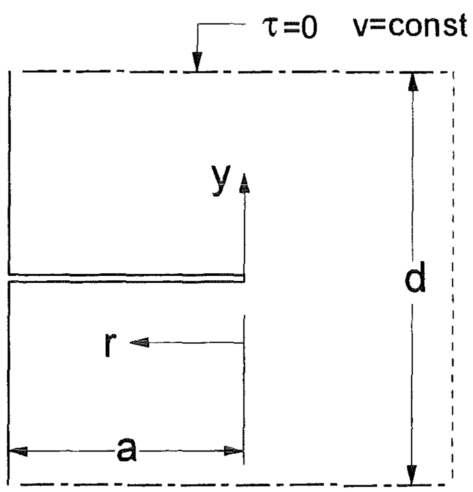

Fig. 16.2 Boundary conditions representing an endless strip with periodical cracks.

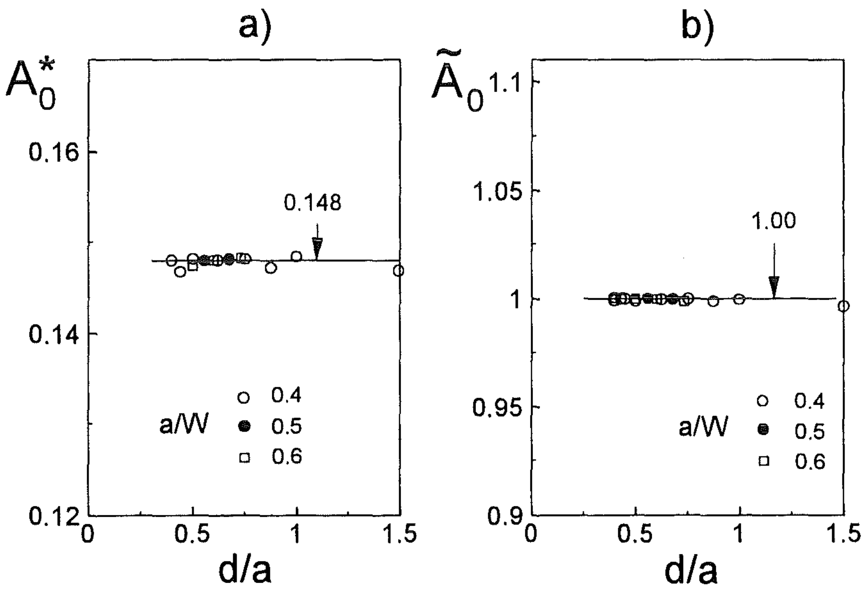

Fig. 16.3 a) Influence of the geometric data on the first regular term of the Williams stress function A^*_0, b) Coefficient A_0 in the normalisation $\tilde{A} = 6A_0\sqrt{\pi W/d}$.

17 Single-edge-cracked plate

17.1 Mixed boundary conditions at the ends

Whereas stress intensity factors for some special crack problems (e.g. semi-infinite crack in a strip of finite height [33]) are available in literature, there is a lack in solutions for the T-stress term in case of displacement-controlled loadings. Such solutions would be of special interest for thermal crack problems.

The single-edge-cracked plate under displacement-controlled loading is shown in Fig. 17.1.1. In Fig. 17.1.1a the plate is extended in y-direction by a constant displacement v. The related stress in the uncracked plate is for plane stress conditions

$$\sigma_0 = \frac{v}{H} E \tag{17.1.1}$$

(E = Young's modulus). For plane strain conditions see Section 20. As the second condition disappearing shear tractions at the ends of the plate may be prescribed leading to a mixed boundary problem. The equivalent description of the crack problem is shown in Fig. 17.1.1b, where the crack faces are loaded by σ_0 and displacements at the ends of the plate are suppressed (v=0).

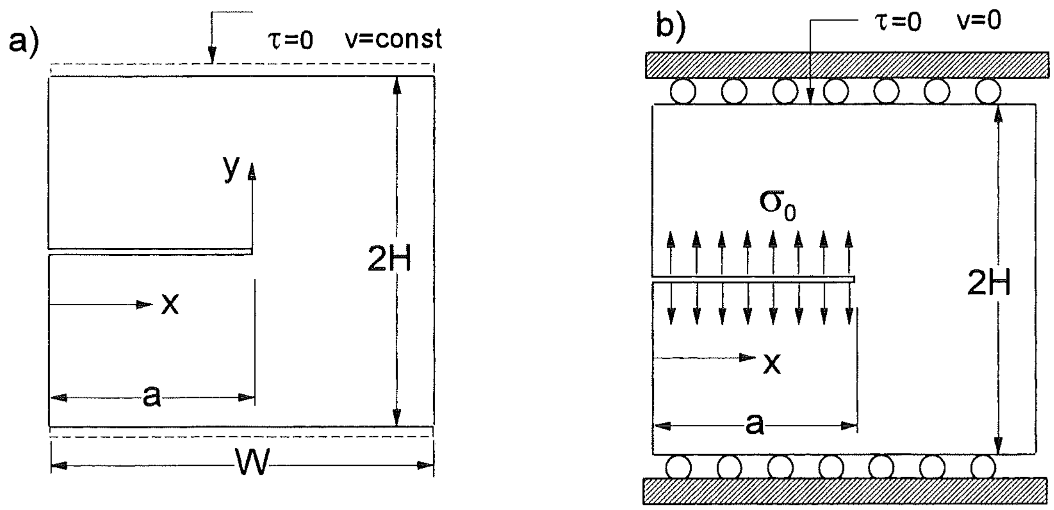

Fig. 17.1.1 Edge-cracked plate under displacement boundary conditions, a) loading by constant displacements v at the plate ends, b) equivalent crack face loading resulting from the superposition principle.

Results for stress intensity factors are illustrated in Fig. 17.1.2a in the form of the geometric function F with $\sigma^* = \sigma_0$. Boundary Collocation results are entered as circles. For $H/W \leq 0.5$ a simple representation of the results is given by [10]

$$F = \sqrt{\frac{H}{\pi a}}\tanh^{1/\gamma}\left(1.1215\sqrt{\frac{\pi a}{H}}\right)^{\gamma} \quad , \quad \gamma = 2.2 \tag{17.1.2}$$

This solution is indicated by the curves in Fig. 17.1.2a. Figure 17.1.2b illustrates the resulting T-stress normalised to σ_0. In the case of H/W=0.25, the T-stress is nearly constant within the range of $0.4 \le a/W \le 0.7$. In order to allow interpolations, Tables 17.1.1 and 17.1.2 provide single values.

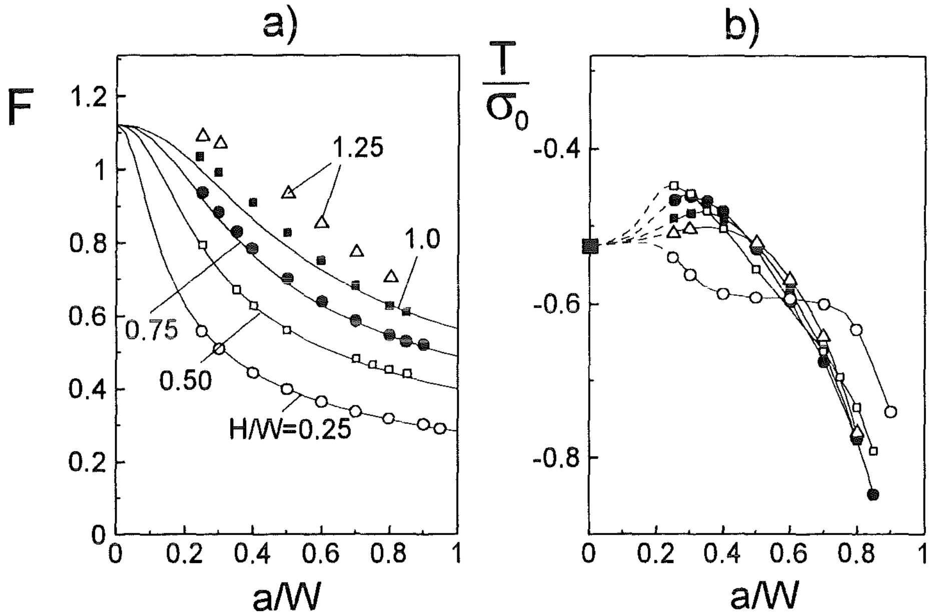

Fig. 17.1.2 Results of BCM computations; a) stress intensity factor, expressed by F (symbols: BCM results, curves: eq.(17.1.2)), b) T-stress (symbols as in a)).

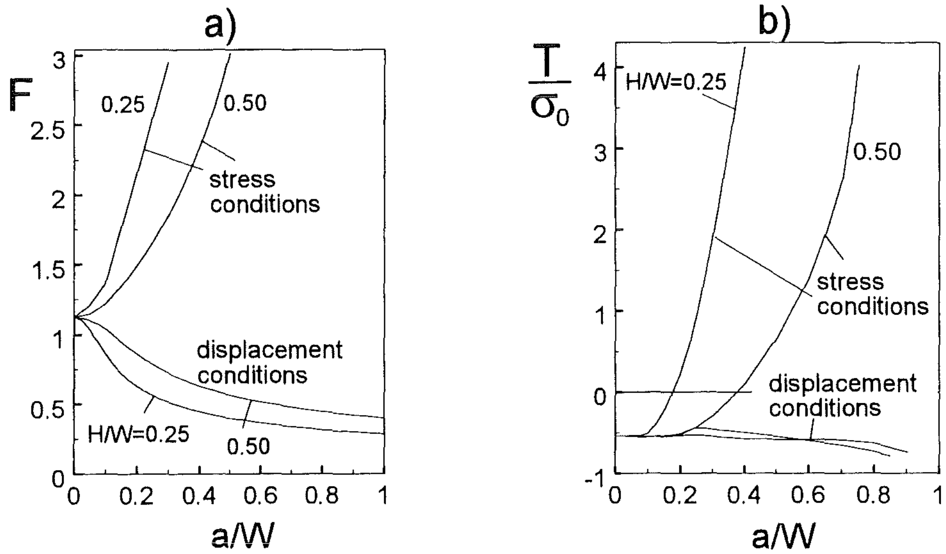

Fig. 17.1.3 Comparison of solutions for constant normal tractions and constant displacements at the plate ends; a) geometric function for stress intensity factor, b) T-stress.

Figure 17.1.3 gives a comparison between the stress intensity factor and T-stress solutions for the stress conditions of ($\sigma_y=\sigma_0$, $\tau_{xy}=0$ at $y=H$) and the results obtained with the displacement condition (v=const., $\tau_{xy}=0$ at $y=H$) for $H/W=0.25$ and $H/W=0.5$.

Strong deviations of the results are obvious from Fig. 17.1.3. Whereas the geometric functions F for the stress boundary conditions increase monotonically with increasing a/W, the geometric function for the displacement boundary conditions decreases with a/W. This result illustrates that the application of the correct boundary conditions is necessary to compute the fracture mechanics parameters for a given crack problem.

As a second displacement condition, the case of prescribed bending displacements

$$v=\sigma_0 \frac{H}{E}\left(1-2\frac{x}{W}\right) \tag{17.1.3}$$

is considered with the outer fibre tensile stress σ_0 in the uncracked plate. The results obtained for this type of loading are compiled in Tables 17.1.3 and 17.1.4. Higher order coefficients of the Williams stress function are entered in Tables 17.1.5-17.1.8

α=a/W	H/W=0.25	0.50	0.75	1.00	1.25
0.00	1.1215	1.1215	1.1215	1.1215	1.1215
0.25	0.558	0.794	0.938	1.030	1.094
0.3	0.510	0.726	0.883	0.992	1.071
0.4	0.445	0.627	0.782	0.909	1.012
0.5	0.399	0.561	0.701	0.826	0.937
0.6	0.364	0.515	0.638	0.750	0.855
0.7	0.338	0.481	0.588	0.684	0.774
0.8	0.318	0.453	0.548	0.629	0.704

Table 17.1.1 Geometric function F for stress intensity factor solution (edge-cracked plate).

α=a/W	H/W=0.25	0.50	0.75	1.00	1.25
0.00	-0.526	-0.526	-0.526	-0.526	-0.526
0.25	-0.536	-0.448	-0.467	-0.490	-0.509
0.3	-0.564	-0.460	-0.462	-0.484	-0.503
0.4	-0.587	-0.505	-0.481	-0.490	-0.498
0.5	-0.592	-0.555	-0.530	-0.525	-0.521
0.6	-0.594	-0.606	-0.596	-0.583	-0.567
0.7	-0.600	-0.662	-0.674	-0.661	-0.641
0.8	-0.634	-0.735	-0.774	-0.776	-0.768

Table 17.1.2 T-stress data T/σ_0 (edge-cracked plate).

α=a/W	H/W=0.25	0.50	0.75	1.00	1.25
0.00	-0.469	-0.469	-0.469	-0.469	-0.469
0.25	-0.961	-0.564	-0.498	-0.476	-0.465
0.3	-1.106	-0.634	-0.523	-0.488	-0.470
0.4	-1.319	-0.805	-0.615	-0.539	-0.492
0.5	-1.484	-0.989	-0.756	-0.636	-0.556
0.6	-1.632	-1.177	-0.934	-0.777	-0.663
0.7	-1.775	-1.376	-1.146	-0.966	-0.828
0.8	-1.994	-1.623	-1.412	-1.234	-1.091

Table 17.1.3 Biaxiality ratio β (edge-cracked plate).

$\alpha=a/W$	H/W=0.25	0.50	1.00
0.3	-0.0737	-0.0459	-0.0356
0.4	-0.0744	-0.0489	-0.0296
0.5	-0.0744	-0.0517	-0.0264
0.6	-0.0744	-0.0532	-0.0235
0.7	-0.0748	-0.0532	-0.0186
0.8	-0.0760	-0.0850	-0.0098

Table 17.1.4 Coefficient A_1 for ν=const. (edge-cracked plate).

$\alpha=a/W$	H/W=0.25	0.50	1.00
0.3	0.2775	0.1945	0.1669
0.4	0.2523	0.1752	0.1450
0.5	0.2464	0.1630	0.1364
0.6	0.2468	0.1589	0.1281
0.7	0.2544	0.1613	0.1156
0.8	0.2834	0.1664	0.1024

Table 17.1.5 Coefficient A^*_1 for ν=const. (edge-cracked plate).

$\alpha=a/W$	H/W=0.25	0.50	1.00
0.3	-0.1052	-0.0785	-0.0356
0.4	-0.0900	-0.0610	-0.0340
0.5	0.0886	-0.0468	-0.0166
0.6	-0.0895	-0.0343	0.0123
0.7	-0.0919	-0.0111	0.0649
0.8	-0.0806	0.0590	0.192

Table 17.1.6 Coefficient A_2 for ν=const. (edge-cracked plate).

$\alpha=a/W$	H/W=0.25	0.50	1.00
0.3	-0.1880	-0.1082	-0.1501
0.4	-0.1282	-0.0685	-0.0758
0.5	-0.1091	-0.0498	-0.0635
0.6	-0.1017	-0.0394	-0.0870
0.7	-0.0836	-0.0577	-0.153
0.8	-0.0736	-0.1636	-0.380

Table 17.1.7 Coefficient A^*_2 for ν=const. (edge-cracked plate).

α=a/W	H/W=0.25	0.50	0.75	1.00	1.25
0.00	1.1215	1.1215	1.1215	1.1215	1.1215
0.2	0.431	0.639	0.740	0.798	0.829
0.3	0.250	0.412	0.531	0.614	0.677
0.4	0.129	0.238	0.344	0.432	0.503
0.5	0.035	0.102	0.186	0.262	0.330
0.6	-0.041	-0.008	0.050	0.109	0.164
0.7	-0.105	-0.103	-0.070	-0.032	0.007
0.8	-0.162	-0.188	-0.183	-0.168	-0.148

Table 17.1.8 Geometric function F for bending displacements (edge-cracked plate).

α=a/W	H/W=0.25	0.50	0.75	1.00	1.25
0.00	-0.526	-0.526	-0.526	-0.526	-0.526
0.2	-0.165	-0.121	-0.146	-0.165	-0.182
0.3	-0.072	0.033	0.033	0.016	0.003
0.4	0.040	0.161	0.184	0.176	0.171
0.5	0.158	0.282	0.318	0.323	0.326
0.6	0.276	0.402	0.446	0.462	0.476
0.7	0.396	0.525	0.580	0.608	0.631
0.8	0.525	0.662	0.741	0.790	0.828

Table 17.1.9 T-stress data T/σ_0 for bending displacements (edge-cracked plate).

α=a/W	H/W=0.25	0.50	0.75	1.00	1.25
0.00	-0.469	-0.469	-0.469	-0.469	-0.469
0.2	-0.383	-0.189	-0.197	-0.207	-0.219
0.3	-0.288	0.080	0.062	0.026	0.004
0.4	0.310	0.676	0.535	0.407	0.340
0.5	4.514	2.765	1.710	1.233	0.988
0.6	-6.732	-0.020	8.92	4.238	2.902
0.7	-3.771	-5.097	-8.285	-1.906	90.14
0.8	-3.241	-3.521	-4.050	-4.702	-5.590

Table 17.1.10 Biaxiality ratio β for bending displacements (edge-cracked plate).

α=a/W	H/W=0.25	0.50	1.00
0.3	0.0170	0.0406	0.0487
0.4	0.0318	0.0534	0.0674
0.5	0.0466	0.0647	0.0822
0.6	0.0615	0.0757	0.0959
0.7	0.0764	0.0870	0.1107
0.8	0.0917	0.0997	0.1304

Table 17.1.11 Coefficient A_1 for bending displacements.

α=a/W	H/W=0.25	0.50	1.00
0.3	-0.0206	-0.0843	-0.1074
0.4	-0.0768	-0.1107	-0.1344
0.5	-0.1264	-0.1318	-0.1512
0.6	-0.1754	-0.1518	-0.1681
0.7	-0.2255	-0.1759	-0.1960
0.8	-0.2849	-0.2177	-0.2560

Table 17.1.12 Coefficient A^*_1 for bending displacements.

A weight function for the crack problem illustrated in Fig. 17.1.1 has been given in [34] as

$$h = \sqrt{\frac{2}{\pi a}}\left[\frac{1}{\sqrt{1-\rho}} + \sum_{n=1}^{4} C_n (1-\rho)^{n-1/2}\right] \quad , \quad \rho = x/a \tag{17.1.4}$$

with the coefficients C_n compiled in Table 17.1.13. In order to allow wide range interpolations of the weight function it is of advantage to know also the solution for the limit case H/W→0 which may be approximated by [10]

$$h = \sqrt{\frac{2}{\pi a}} \frac{1}{\sqrt{1-\rho}} \left[1 - 2\left(\frac{a}{H}\right)^2 (1-\rho)^2 \right] \exp\left(-3\frac{a}{H}(1-\rho) - (a/H)^3(1-\rho)^3 \right) \quad (17.1.5)$$

H/W		a/W=0.3	0.4	0.5	0.6	0.7	0.8
0.25	C_1	-1.6924	-2.3107	-2.9654	-3.6544	-4.3576	-50441
	C_2	0.4181	1.1296	2.3576	4.15225	6.4217	9.0209
	C_3	0.8616	1.0018	0.4213	-1.1047	-3.5700	-6.7893
	C_4	-0.7010	-0.9450	-0.9149	-0.4561	0.4673	1.7795
0.50	C_1	-0.7560	-1.0480	-1.3366	-1.5870	-1.8665	-2.2770
	C_2	0.0813	0.0515	0.1397	0.3347	0.3478	0.0345
	C_3	0.5542	0.6190	0.6893	0.7303	1.3338	3.0820
	C_4	-0.3818	-0.4584	-0.5345	-0.6192	-0.9558	-1.7863
1.00	C_1	0.1158	-0.1735	-0.4305	-0.6369	-0.7176	-0.5953
	C_2	0.1943	0.1825	0.1079	-0.0455	-0.4514	-1.3617
	C_3	0.4413	0.4832	0.5914	0.7634	1.1138	1.8879
	C_4	-0.3196	-0.3369	-0.3962	-0.4931	-0.6423	-0.9200

Table 17.1.13 Coefficients for the weight function representation eq.(17.1.4).

17.2 Pure displacement conditions at the plate ends

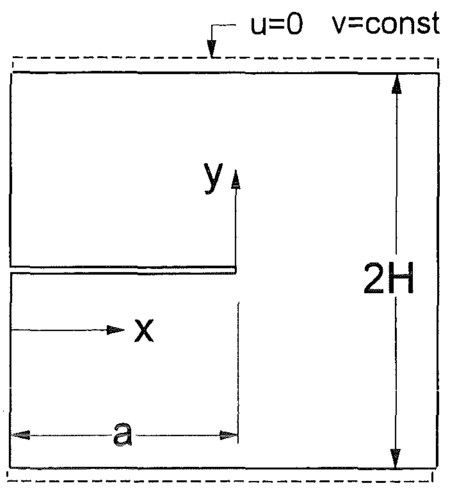

Fig. 17.2.1 Edge crack under pure displacement boundary conditions.

In the loading situation illustrated in Fig. 17.2.1 the displacements u are also kept constant. Since a rigid body motion has no influence on the stresses we restrict the considerations to the case $u = 0$. T-stress solutions for several Poisson's ratios ν are compiled in Tables 17.2.1-17.2.3, normalised on the characteristic stress

$$\sigma_0 = \frac{v}{H} E \tag{17.2.1}$$

Geometric functions F for stress intensity factors, defined by

$$K = \sigma F \sqrt{\pi a}\,, \tag{17.2.2}$$

are represented in Tables 17.2.1-17.2.3. An impression of the influence of the Poisson's ratio on the geometric function is shown in Fig. 17.2.2.

For short plate heights a simple representation of geometric functions has been given in [10]

$$F = \sqrt{\frac{H}{\pi a}} \tanh^{1/\gamma}\left(1.1215\sqrt{\frac{\pi a}{H}}\right)^{\gamma} \quad , \quad \gamma = 2.2 \tag{17.2.3}$$

This relation represents the data of Table 1 with maximum deviations of less than 1.5% for $H/W \leq 0.5$ and less than 2.5% for $H/W = 0.75$.

Results obtained for pure displacement boundary conditions are compiled in Tables 2 and 3.

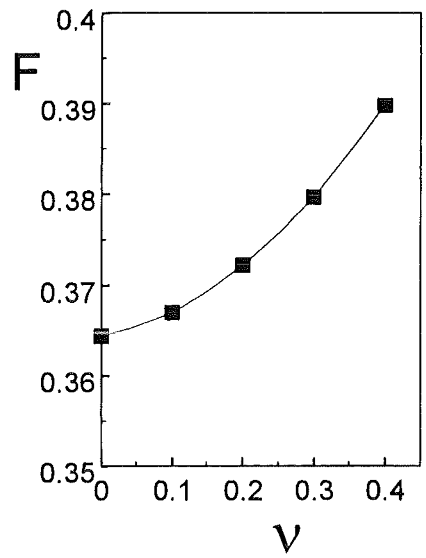

Fig. 17.2.2 Influence of Poisson's ratio ν on geometric function F for stress intensity factor.

a/W	ν=0	0.1	0.2	0.3	0.4
0	1.1215				
0.3	0.512	0.516	0.524	0.537	0.555
0.4	0.444	0.447	0.455	0.466	0.482
0.5	0.398	0.401	0.407	0.417	0.430
0.6	0.364	0.367	0.372	0.380	0.390
0.7	0.338	0.341	0.345	0.351	0.358
0.8	0.318	0.320	0.322	0.326	0.330

Table 17.2.1 Geometric function for $H/W = 0.25$.

a/W	ν=0	0.1	0.2	0.3	0.4
0	1.1215				
0.3	0.727	0.730	0.736	0.744	0.754
0.4	0.630	0.636	0.643	0.652	0.664
0.5	0.563	0.568	0.575	0.584	0.595
0.6	0.516	0.520	0.525	0.532	0.540
0.7	0.480	0.482	0.485	0.490	0.496
0.8	0.451	0.452	0.453	0.455	0.458

Table 17.2.2 Geometric function for $H/W = 0.5$.

a/W	ν=0	0.1	0.2	0.3	0.4
0	1.1215				
0.3	0.993	0.994	0.996	1.000	1.005
0.4	0.909	0.911	0.914	0.918	0.924
0.5	0.827	0.828	0.831	0.835	0.840
0.6	0.751	0.752	0.754	0.757	0.762
0.7	0.684	0.685	0.686	0.688	0.692
0.8	0.629	0.629	0.630	0.632	0.635

Table 17.2.3 Geometric function for $H/W = 1.0$.

a/W	ν=0	0.1	0.2	0.3	0.4
0	-0.526				
0.3	-0.547	-0.522	-0.506	-0.498	-0.499
0.4	-0.577	-0.547	-0.525	-0.511	-0.505
0.5	-0.590	-0.563	-0.544	-0.533	-0.529
0.6	-0.599	-0.579	-0.568	-0.565	-0.570
0.7	-0.614	-0.607	-0.605	-0.608	-0.616
0.8	-0.651	-0.653	-0.659	-0.669	-0.682

Table 17.2.4 T/σ_0 for $H/W = 0.25$.

a/W	ν=0	0.1	0.2	0.3	0.4
0	-0.526				
0.3	-0.468	-0.479	-0.494	-0.513	-0.535
0.4	-0.509	-0.518	-0.531	-0.549	-0.571
0.5	-0.557	-0.564	-0.575	-0.591	-0.611
0.6	-0.608	-0.614	-0.623	-0.635	-0.651
0.7	-0.664	-0.668	-0.674	-0.684	-0.696
0.8	-0.740	-0.740	-0.742	-0.747	-0.754

Table 17.2.5 T/σ_0 for $H/W = 0.5$.

a/W	ν=0	0.1	0.2	0.3	0.4
0	-0.526				
0.3	-0.484	-0.488	-0.494	-0.501	-0.510
0.4	-0.492	-0.497	-0.504	-0.512	-0.521
0.5	-0.526	-0.531	-0.538	-0.546	-0.555
0.6	-0.583	-0.587	-0.592	-0.599	-0.607
0.7	-0.661	-0.664	-0.668	-0.673	-0.678
0.8	-0.776	-0.776	-0.779	-0.784	-0.791

Table 17.2.6 T/σ_0 for $H/W = 1.0$.

a/W	ν=0	0.1	0.2	0.3	0.4
0.3	-0.0752	-0.0775	-0.0815	-0.0871	-0.0944
0.4	-0.0761	-0.0782	-0.0817	-0.0868	-0.0933
0.5	-0.0762	-0.0783	-0.0817	-0.0863	-0.0922
0.6	-0.0763	-0.0785	-0.0817	-0.0859	-0.0911
0.7	-0.0767	-0.0787	-0.0815	-0.0850	-0.0891
0.8	-0.0771	-0.0784	-0.0799	-0.0818	-0.0839

Table 17.2.7 Coefficient A_1 for $H/W=0.25$.

a/W	ν=0	0.1	0.2	0.3	0.4
0.3	-0.0489	-0.0518	-0.0551	-0.0589	-0.0632
0.4	-0.0509	-0.0531	-0.0558	-0.0589	-0.0625
0.5	-0.0528	-0.0544	-0.0564	-0.0588	-0.0616
0.6	-0.0538	-0.0549	-0.0562	-0.0578	-0.0596
0.7	-0.0536	-0.0539	-0.0545	-0.0552	-0.0562
0.8	-0.0506	-0.0503	-0.0501	-0.0500	-0.0501

Table 17.2.8 Coefficient A_1 for $H/W=0.5$.

a/W	ν=0	0.1	0.2	0.3	0.4
0.3	-0.0356	-0.0363	-0.0370	-0.0378	-0.0387
0.4	-0.0298	-0.0302	-0.0310	-0.0321	-0.0326
0.5	-0.0265	-0.0269	-0.0274	-0.0280	-0.0286
0.6	-0.0234	-0.0236	-0.0239	-0.0243	-0.0248
0.7	-0.0188	-0.0189	-0.0190	-0.0192	-0.0195
0.8	-0.0106	-0.0105	-0.0106	-0.0108	-0.0112

Table 17.2.9 Coefficient A_1 for $H/W=1.0$.

a/W	ν=0	0.1	0.2	0.3	0.4
0.3	0.2742	0.2626	0.2559	0.2542	0.2574
0.4	0.2532	0.2494	0.2506	0.2568	0.2679
0.5	0.2466	0.2489	0.2561	0.2682	0.2852
0.6	0.2472	0.2555	0.2672	0.2822	0.3006
0.7	0.2552	0.2673	0.2815	0.2978	0.3163
0.8	0.2778	0.2868	0.2951	0.3027	0.3095

Table 17.2.10 Coefficient A^*_1 for $H/W=0.25$.

a/W	ν=0	0.1	0.2	0.3	0.4
0.3	0.1936	0.1953	0.1993	0.2056	0.2141
0.4	0.1744	0.1759	0.1790	0.1837	0.1899
0.5	0.1647	0.1672	0.1706	0.1749	0.1801
0.6	0.1611	0.1635	0.1663	0.1695	0.1731
0.7	0.1628	0.1632	0.1637	0.1643	0.1649
0.8	0.1726	0.1699	0.1672	0.1645	0.1619

Table 17.2.11 Coefficient A^*_1 for H/W=0.5.

a/W	ν=0	0.1	0.2	0.3	0.4
0.3	0.1684	0.1713	0.1743	0.1775	0.1809
0.4	0.1455	0.1468	0.1486	0.1509	0.1536
0.5	0.1363	0.1363	0.1367	0.1375	0.1386
0.6	0.1280	0.1271	0.1265	0.1263	0.1264
0.7	0.1171	0.1155	0.1144	0.1138	0.1136
0.8	0.1058	0.1066	0.1073	0.1078	0.1081

Table 17.2.12 Coefficient A^*_1 for H/W=1.0.

18 The double-edge-cracked plate

18.1 Mixed boundary conditions at the end

The double-edge-cracked plate under displacement-controlled loading is shown in Fig. 18.1.1. Results for stress intensity factors (expressed by F) are illustrated in Fig. 18.1.1a. Also in this case the curves introduced are described by eq.(18.1.1). The numerical data are represented well up to H/W=0.5 by

$$F = \sqrt{\frac{H}{\pi a}} \tanh^{1/\gamma}\left(1.1215\sqrt{\frac{\pi a}{H}}\right)^{\gamma} \quad , \quad \gamma = 2.2 \tag{18.1.1}$$

with a maximum deviation of less than 3%. For the characteristic stress $\sigma^*=\sigma_0$ see eq.(17.1.1). Figure 18.1.2 represents the resulting T-stress.

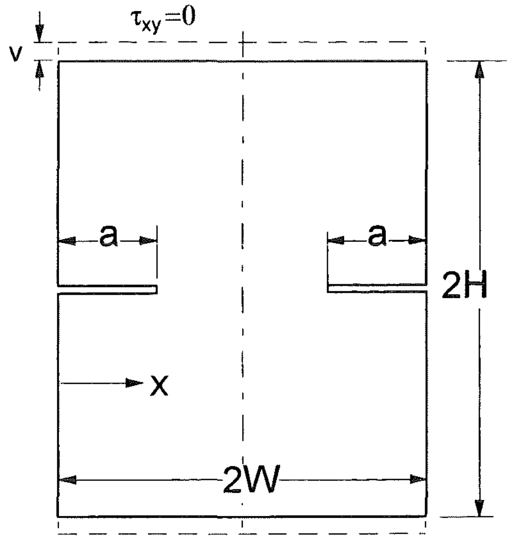

Fig. 18.1.1 Double-edge-cracked plate under mixed boundary conditions

α=a/W	H/W=0.25	0.50	0.75	1.00	1.25
0.00	-0.526	-0.526	-0.526	-0.526	-0.526
0.3	-0.5632	-0.456	-0.443	-0.455	-0.471
0.4	-0.5872	-0.494	-0.434	-0.423	-0.433
0.5	-0.5919	-0.530	-0.437	-0.396	-0.396
0.6	-0.5922	-0.546	-0.436	-0.369	-0.359
0.7	-0.5903	-0.534	-0.417	-0.336	-0.315
0.8	-0.5740	-0.480	-0.370	-0.290	-0.290

Table 18.1.1 T-stress data T/σ_0 for the double-edge-cracked plate.

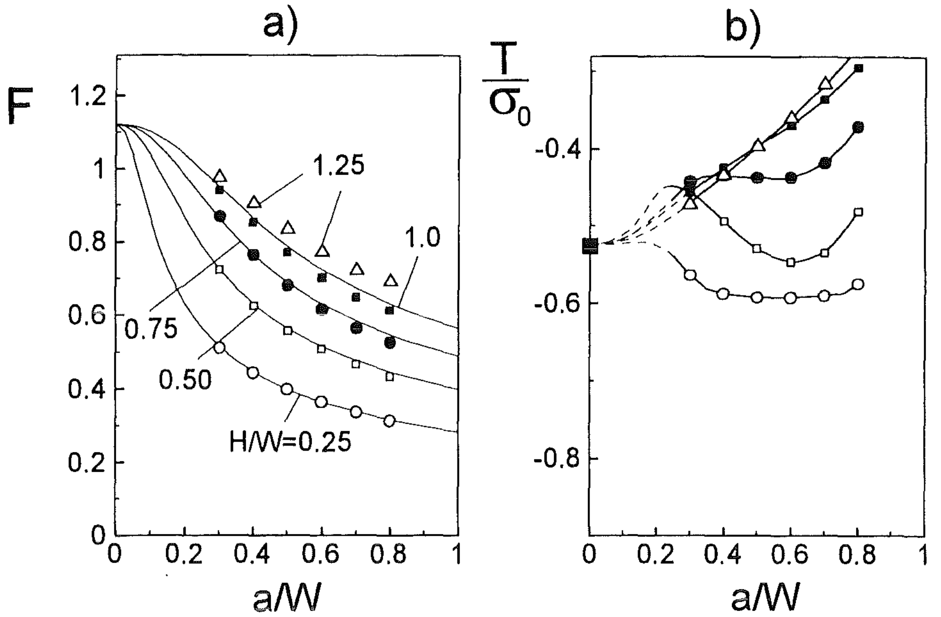

Fig. 18.1.2 Results of BCM computations for the double-edge-cracked plate; a) stress intensity factor, expressed by the geometric function F (symbols: BCM results, curves: eq.(8)), b) T-stress (symbols as in a)).

α=a/W	H/W=0.25	0.50	0.75	1.00	1.25
0.00	1.1215	1.1215	1.1215	1.1215	1.1215
0.3	0.5104	0.726	0.868	0.940	0.976
0.4	0.4446	0.625	0.764	0.853	0.905
0.5	0.3987	0.557	0.680	0.772	0.834
0.6	0.3641	0.508	0.614	0.703	0.772
0.7	0.337	0.468	0.563	0.648	0.722
0.8	0.314	0.480	0.527	0.612	0.693

Table 18.1.2 Geometric function *F* for the double-edge-cracked plate.

α=a/W	H/W=0.25	0.50	0.75	1.00	1.25
0.0	-0.469	-0.469	-0.469	-0.469	-0.469
0.3	-1.103	-0.628	-0.510	-0.484	-0.483
0.4	-1.321	-0.790	-0.568	-0.496	-0.478
0.5	-1.485	-0.952	-0.643	-0.513	-0.475
0.6	-1.626	-1.075	-0.710	-0.525	-0.465
0.7	-1.752	-1.141	-0.741	-0.519	-0.436
0.8	-1.828	-1.00	-0.702	-0.474	-0.418

Table 18.1.3 Biaxiality ratio β for the double-edge-cracked plate.

α=a/W	H/W=0.25	0.50	0.75	1.00	1.25
0.3	-0.0737	-0.0457	-0.0387	-0.0386	-0.0397
0.4	-0.0744	-0.0744	-0.0364	-0.0335	-0.0342
0.5	-0.0743	-0.0504	-0.0366	-0.0314	-0.0315
0.6	-0.0742	-0.0509	-0.0372	-0.0313	-0.0311
0.7	-0.0740	-0.0501	-0.0383	-0.0334	-0.0337
0.8	-0.0726	-0.0495	-0.0424	-0.0409	-0.0433

Table 18.1.4 Coefficient A_1 for the double-edge-cracked plate.

α=a/W	H/W=0.25	0.50	0.75	1.00	1.25
0.3	0.2776	0.1913	0.1543	0.1426	0.1368
0.4	0.2522	0.2523	0.1245	0.1021	0.0960
0.5	0.2461	0.1470	0.1044	0.0772	0.0676
0.6	0.2449	0.1266	0.0841	0.0573	0.0465
0.7	0.2420	0.1027	0.0610	0.0394	0.0303
0.8	0.2220	0.0697	0.0371	0.0236	0.0200

Table 18.1.5 Coefficient A^*_1 for the double-edge-cracked plate.

α=a/W	H/W=0.25	0.50	1.00
0.3	-0.1054	-0.0773	-0.0416
0.4	-0.0899	-0.0900	-0.0291
0.5	-0.0885	-0.0432	-0.0242
0.6	-0.0884	-0.0326	-0.0233
0.7	-0.0866	-0.0264	-0.0312
0.8	-0.0766	-0.0362	-0.0694

Table 18.1.6 Coefficient A_2.

α=a/W	H/W=0.25	0.50	1.00
0.3	-0.188	-0.113	-0.159
0.4	-0.128	-0.128	-0.088
0.5	-0.110	-0.067	-0.058
0.6	-0.108	-0.065	-0.047
0.7	-0.117	-0.074	-0.041
0.8	-0.176	-0.091	-0.032

Table 18.1.7 Coefficient A^*_2.

18.2 Displacement boundary conditions at the ends

The T-stress, geometric function and the higher coefficients A_1 and A^*_1 for the double-edge-cracked rectangular plate under pure displacement conditions at the plate ends are given in Tables 18.2.1-18.2.14.

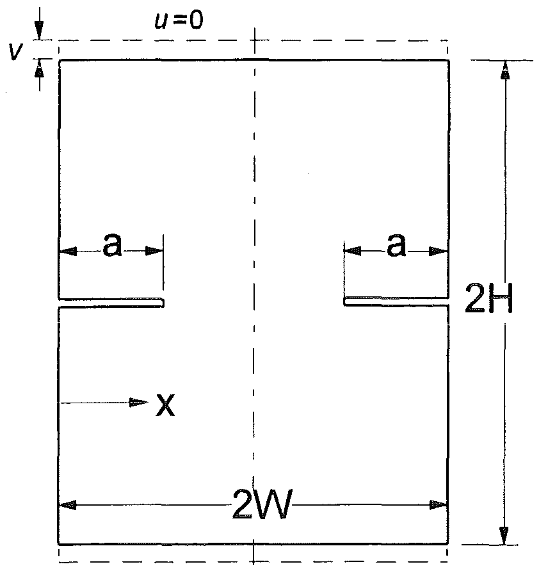

Fig. 18.2.1 Double-edge-cracked plate under displacement boundary conditions.

a/W	v=0	0.1	0.2	0.3	0.4
0	-0.526				
0.3	-0.5460	-0.5152	-0.4915	-0.4749	-0.4654
0.4	-0.5744	-0.5337	-0.4997	-0.4724	-0.4517
0.5	-0.5845	-0.5404	-0.5024	-0.4705	-0.4448
0.6	-0.5856	-0.5412	-0.5030	-0.4709	-0.4449
0.7	-0.5794	-0.5375	-0.5021	-0.4732	-0.4507
0.8	-0.5578	-0.5232	-0.4953	-0.4741	-0.4596

Table 18.2.1 T-stress T/σ_0 for $H/W=0.25$.

a/W	v=0	0.1	0.2	0.3	0.4
0	1.1215				
0.3	0.5119	0.5156	0.5243	0.5381	0.557
0.4	0.4443	0.4471	0.4549	0.4677	0.4854
0.5	0.3982	0.4003	0.4071	0.4185	0.4346
0.6	0.3637	0.3656	0.3717	0.3821	0.3967
0.7	0.3365	0.3384	0.3441	0.3536	0.3670
0.8	0.3137	0.3159	0.3214	0.3301	0.3420

Table 18.2.2 Geometric function F for $H/W=0.25$.

a/W	ν=0	0.1	0.2	0.3	0.4
0.3	-0.0752	-0.0774	-0.0816	-0.0879	-0.0960
0.4	-0.0760	-0.0778	-0.0816	-0.0873	-0.0950
0.5	-0.0760	-0.0778	-0.0815	-0.0872	-0.0948
0.6	-0.0759	-0.0778	-0.0815	-0.0871	-0.0947
0.7	-0.0757	-0.0777	-0.0815	-0.0871	-0.0944
0.8	-0.0747	-0.0770	-0.0809	-0.0863	-0.0932

Table 18.2.3 Coefficient A_1 for $H/W=0.25$.

a/W	ν=0	0.1	0.2	0.3	0.4
0.3	0.2737	0.2568	0.2442	0.2359	0.2318
0.4	0.2518	0.2412	0.2355	0.2347	0.2387
0.5	0.2432	0.2354	0.2331	0.2361	0.2446
0.6	0.2388	0.2327	0.2322	0.2374	0.2483
0.7	0.2330	0.2292	0.2311	0.2386	0.2517
0.8	0.2149	0.2156	0.2214	0.2324	0.2485

Table 18.2.4 Coefficient A^*_1 for $H/W=0.25$.

a/W	ν=0	0.1	0.2	0.3	0.4
0	-0.526				
0.3	-0.456	-0.458	-0.466	-0.481	-0.502
0.4	-0.479	-0.472	-0.473	-0.481	-0.496
0.5	-0.502	-0.488	-0.481	-0.482	-0.491
0.6	-0.512	-0.494	-0.483	-0.480	-0.485
0.7	-0.500	-0.482	-0.472	-0.496	-0.473
0.8	-0.455	-0.441	-0.433	-0.460	-0.436

Table 18.2.5 T-stress T/σ_0 for $H/W=0.5$.

a/W	ν=0	0.1	0.2	0.3	0.4
0	1.1215				
0.3	0.722	0.722	0.725	0.732	0.742
0.4	0.625	0.629	0.637	0.649	0.666
0.5	0.558	0.563	0.573	0.587	0.605
0.6	0.509	0.515	0.524	0.538	0.555
0.7	0.469	0.475	0.484	0.496	0.512
0.8	0.437	0.441	0.449	0.460	0.474

Table 18.2.6 Geometric function F for $H/W=0.5$.

a/W	ν=0	0.1	0.2	0.3	0.4
0.3	-0.0439	-0.0529	-0.0578	-0.0638	-0.0711
0.4	-0.0506	-0.0534	-0.0574	-0.0626	-0.0690
0.5	-0.0519	-0.0541	-0.0575	-0.0620	-0.0676
0.6	-0.0523	-0.0542	-0.0572	-0.0613	-0.0664
0.7	-0.0518	-0.0539	-0.0564	-0.0592	-0.0646
0.8	-0.0515	-0.0532	-0.0556	-0.0587	-0.0624

Table 18.2.7 Coefficient A_1 for $H/W=0.50$.

a/W	ν=0	0.1	0.2	0.3	0.4
0.3	0.1808	0.1726	0.1678	0.1664	0.1683
0.4	0.1550	0.1460	0.1398	0.1364	0.1357
0.5	0.1368	0.1302	0.1261	0.1245	0.1254
0.6	0.1207	0.1173	0.1162	0.1174	0.1210
0.7	0.1012	0.1007	0.1022	0.1058	0.1114
0.8	0.0716	0.0727	0.0753	0.0793	0.0847

Table 18.2.8 Coefficient A^*_1 for $H/W=0.50$.

a/W	ν=0	0.1	0.2	0.3	0.4
0	-0.526				
0.3	-0.460	-0.473	-0.486	-0.498	-0.509
0.4	-0.434	-0.446	-0.460	-0.477	-0.497
0.5	-0.411	-0.425	-0.441	-0.460	-0.482
0.6	-0.385	-0.399	-0.416	-0.436	-0.459
0.7	-0.351	-0.364	-0.379	-0.398	-0.419
0.8	-0.302	-0.316	-0.329	-0.342	-0.354

Table 18.2.9 T-stress T/σ_0 for $H/W=1.0$.

a/W	ν=0	0.1	0.2	0.3	0.4
0	1.1215				
0.3	0.925	0.918	0.913	0.911	0.912
0.4	0.841	0.839	0.840	0.844	0.851
0.5	0.767	0.769	0.774	0.781	0.791
0.6	0.703	0.708	0.715	0.724	0.736
0.7	0.653	0.658	0.666	0.676	0.688
0.8	0.619	0.627	0.634	0.642	0.649

Table 18.2.10 Geometric function F for $H/W=1.0$.

a/W	ν=0	0.1	0.2	0.3	0.4
0.3	-0.0409	-0.0433	-0.0459	-0.0488	-0.0520
0.4	-0.0371	-0.0395	-0.0422	-0.0452	-0.0484
0.5	-0.0354	-0.0377	-0.0403	-0.0432	-0.0463
0.6	-0.0351	-0.0371	-0.0395	-0.0422	-0.0452
0.7	-0.0367	-0.0384	-0.0404	-0.0426	-0.0451
0.8	-0.0433	-0.0452	-0.0469	-0.0483	-0.0493

Table 18.2.11 Coefficient A_1 for $H/W = 1.0$.

a/W	ν=0	0.1	0.2	0.3	0.4
0.3	0.1456	0.1477	0.1521	0.1589	0.1681
0.4	0.1047	0.1082	0.1128	0.1185	0.1252
0.5	0.0783	0.0806	0.0840	0.0883	0.0937
0.6	0.0575	0.0592	0.0616	0.0647	0.0686
0.7	0.0391	0.0402	0.0418	0.0439	0.0465
0.8	0.0239	0.0245	0.0252	0.0259	0.0266

Table 18.2.12 Coefficient A^*_1 for $H/W = 1.0$.

a/W	ν=0	0.2	0.4
0	-0.526		
0.3	-0.477	-0.490	-0.509
0.4	-0.442	-0.462	-0.488
0.5	-0.411	-0.436	-0.469
0.6	-0.377	-0.404	-0.432
0.7	-0.338	-0.356	-0.399

Table 18.2.13 T-stress T/σ_0 for $H/W = 1.25$.

a/W	ν=0	0.2	0.4
0	1.1215		
0.3	0.964	0.954	0.958
0.4	0.895	0.894	0.904
0.5	0.829	0.833	0.847
0.6	0.770	0.779	0.795
0.7	0.724	0.733	0.752

Table 18.2.14 Geometric function F for $H/W = 1.25$.

19 Internally cracked plate

19.1 Mixed boundary conditions at the ends

The T-stress, geometric function and the higher coefficients A_1 and A^*_1 for the internally cracked rectangular plate under mixed boundary conditions at the plate ends are given in Tables 19.1.1-19.1.7. The characteristic stress σ_0 is defined according to eq.(17.1.1).

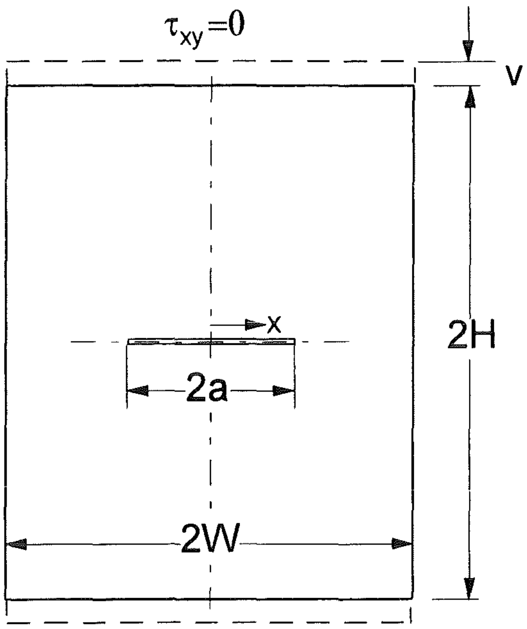

Fig. 19.1.1 Internally cracked plate with mixed boundary conditions at the ends.

α=a/W	H/W=0.25	0.50	0.75	1.00	1.25
0.00	1.00	1.00	1.00	1.00	1.00
0.25	0.570	0.790	0.889	0.937	0.959
0.3	0.518	0.735	0.852	0.913	0.944
0.4	0.446	0.642	0.778	0.860	0.907
0.5	0.399	0.573	0.737	0.805	0.865
0.6	0.364	0.523	0.652	0.751	0.823
0.7	0.338	0.485	0.603	0.702	0.778
0.8	0.319	0.455	0.562	0.667	-

Table 19.1.1 Geometric function F for stress intensity factor solution (internally cracked plate).

α=a/W	H/W=0.25	0.50	0.75	1.00	1.25
0.00	-1.00	-1.00	-1.00	-1.00	-1.00
0.25	-0.606	-0.756	-0.869	-0.932	-0.964
0.3	-0.596	-0.707	-0.832	-0.910	-0.952
0.4	-0.592	-0.646	-0.770	-0.869	-0.928
0.5	-0.592	-0.626	-0.737	-0.840	-0.912
0.6	-0.594	-0.637	-0.734	-0.833	-0.913
0.7	-0.600	-0.674	-0.760	-0.857	-0.965
0.8	-0.635	-0.740	-0.831	-0.98	-

Table 19.1.2 T-stress data T/σ_0 (internally cracked plate).

α=a/W	H/W=0.25	0.50	0.75	1.00	1.25
0.00	-1.00	-1.00	-1.00	-1.00	-1.00
0.25	-1.064	-0.957	-0.977	-0.995	-1.005
0.3	-1.151	-0.962	-0.976	-0.997	-1.008
0.4	-1.327	-1.007	-0.990	-1.010	-1.022
0.5	-1.485	-1.093	-1.037	-1.044	-1.054
0.6	-1.630	-1.219	-1.125	-1.110	-1.109
0.7	-1.777	-1.389	-1.260	-1.220	-1.240
0.8	-1.993	-1.627	-1.477	-1.474	-

Table 19.1.3 Biaxiality ratio β (internally cracked plate).

α=a/W	H/W=0.25	0.50	0.75	1.00	1.25
0.25	-0.0734	-0.0624	-0.0648	-0.0668	-0.0682
0.3	-0.0735	-0.0575	-0.0581	-0.0599	-0.0614
0.4	-0.0740	-0.0533	-0.0499	-0.0503	-0.0515
0.5	-0.0742	-0.0527	-0.0457	-0.0439	-0.0448
0.6	-0.0743	-0.0532	-0.0430	-0.0393	-0.0396
0.7	-0.0748	-0.0528	-0.0398	-0.0349	-0.0416
0.8	-0.0758	-0.0488	-0.0348	-0.0392	

Table 19.1.4 Coefficient A_1 for the internally cracked plate.

α=a/W	H/W=0.25	0.50	0.75	1.00	1.25
0.25	0.2239	0.0514	0.0167	0.0071	0.0038
0.3	0.2384	0.0699	0.0258	0.0116	0.0063
0.4	0.2454	0.1005	0.0466	0.0232	0.0140
0.5	0.2457	0.1220	0.0675	0.0374	0.0261
0.6	0.2468	0.1385	0.0853	0.0542	0.0428
0.7	0.2544	0.1524	0.1001	0.0721	0.0873
0.8	0.2822	0.1634	0.1222	0.1262	

Table 19.1.5 Coefficient A^*_1 for the internally cracked plate.

α=a/W	H/W=0.25	0.50	0.75	1.00	1.25
0.25	-0.087	0.025	0.057	0.068	0.072
0.3	-0.092	0.000	0.035	0.048	0.053
0.4	-0.090	-0.024	0.009	0.026	0.033
0.5	-0.089	-0.032	0.000	0.018	0.024
0.6	-0.089	-0.030	0.004	0.021	0.028
0.7	-0.092	-0.011	0.029	0.049	0.037
0.8	-0.079	0.059	0.109	0.125	

Table 19.1.6 Coefficient A_2 for the internally cracked plate.

α=a/W	H/W=0.25	0.50	0.75	1.00	1.25
0.25	-0.035	0.038	0.018	0.008	0.004
0.3	-0.077	0.032	0.020	0.010	0.006
0.4	-0.104	0.014	0.020	0.011	0.008
0.5	-0.106	0.000	0.011	0.007	0.007
0.6	-0.101	-0.011	-0.009	-0.006	-0.002
0.7	-0.084	-0.042	-0.052	-0.061	-0.033
0.8	-0.072	-0.159	-0.188	-0.276	

Table 19.1.7 Coefficient A^*_2 for the internally cracked plate.

19.2 Displacement boundary conditions at the ends

The T-stress, geometric function and the higher coefficients A_1 and A^*_1 for the internally cracked rectangular plate under pure displacement conditions at the plate ends are given in Tables 19.2.1-19.2.4. The characteristic stress σ_0 is defined by eq.(17.1.1).

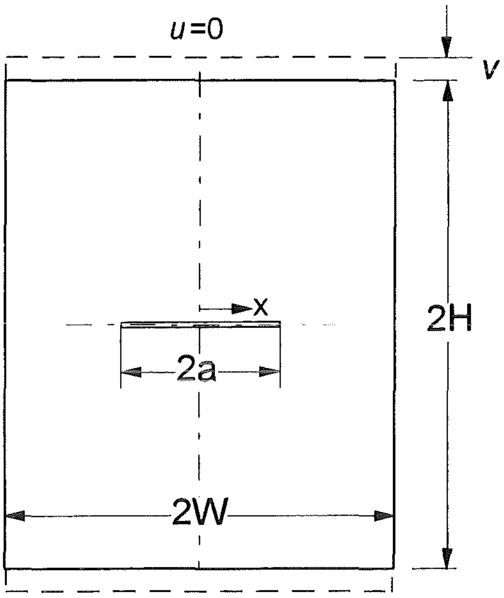

Fig. 19.2.1 Internally cracked plate with pure displacement conditions at the ends.

a/W	ν=0	0.1	0.2	0.3	0.4
0	-1.000				
0.3	-0.612	-0.567	-0.527	-0.492	-0.462
0.4	-0.600	-0.563	-0.533	-0.509	-0.491
0.5	-0.598	-0.568	-0.545	-0.529	-0.520
0.6	-0.602	-0.578	-0.561	-0.551	-0.549

Table 19.2.1 T-stress T/σ_0 for H/W=0.25.

a/W	ν=0	0.1	0.2	0.3	0.4
0	1.000				
0.3	0.518	0.519	0.527	0.541	0.561
0.4	0.447	0.449	0.456	0.467	0.483
0.5	0.399	0.402	0.408	0.417	0.430
0.6	0.365	0.367	0.372	0.380	0.391

Table 19.2.2 Geometric function F for H/W=0.25.

a/W	ν=0	0.1	0.2	0.3	0.4
0	-1.000				
0.3	-1.182	-1.090	-1.000	-0.992	-0.825
0.4	-1.343	-1.253	-1.169	-1.090	-1.016
0.5	-1.499	-1.413	-1.336	-1.268	-1.210
0.6	-1.651	-1.575	-1.508	-1.451	-1.404

Table 19.2.3 Biaxiality ratio β for $H/W=0.25$.

a/W	ν=0	0.1	0.2	0.3	0.4
0.3	-0.0757	-0.0777	-0.0813	-0.0865	-0.0932
0.4	-0.0759	-0.0780	-0.0816	-0.0866	-0.0931
0.5	-0.0761	-0.0783	-0.0817	-0.0864	-0.0924
0.6	-0.0767	-0.0787	-0.0817	-0.0857	-0.0908

Table 19.2.4 Coefficient A_1 for $H/W=0.25$.

a/W	ν=0	0.1	0.2	0.3	0.4
0.3	0.2287	0.2302	0.2380	0.2520	0.2723
0.4	0.2376	0.2386	0.2455	0.2582	0.2768
0.5	0.2411	0.2444	0.2530	0.2668	0.2858
0.6	0.2451	0.2575	0.2740	0.2945	0.319

Table 19.2.5 Coefficient A^*_1 for $H/W=0.25$.

a/W	ν=0	0.1	0.2	0.3	0.4
0	-1.000				
0.3	-0.729	-0.697	-0.673	-0.657	-0.648
0.4	-0.675	-0.656	-0.643	-0.636	-0.634
0.5	-0.660	-0.650	-0.645	-0.645	-0.651
0.6	-0.667	-0.665	-0.666	-0.671	-0.679
0.7	-0.697	-0.698	-0.701	-0.707	-0.715

Table 19.2.6 T-stress T/σ_0 for $H/W=0.50$.

a/W	ν=0	0.1	0.2	0.3	0.4
0	1.000				
0.3	0.731	0.735	0.745	0.762	0.786
0.4	0.640	0.642	0.649	0.661	0.677
0.5	0.572	0.574	0.579	0.587	0.599
0.6	0.522	0.523	0.527	0.533	0.541
0.7	0.484	0.485	0.487	0.490	0.495

Table 19.2.7 Geometric function F for $H/W=0.50$.

a/W	ν=0	0.1	0.2	0.3	0.4
0	-1.000				
0.3	-0.998	-0.949	-0.904	-0.863	-0.825
0.4	-1.056	-1.022	-0.991	-0.963	-0.937
0.5	-1.152	-1.132	-1.114	-1.099	-1.087
0.6	-1.278	-1.269	-1.263	-1.259	-1.257
0.7	-1.440	-1.439	-1.439	-1.440	-1.443

Table 19.2.8 Biaxiality ratio β for $H/W=0.50$.

a/W	ν=0	0.1	0.2	0.3	0.4
0.3	-0.0586	-0.0597	-0.0614	-0.0637	-0.0665
0.4	-0.0548	-0.0561	-0.0579	-0.0601	-0.0628
0.5	-0.0541	-0.0554	-0.0571	-0.0591	-0.0614
0.6	-0.0542	-0.0552	-0.0565	-0.0580	-0.0597
0.7	-0.0540	-0.0543	-0.0549	-0.0557	-0.0567

Table 19.2.9 Coefficient A_1 for $H/W=0.50$.

a/W	ν=0	0.1	0.2	0.3	0.4
0.3	0.0717	0.0806	0.0904	0.1012	0.1129
0.4	0.1000	0.1089	0.1190	0.1303	0.1429
0.5	0.1172	0.1257	0.1348	0.1446	0.1550
0.6	0.1309	0.1370	0.1433	0.1499	0.1569
0.7	0.1499	0.1489	0.1492	0.1509	0.1540

Table 19.2.10 Coefficient A^*_1 for $H/W=0.50$.

a/W	ν=0	0.1	0.2	0.3	0.4
0	-1.000				
0.3	-0.910	-0.911	-0.918	-0.930	-0.947
0.4	-0.871	-0.870	-0.873	-0.880	-0.892
0.5	-0.845	-0.842	-0.843	-0.847	-0.855
0.6	-0.842	-0.838	-0.837	-0.838	-0.842
0.7	-0.872	-0.867	-0.864	-0.863	-0.865
0.8	-0.958	-0.960	-0.963	-0.967	-0.973

Table 19.2.11 T-stress T/σ_0 for $H/W=1.0$.

a/W	ν=0	0.1	0.2	0.3	0.4
0	1.000				
0.3	0.905	0.915	0.929	0.948	0.971
0.4	0.851	0.857	0.866	0.879	0.895
0.5	0.795	0.798	0.803	0.811	0.822
0.6	0.744	0.744	0.746	0.750	0.757
0.7	0.699	0.698	0.698	0.700	0.703
0.8	0.666	0.665	0.665	0.667	0.669

Table 19.2.12 Geometric function F for H/W= 1.0.

a/W	ν=0	0.1	0.2	0.3	0.4
0	-1.000				
0.3	-1.006	-0.996	-0.988	-0.981	-0.975
0.4	-1.024	-1.015	-1.008	-1.002	-0.997
0.5	-1.063	-1.056	-1.050	-1.045	-1.040
0.6	-1.132	-1.127	-1.122	-1.117	-1.113
0.7	-1.247	-1.242	-1.238	-1.234	-1.231
0.8	-1.440	-1.444	-1.448	-1.451	-1.454

Table 19.2.13 Biaxiality ratio β for H/W= 1.0.

a/W	ν=0	0.1	0.2	0.3	0.4
0.3	-0.0599	-0.0602	-0.0608	-0.0616	-0.0626
0.4	-0.0507	-0.0506	-0.0507	-0.0510	-0.0514
0.5	-0.0451	-0.0447	-0.0445	-0.0444	-0.0444
0.6	-0.0416	-0.0410	-0.0405	-0.0401	-0.0398
0.7	-0.0388	-0.0380	-0.0374	-0.0369	-0.0365
0.8	-0.0329	-0.0338	-0.0346	-0.0353	-0.0359

Table 19.2.14 Coefficient A_1 for H/W= 1.0.

a/W	ν=0	0.1	0.2	0.3	0.4
0.3	0.0123	0.0127	0.0127	0.0124	0.0118
0.4	0.0245	0.0248	0.0248	0.0245	0.0238
0.5	0.0402	0.0399	0.0395	0.0389	0.0381
0.6	0.0594	0.0583	0.0572	0.0561	0.0549
0.7	0.0842	0.0817	0.0797	0.0781	0.0770
0.8	0.1202	0.1227	0.1252	0.1278	0.1304

Table 19.2.15 Coefficient A^*_1 for H/W=1.0.

20 Poisson's ratio and boundary conditions

As could be seen from the results presented in Section 17, the mixed boundary conditions yielded results independent of the Poisson's ratio, whereas in case of displacement boundary conditions at $y=H$ an influence of ν is obvious. This behaviour is known for stress intensity factors [33-38] and will be discussed according to [34] for the T-stress term.

Figure 20.1 illustrates three different loading situations at the ends of a rectangular plate. Pure stress conditions are represented as case a), mixed boundary conditions as case b) and pure displacement conditions as case c).

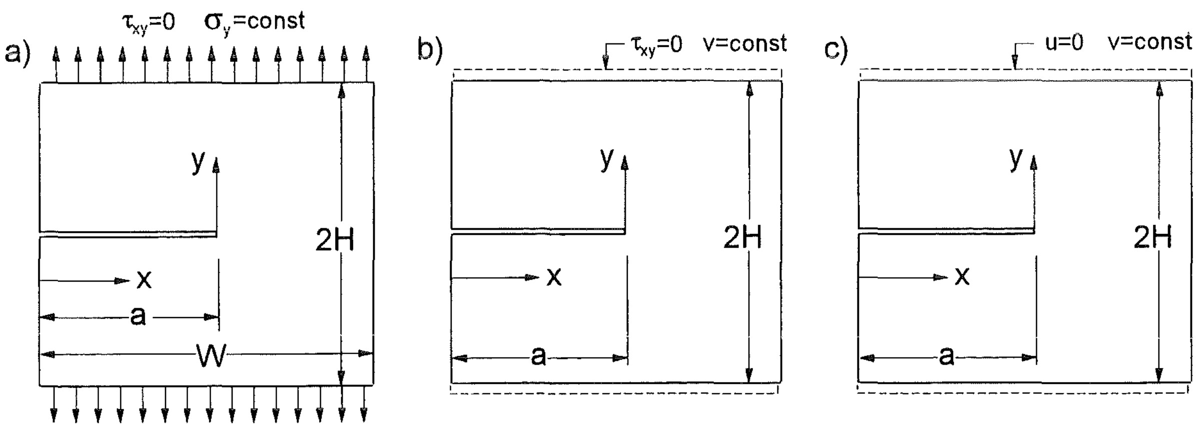

Fig. 20.1 Edge crack under different boundary conditions; a) pure stress conditions, b) mixed boundary conditions, c) displacement boundary conditions.

20.1 Influence of ν on the Airy stress function

A simple consideration in terms of the Airy stress function may illustrate this. A fracture mechanics problem is solved if the Airy stress function Φ has been determined as the solution of the biharmonic differential equation

$$\Delta\Delta\Phi = 0 \tag{20.1}$$

For cracked structures the Airy stress function is of the Williams type [15]. A possible influence of Poisson's ratio ν can only result from the boundary conditions which must be fulfilled by Φ. The following considerations are made for plane stress conditions.

The common boundary conditions for all three cases, illustrated in Fig.20.2, are

$$
\begin{array}{lll}
v = 0 & \tau_{xy} = 0 & \text{for } L_0 \\
\sigma_y = 0 & \tau_{xy} = 0 & \text{for } L_1 \\
\sigma_x = 0 & \tau_{xy} = 0 & \text{for } L_2 \\
\sigma_x = 0 & \tau_{xy} = 0 & \text{for } L_4
\end{array}
\tag{20.2}
$$

with the boundaries L_0, L_1, L_2 and L_4 shown in Fig. 20.2. The Williams stress function [15] automatically satisfies the displacement and stress conditions along lines L_0 and L_1.

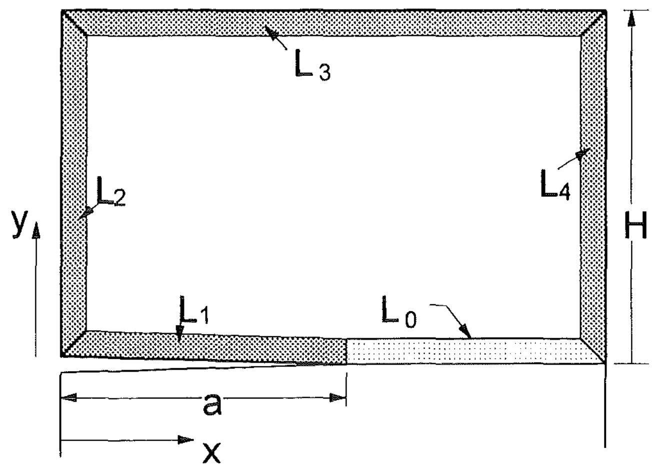

Fig. 20.2 Notation of boundary lines.

The different conditions at boundary L_3 read for cases a), b) and c) in Fig. 20.1

$$
\begin{array}{lll}
\sigma_y = \sigma_0 & \tau_{xy} = 0 & \text{case a)} \\
v = const & \tau_{xy} = 0 & \text{case b)} \\
v = const & u = 0 & \text{case c)}
\end{array}
\tag{20.3}
$$

Let us use Hooke's relations written in terms of the stress function

$$
\varepsilon_x = \frac{\partial u}{\partial x} = \frac{1}{E'}\left(\frac{\partial^2\Phi}{\partial y^2} - \nu'\frac{\partial^2\Phi}{\partial x^2}\right)
\tag{20.4}
$$

$$
\varepsilon_y = \frac{\partial v}{\partial y} = \frac{1}{E'}\left(\frac{\partial^2\Phi}{\partial x^2} - \nu'\frac{\partial^2\Phi}{\partial y^2}\right)
\tag{20.5}
$$

with

$$
\nu' = \begin{cases} \nu & \text{plane stress} \\ \nu/(1-\nu) & \text{plane strain} \end{cases}
\tag{20.6}
$$

and as an additional relation between the displacements

$$\frac{\partial v}{\partial x}+\frac{\partial u}{\partial y}=\gamma=\frac{\tau_{xy}}{G} \tag{20.7}$$

with the shear modulus G.

Stress boundary conditions (case a):

From eq.(20.3), expressed by the stress function Φ

$$\tau_{xy}=0=-\frac{\partial^2\Phi}{\partial x\partial y}, \quad \sigma_y=\sigma_0=\frac{\partial^2\Phi}{\partial x^2}, \tag{20.8}$$

we can conclude that this boundary condition only introduces σ_0 into the solution.

Mixed boundary conditions (case b):

Starting with

$$\tau_{xy}=0=-\frac{\partial^2\Phi}{\partial x\partial y}, \quad v=const. \tag{20.9}$$

we obtain from (20.7) with $\partial v/\partial x=0$ and $\tau_{xy}=0$:

$$\frac{\partial u}{\partial y}=0 \quad \forall x \tag{20.10}$$

leading to

$$\frac{\partial^2 u}{\partial x\partial y}=0=\frac{1}{E'}\left(\frac{\partial^3\Phi}{\partial y^3}-\nu'\frac{\partial^3\Phi}{\partial x^2\partial y}\right)=\frac{1}{E'}\left(\frac{\partial^3\Phi}{\partial y^3}+\nu'\frac{\partial\tau_{xy}}{\partial x}\right) \tag{20.11}$$

The boundary conditions (20.9), rewritten in terms of the stress function, are given by

$$\frac{\partial^3\Phi}{\partial y^3}=0, \quad \frac{\partial^2\Phi}{\partial x\partial y}=0 \tag{20.12}$$

Since the boundary conditions do not contain ν, the stress function for case b) must also be independent of ν.

Displacement boundary conditions (case c):

From (20.4) we obtain with u=const, i.e. $\partial u/\partial x=0$

$$\frac{\partial u}{\partial x}=\frac{1}{E'}\left(\frac{\partial^2\Phi}{\partial y^2}-\nu'\frac{\partial^2\Phi}{\partial x^2}\right)=0 \tag{20.13}$$

providing the boundary condition for Φ

$$\frac{\partial^2\Phi}{\partial y^2} = \nu' \frac{\partial^2\Phi}{\partial x^2} \Rightarrow \Phi = f(\nu) \tag{20.14}$$

i.e. the stress function will depend on ν.

20.2 Influence of ν on the T-stress

From the numerical results we can conclude that the stress intensity factors and weight functions for mixed boundary conditions at the plate ends (v=const., τ_{xy}=0) are independent of the Poisson's ratio within the accuracy of the BCM procedure. In case of pure displacement conditions (v=const., u=const.) an influence of ν could be clearly stated.

In order to give a theoretical explanation let us use the Williams expansion [15] for the stress function Φ

$$\Phi = \sigma * W^2 \sum_{n=0}^{\infty} (r/W)^{n+3/2} A_n \left[\cos(n+\tfrac{3}{2})\varphi - \frac{n+\frac{3}{2}}{n-\frac{1}{2}} \cos(n-\tfrac{1}{2})\varphi \right]$$

$$+ \sigma * W^2 \sum_{n=0}^{\infty} (r/W)^{n+2} A^*_n [\cos(n+2)\varphi - \cos n\varphi] \tag{20.15}$$

with polar coordinates r, φ (origin at the crack tip). Since in case of the mixed boundary conditions this function has to be independent of ν for all locations of the component, the coefficients A_n have to be independent of ν. Due to

$$\sigma_r = \frac{1}{r}\frac{\partial\Phi}{\partial r} + \frac{1}{r^2}\frac{\partial^2\Phi}{\partial\varphi^2}\,, \quad \sigma_\varphi = \frac{\partial^2\Phi}{\partial r^2}\,, \quad \tau_{r\varphi} = \frac{1}{r^2}\frac{\partial\Phi}{\partial\varphi} - \frac{1}{r}\frac{\partial^2\Phi}{\partial r\partial\varphi} \tag{20.16}$$

also the stresses in the component must be independent on ν. This especially holds for the singular stress term, consequently for the stress intensity factor K and for the constant stress term, the T-stress.

Finally, it should be mentioned that in case of plane strain conditions Poisson's ratio only affects the results via the characteristic stress σ*.

21 Nomenclature

a	Crack length
a_0	Depth of a notch
A_n	Coefficient of the Williams stress function
A^*_n	Coefficient of the Williams stress function
C_n	Coefficient of the Green's function for T-stresses
d	Spacing of a crack array
D	Diameter of a disk
D_n	Coefficient for weight function representation
E	Young's modulus
F	Geometric function for stress intensity factors
G	Shear modulus
h	Weight function (Green's function) for stress intensity factors
H	Height of a rectangular specimen
K	Stress intensity factor
ℓ	Length of a small crack ahead of a notch
L	Length of a 3-point bending bar
L_n	Notation of boundaries
M	Bending moment
p	Pressure on crack faces
P	concentrated forces
r	distance from crack tip
R	Radius of a disk, notch root radius
t	Weight function (Green's function) for T-stress, thickness of a component
t_0	asymptotic part of t (near-tip solution)
T	total T-stress, eq.(2.9)
T_c	T-stress contribution caused by the crack, eq.(2.11)
$T^{(0)}$	T-stress contribution caused by the x-stress in the uncracked body, eq.(2.10)

u	Displacements in x-direction
v	Displacements in y-direction
W	Width of a rectangular plate
x	Coordinate parallel to a crack
y	Coordinate perpendicular to a crack
z	Complex coordinate $(x+iy)$
Z	Westergaard stress function
α	Relative crack length a/W
β	Biaxiality ratio, eq.(2.12)
ν	Poisson's ratio
φ	Polar angle
σ_0	constant stresses at the plate ends in case of stress boundary conditions; for displacement boundary conditions $\sigma_0=vE/H$
σ^*	characteristic stress
σ_n	Normal tractions
τ	Shear stresses
Φ	Airy stress function, Williams stress function
Θ	Angle between crack and force in a Brazilian disk test

22 References

[1] Larssen, S.G., Carlsson, A.J., J. of Mech. and Phys. of Solids **21**(1973), 263-277

[2] Sumpter, J.D., The effect of notch depth and orientation on the fracture toughness of multipass weldments, Int. J. Press. Ves. and Piping **10**(1982), 169-180

[3] Cotterell, B., Li, Q.F., Zhang, D.Z., Mai, Y.W., On the effect of plastic constraint on ductile tearing in a structural steel, Eng. Fract. Mech. **21**(1985), 239-244.

[4] Sumpter, J.D., Hancock, J.W., Shallow crack toughness of HY80 welds: An analysis based on T-stresses, Int. J. Pres. Ves. & Piping **45**(1991), 207-221.

[5] Leevers, P.S., Radon, J.C., Inherent stress biaxiality in various fracture specimen geometries, Int. J. Fract. **19**(1982), 311-325.

[6] Kfouri, A.P., Some evaluations of the elastic T-term using Eshelby's method, Int. J. Fract. **30**(1986), 301-315.

[7] Sham, T.L., The theory of higher order weight functions for linear elastic plane problems, Int. J. Solids and Struct. **25**(1989), 357-380.

[8] Sham, T.L., The determination of the elastic T-term using higher order weight functions, Int. J. Fract. **48**(1991), 81-102.

[9] Fett, T., A Green's function for T-stresses in an edge-cracked rectangular plate, Eng. Fract. Mech. **57**(1997), 365-373.

[10] Fett, T., Munz, D., Stress intensity factors and weight functions, Computational Mechanics Publications, Southampton, 1997.

[11] Wang, Y.Y., Parks, D.M., Evaluation of the elastic T-stress in surface-cracked plates using the line-spring method, Int. J. Fract **56**(1992), 25-40.

[12] Sherry, A.H., France, C.C., Goldthorpe, M.R., Compendium of T-stress solutions for two and three-dimensional cracked geometries, Engng. Fract. Mech. **18**(1995), 141-155.

[13] Fett, T., T-stress in edge-cracked specimens, FZKA 5802, Forschungszentrum Karlsruhe, 1996.

[14] Fett, T., A compendium of T-stress solutions, FZKA 6057, Forschungszentrum Karlsruhe, 1998.

[15] Williams, M.L., On the stress distribution at the base of a stationary crack, J. Appl. Mech. **24**(1957), 109-114.

[16] Bückner, H., A novel principle for the computation of stress intensity factors, ZAMM **50**(1970), 529-546.

[17] Irwin, G.R., Analysis of stresses and strains near the end of a crack transversing a plate, J. Appl. Mech. **24** (1957), 361-364.

[18] Gröbner, W., Hofreiter, N., Integraltafel, Teil 1, Springer Verlag, Wien New York, 1975.

[19] Gross, B., Srawley, J.E., Brown, W.F., Stress intensity factors for a single-edge-notched tension specimen by Boundary Collocation of a stress function, NASA, Technical Note, D-2395, 1965.

[20] Gross, B., Srawley, W.F., Stress intensity factors for a single-edge-notched tension specimen by Boundary Collocation of a stress function, NASA, Technical Note, D-2395, 1965.

[21] Newman, J.C., An improved method of collocation for the stress analysis of cracked plates with various shaped boundaries, NASA TN D-6376, 1971.

[22] Atkinson, C., Smelser, R.E., Sanchez, J., Combined mode fracture via the cracked Brazilian disk test, Int. J. Fract. **18**(1982), 279-291

[23] Awaji, H., Sato, S., Combined mode fracture toughness measurement by the disk test, J. Engng. Mat. Tech. **100**(1978), 175-182.

[24] Fett, T., Mode-II weight function for circular disks with internal radial crack and application to the Brazilian disk test, Int. J. Fract..

[25] Tada, H., Paris, P.C., Irwin, G.R., The stress analysis of cracks handbook, Del Research Corporation, 1986.

[26] Filon, L.N.G., On an approximate solution for the bending of a beam of rectangular cross-section under any system of load, with special reference to points of concentrated or discontinuos loading, Phil. Trans., A, **201**(1903), 63-155.

[27] Cotterell, B., On the fracture path stability in the compact tension test, Int. J. Fract. Mech. **6**(1970), 189-192.

[28] Rödel, J., Kelly, J.F., Lawn, B.R., In situ measurements of bridge crack interfaces in the scanning electron microscope, J. Am. Ceram. Soc. **73**(1990), 3313-3318.

[29] Schneider, G.A., Magerl, F., Hahn, I., Petzow, G., In-situ observations of unstable and stable crack propagation and R-curve behaviour in thermally loaded disks, in: G.A. Schneider, G. Petzow (eds,), Thermal Shock and Thermal Fatigue Behaviour of Advanced Ceramics, 105-117, 1993 Kluwer Academic Publishers, Dordrecht, Netherlands.

[30] Wigglesworth, L.A., Stress distribution in a notched plate, Mathematica **4**(1957), 76-96.

[31] Timoshenko, S.P., Goodier, J.N., Theory of Elasticity, McGraw-Hill Kogagusha, Ltd., Tokyo.

[32] Creager, M., Paris, P.C., Elastic field equations for blunt cracks with reference to stress corrosion cracking, Int. J. Fract. **3**(1967), 247-252.

[33] Rice, J.R., Stress in an infinite strip containing a semi-infinite crack, Trans. ASME, Ser. E, J. Appl. Mech., **34**(1967), 248-249.

[34] Fett, T., Bahr, H.-A., Crack-face weight functions for short plates under different boundary conditions, submitted to Engng. Fract. Mech.

[35] Benthem, J.P., Koiter, W.T., Asymptotic approximations to crack problems, in "Methods of Analysis of Crack Problems" edited by G.C. Sih, 1972, Noordhoff International Publishing

[36] Fichter, W.B., Stresses at the tip of a longitudinal crack in a plate strip, NASA Technical Report TR-R-265, 1967, Langley.

[37] Isida, M., On the determination of stress intensity factors for some common structural problems, Engng. Fract. Mech. **2**(1970), 61.

[38] Torvik, P.J., On the determination of stresses, displacements, and stress intensity factors in edge-cracked sheets with mixed boundary conditions, Trans. ASME, J. Appl. Mech. **46**(1979), 611-617.